Static force capabilities and dynamic capabilities of parallel mechanisms equipped with safety clutches

Mémoire

Wei Chen

Maîtrise en génie mécanique
Maître ès sciences (M.Sc.)

Québec, Canada

Résumé

Cette thèse étudie les forces potentielles des mécanismes parallèles plans à deux degrés de liberté équipés d'embrayages de sécurité (limiteur de couple). Les forces potentielles sont étudiées sur la base des matrices jacobienne. La force maximale qui peut être appliquée à l'effecteur en fonction des limiteurs de couple ainsi que la force maximale isotrope sont déterminées. Le rapport entre ces deux forces est appelé l'efficacité de la force et peut être considéré ; comme un indice de performance. Enfin, les résultats numériques proposés donnent un aperçu sur la conception de robots coopératifs reposant sur des architectures parallèles.

En isolant chaque lien, les modèles dynamiques approximatifs sont obtenus à partir de l'approche Newton-Euler et des équations de Lagrange pour du tripteron et du quadrupteron. La plage de l'accélération de l'effecteur et de la force externe autorisée peut être trouvée pour une plage donnée de forces d'actionnement.

Abstract

This thesis investigates the force capabilities of two-degree-of-freedom planar parallel mechanisms that are equipped with safety clutches (torque limiters). The force capabilities are studied based on the Jacobian matrices. The maximum force that can be applied at the end-effector for given torque limits (safety index) is determined together with the maximum isotropic force that can be produced. The ratio between these two forces, referred to as the force effectiveness, can be considered as a performance index. Finally, some numerical results are proposed which can provide insight into the design of cooperation robots based on parallel architectures.

Considering each link and slider system as a single body, approximate dynamic models are derived based on the Newton-Euler approach and Lagrange equations for the tripteron and the quadrupteron. The acceleration range or the external force range of the end-effector are determined and given as a safety consideration with the dynamic models.

Contents

List of Figures

Foreword

First, I want to thank my supervisor Dr. Clément Gosselin for his support and guidance. I am very gratefull not only for all the great advise and stimulating discussions, but his broad-mindedness and generous support on my research and my life. He has shown me a professional standard which will always stay with me.

I would like to thank my thesis committee Dr. Marc Richard and Dr. Alain Curodeau for their precious time and support.

I would like to acknowledge all the members of the Robotics Laboratory for their help and camaraderie.

Finally and most specially, my gratitude also belongs to my wife, Hanwei Liu. She has given me her love and support throughout my graduate studies. And together with her, I look forward to whatever the future may bring.

Chapter 1

Introduction

Some of the parallel mechanisms that have been developed in the last several decades are briefly described in this chapter. The research methodology regarding the force capability analysis and the dynamic analysis are also introduced briefly. The literature review on force capabilities and dynamic analysis for parallel mechanisms is presented in the following. In the end, the main contributions of this thesis are introduced.
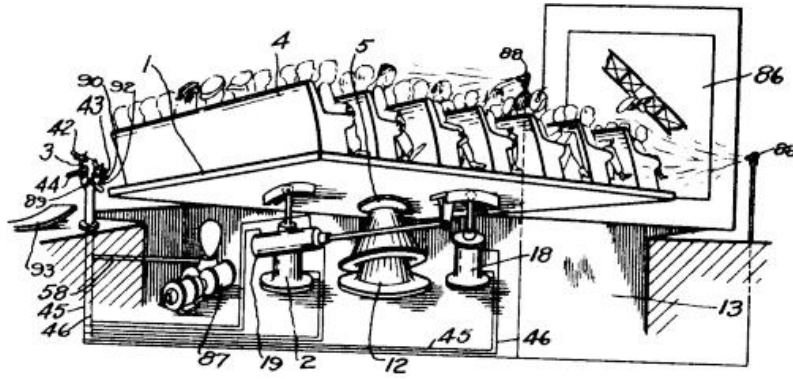
Figure 1.1: Parallel structure used for entertainment (from US Patent No. 1789680).
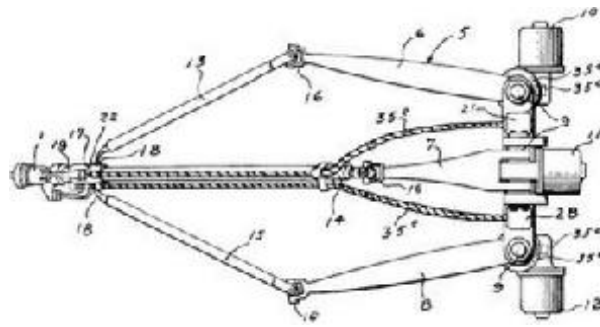
Figure 1.2: Parallel structure proposed by Pollard (from US Patent No. 2213108).

1.1 Parallel Mechanisms

1.1.1 1.1.1 Development of Parallel Mechanisms

The first theoretical works on mechanical parallel structures appeared a long time ago, even before the notion of robot. It can be said that the first parallel mechanism (shown in Fig. 1.1) was patented in 1931 (US Patent No. 1789680) and was designed by James E. Gwinnett (Gwinnett 1931). In 1940 Willard Pollard presented a robot with 5 degrees of freedom dedicated to painting tasks (US Patent No. 2213108). The robot was composed of three legs of two links each. The three actuators of the base drive the position of the tool (shown in Fig. 1.2).

More significant parallel mechanisms have been achieved since then. In 1947, Gough established the basic principles of a mechanism with a closed-loop kinematic structure (shown in Fig. 1.3), that allows the positioning and the orientation of a moving platform so as to test tire wear and tear [1, 2]. In 1965, Stewart described a movement platform with 6 degrees of freedom (shown in Fig. 1.4) designed to be used as a flight simulator. Contrary to the general belief, the Stewart mechanism is different from the one previously presented by Gough.
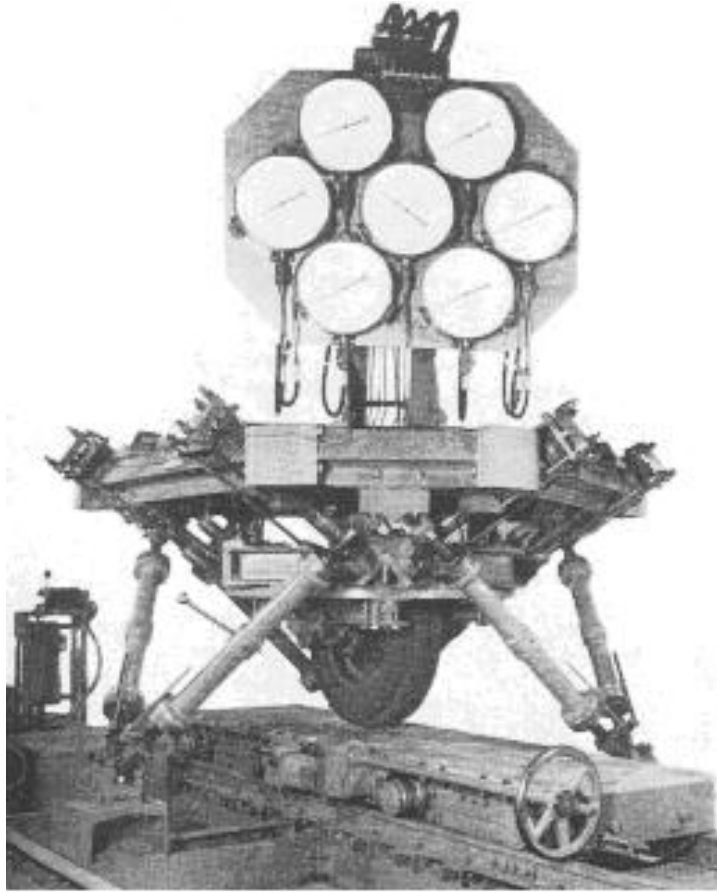
Figure 1.3: Gough platform (from [2]).

The work presented by Stewart has had a great influence in the academic world, and it is considered one of the first works of analysis of parallel structures [3].

Over the last three decades, parallel mechanisms evolved from rather marginal machines to widely used mechanical architectures. Current applications of parallel mechanisms include motion simulators, industrial robots, nano-manipulators and micro-manipulators, to name only a few.

1.1.2   1.1.2 Definition of a Parallel Mechanism

The definition of a general parallel manipulator is a closed-loop kinematic chain mechanism whose end-effector is linked to the base by several independent kinematic chains [4]. This type of mechanism is interesting for the following reasons:
– a minimum of two chains allow us to distribute the load on the chains;
– the number of sensors necessary for the closed-loop control of the mechanism is minimal;
– when the actuators are locked, the manipulator remains in its pose. This is an important
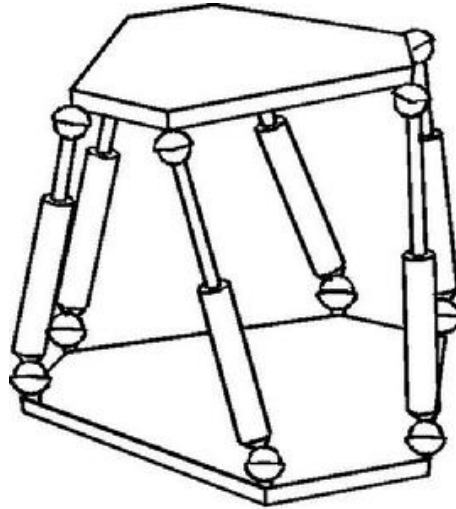
Figure 1.4: Stewart platform.

safety aspect for certain applications, such as medical robotics.
Correspondingly, parallel robots can be defined as:

A parallel robot is made up of an end-effector with n degrees of freedom, and of a fixed base, linked together by at least two independent kinematic chains. Actuation takes place through n simple actuators [4].

1.1.3   1.1.3 Characteristics and Applications

In comparison with serial mechanisms, properly designed parallel mechanisms generally have higher stiffness and higher accuracy, although their workspace is usually smaller (except for cable-driven parallel mechanisms). The variety of applications in which parallel mechanisms are used is constantly expanding.

One of the most successful parallel robot designs is Delta parallel robot. In the early 80's, Professor Reymond Clavel came up with the idea of using parallelograms to build a parallel robot with three translational and one rotational degree of freedom (schematically shown in Fig. 1.5). During the last decades, Delta robots have been used for packaging, aiding surgery and industry product (Fig. 1.6) [5].

Also, there are many other applications for different parallel mechanisms. There are parallel mechanisms used for camera orienting devices, haptic devices [6] and alignment devices. The agile eye [7, 8](Fig. 1.7) developed in the robotics laboratory of Laval University is based on a spherical 3-DOF parallel manipulator. It is capable of an orientation workspace larger than that of the human eye and it can be used as a high performance camera-orienting device. The haptic device SHaDe [9] which was also developed based on the spherical parallel mechanism is
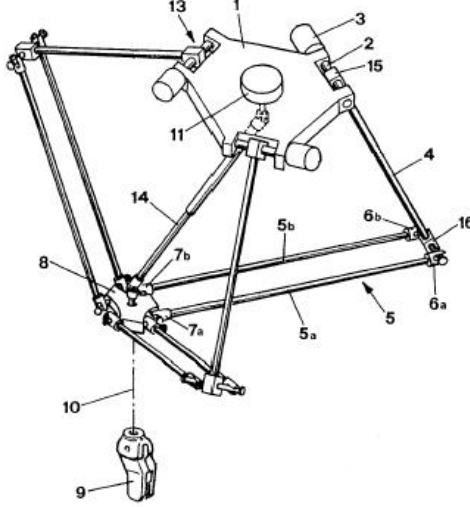
Figure 1.5: Schematic of the Delta robot (from US patent No. 4976582).

shown in Fig. 1.8. The general spherical kinematics lead to an optimal design, well-conditioned and without singularities in a large workspace. The two figure haptic device MasterFinger-2 [10] (Fig. 1.9) can be used for capturing one massage technique and one joint manipulation technique, and also for simulating this manipulation technique that can be used in both assessment and treatment of the hand. The PreXYT [11, 12] (Fig. 1.10) is both partially decoupled, rigid in all directions, and having a relatively large workspace, and proposes a geometric procedure for the kinematic calibration of the robot. It is one of the best candidates for alignment.

In order to meet the needs for the development of nanotechnology and microsystem or micro-electromechanical systems, nano-manipulators and micro-manipulators were developed based on parallel mechanisms. The finger module mechanism for micromanipulation is proposed in [13, 14]. The 3DOF parallel mechanisms (Fig. 1.11) can succeed in performing basic micro manipulations, including the grasp and release. And a planar three-degree-of-freedom parallel-type micropositioning mechanism, schematically shown in Fig. 1.12, is designed with the intention of accurate flexure hinge modeling [15], the design has mobility six and exhibits good position accuracy. Li and Xu proposed a totally decoupled flexure-based XY parallel micromanipulator and a nearly decoupled XYZ translational compliant parallel micromanipu-lator in [16–18] as shown in Fig. 1.13. In [19], many XYZ micromanipulators (Fig. 1.14) have been fabricated and tested successfully using two surface micromachining processes and found to achieve out-of-plane displacement with three linear inputs while maintaining a horizontal position of the platform throughout its motion. Culpepper [20] proposed a low-cost nano-manipulator which uses a six-axis compliant mechanism which is driven by electromagnetic actuators (Fig. 1.15(a)) and a pure spatial translational nanomanipulator is also introduced in [21, 22].
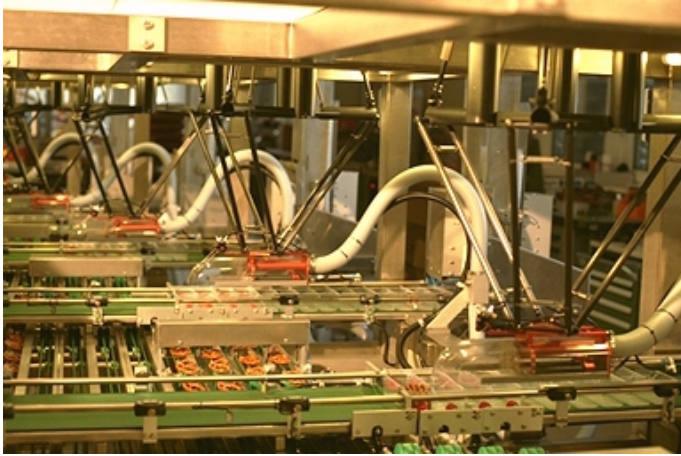
(a)

(b)

(c)

Figure 1.6: Applications of Delta mechanism: (a) Demaurex's Line-Placer installation for the packaging of pretzels in an industrial bakery (courtesy of Demaurex), (b) SurgiScope in action at the Surgical Robotics Lab, Humboldt-University at Berlin (courtesy of Prof. Dr. Tim C. Lueth), (c) Hitachi Seiki's Delta robots for pick-and-place and drilling (courtesy of Hitachi Seiki).
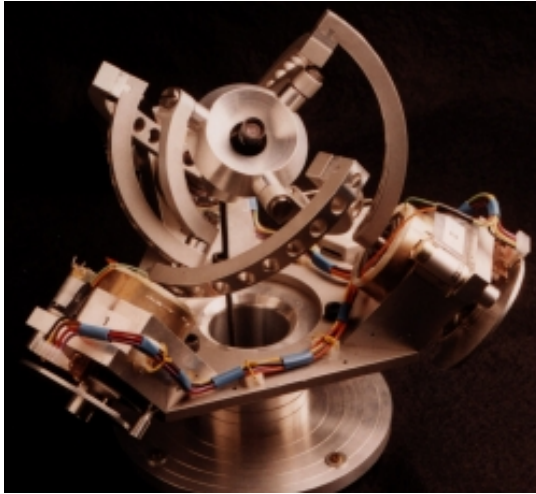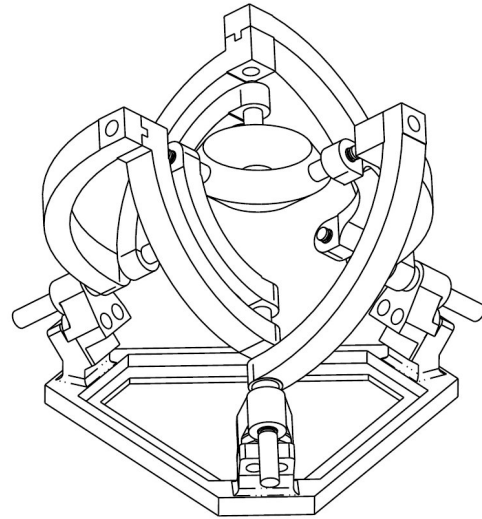
(a) Prototype   (b) CAD model

Figure 1.7: The agile eye (from [8]).
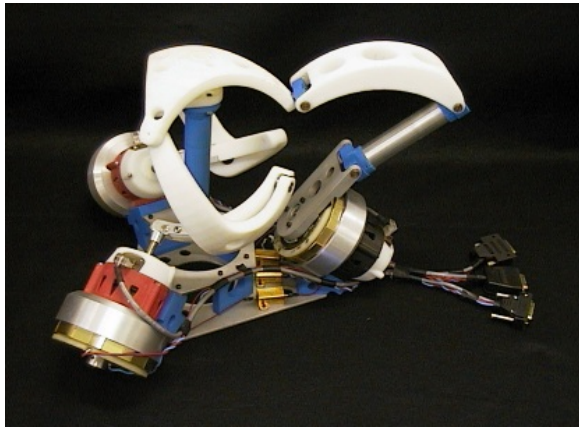
(a) Prototype of SHaDe   (b) CAD model of SHaDe
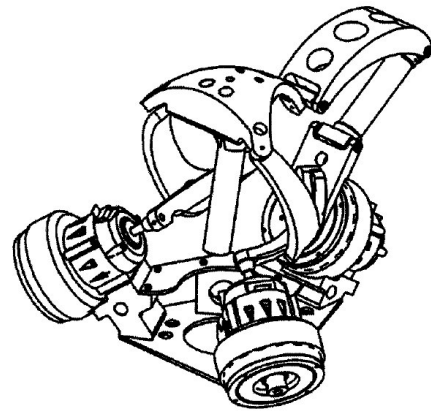
Figure 1.8: The 3-DOF spherical haptic device, SHaDe (from [9]).
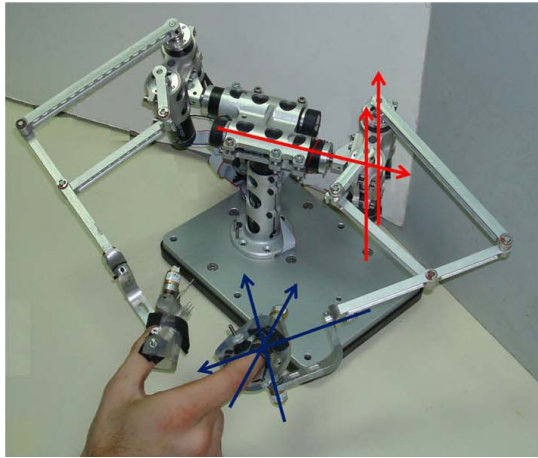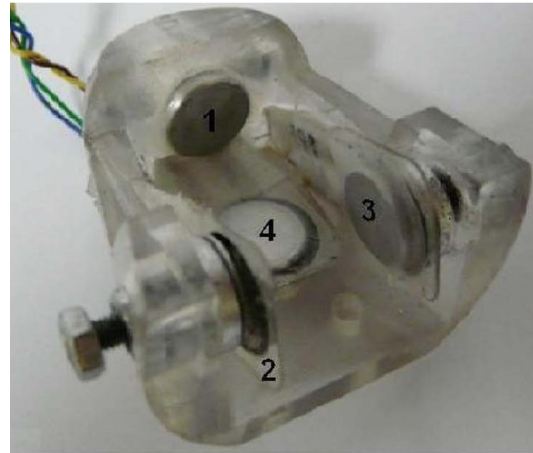
(a)   (b)

Figure 1.9: MasterFinger-2: (a) Two-figure haptic device, (b) User inserts the index or thunb in the timble (from [10]).
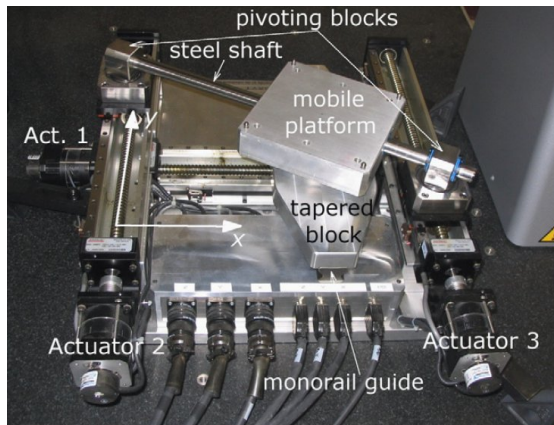
(a) Experimental setup   (b) Schematic diagram
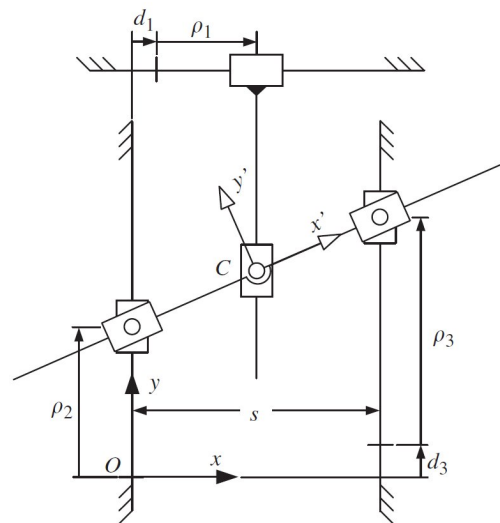
Figure 1.10: PreXYT: a planar 3-DOF parallel robot (from [12]).

Figure 1.11: Translational 3-DOF micro-parallel mechanisms (from [13]).
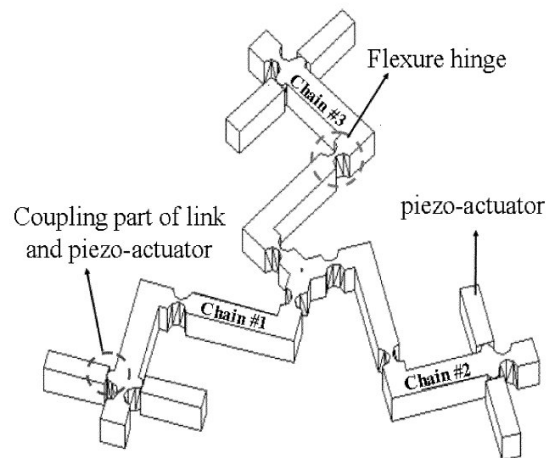
Figure 1.12: Schematic of a 3-DOF microparallel manipulator (from [15]).

1.2 Force Capabilities Analysis for Parallel Mechanisms

The analysis for the relations existing between the articular forces or torques of the robot and the wrench (constituted of the force and the torque) that is applied on the end-effector is called static analysis. The wrench that may be applied on the platform when the articular forces are bounded and the extrema of the articular forces when the wrench applied on the robot is bounded should be analyzed. This is particularly important in the context of the development of human-friendly robots in which the external forces should be limited mechanically, for safety reasons.
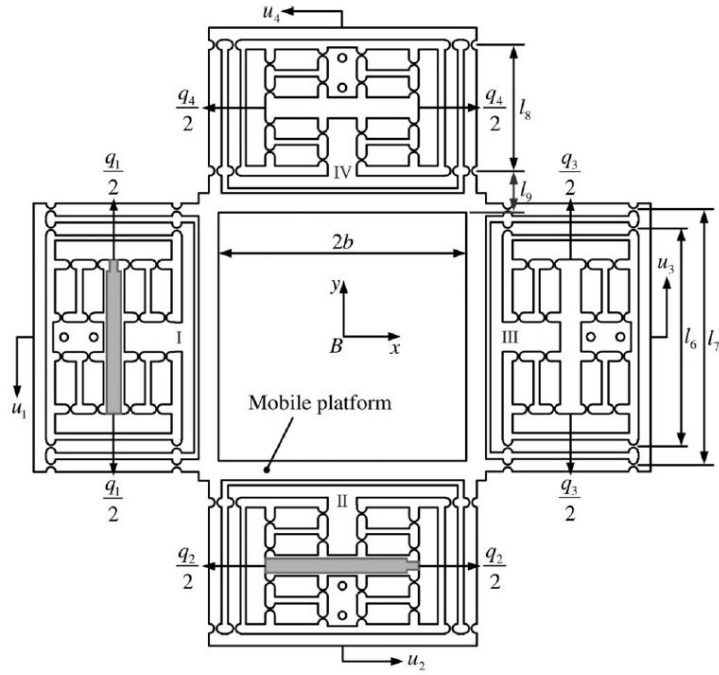
(a) Symmetric XY TDPS with displacement amplifier
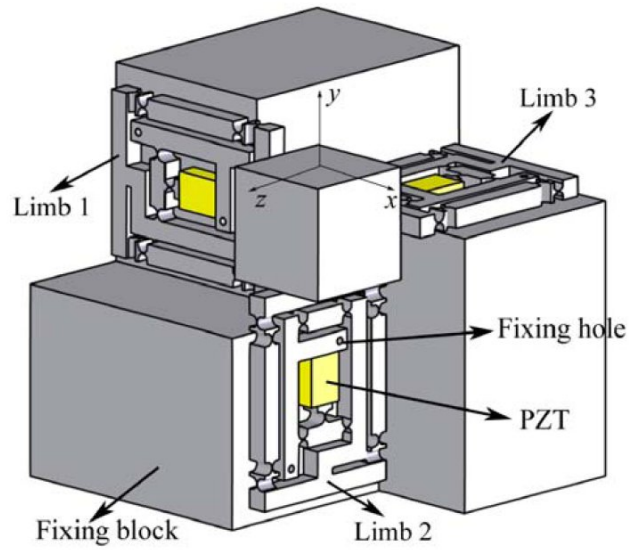
(b) CAD model of the compliant parallel mechanism

Figure 1.13: Two decoupled micromanipulators (from [16, 17]).
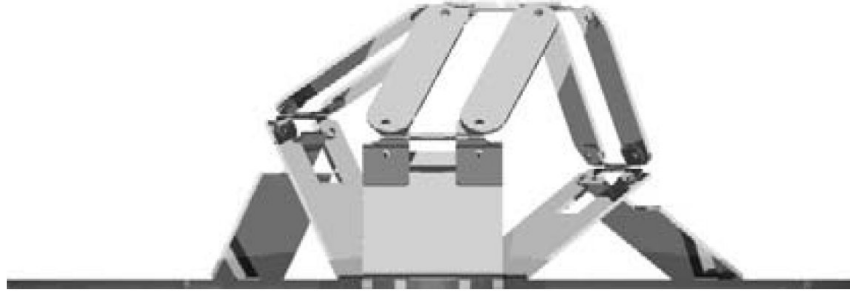
(a) A rendering of the XYZ micromanipulator in a raised position
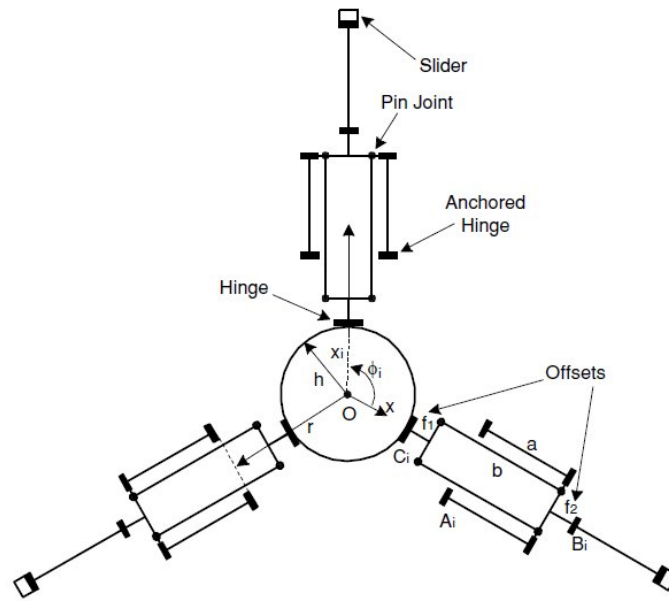
(b) Schematic of top view for offset three degree of freedom XYZ micromanipulator

Figure 1.14: An XYZ micromanipulator with three translational degrees of freedom (from [19]).

1.2.1   1.2.1 Relations Between Generalized and Articular Forces/Torques

The fundamental relation between the articular and the end-effector forces/torques, which is valid for serial manipulators as well as for parallel manipulations, is the following:

$$\boldsymbol{\tau} = \mathbf{J}^T \mathbf{F}$$

where $\boldsymbol{\tau}$ is the vector of the articular forces, $\mathbf{F}$ is the vector of the generalized end-effector or Cartesian forces and $\mathbf{J}$ is the kinematic Jacobian matrix. From this relation we get

$$\mathbf{F} = \mathbf{J}^{-T} \boldsymbol{\tau}$$

Being given the pose of the moving platform and the articular forces, we may calculate the
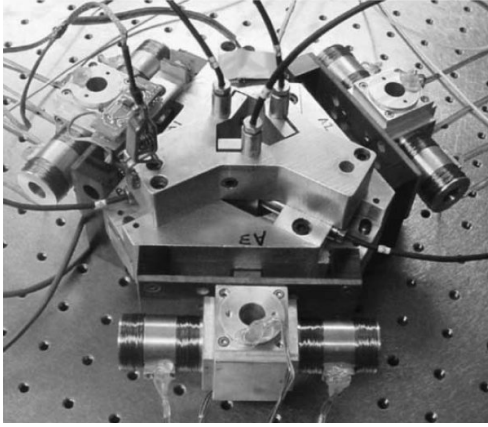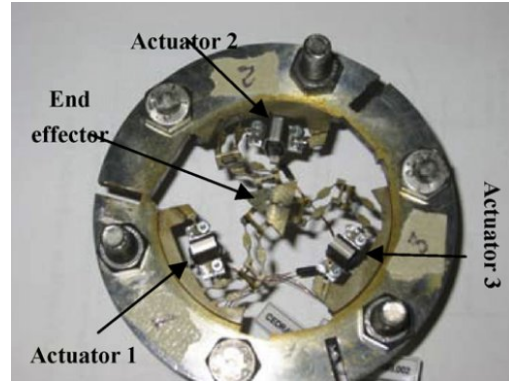
Figure 1.15: Two nano-manipulators based on parallel mechanisms (from [20, 21]).

inverse kinematic Jacobian matrix, therefore allowing us to determine the wrench that acts on the moving platform.

When designing a parallel robot, it is quite common to know the wrench that will be applied on the moving platform. It will therefore be useful to calculate the extremal values of the articular forces in order to choose the linear actuators and passive joints. On the other hand we may have limited possibilities for the actuators and passive joints, which determine the maximal value of the articular forces, and may want to calculate what will be the corresponding maximal Cartesian forces.

The simple relation existing between the Cartesian forces and the articular forces enticed numerous researchers to use parallel structures as force sensors. For example, a general robot with segments that are submitted almost only to traction-compression stresses will require only a force cell in each link to get the measurement of the articular forces. Then, we may calculate the Cartesian forces acting on the moving platform with the help of the inverse Jacobian matrix. This principle was suggested as early as 1979 by Jones [23], and later by Berthomieu [24], and is now widely used.

The stiffness of a manipulator has many consequences for its control since it conditions its bandwidth. For serial manipulators, the bandwidth is low, only reaching a few Hz at best. The stiffness of a parallel robot may be evaluated by using an elastic model for the variations of the articular variables as functions of the forces that are applied on the end-effector. In this model the change $\Delta\Theta$ in the articular variable Θ when an articular force $\boldsymbol{\tau}$ is applied at the joints is

$$\Delta\boldsymbol{\tau} = \mathbf{K}\Delta\Theta \tag{1.1}$$

where $\mathbf{K}$ is the diagonal elastic stiffness matrix of the joints. However, we have

$$\Delta\Theta = \mathbf{J}^{-1}\Delta\mathbf{X}, \tag{1.2}$$

where $\Delta \mathbf{X}$ is the small Cartesian displacement corresponding to $\Delta \Theta$. Also, from the above, one has

$$\Delta \mathbf{F} = \mathbf{J}^{-T} \Delta \boldsymbol{\tau}, \tag{1.3}$$

Substituting Eqn. (1.1) and Eqn. (1.2) into Eqn. (1.3) leads to

$$\Delta \mathbf{F} = \mathbf{J}^{-T} \mathbf{K} \mathbf{J}^{-1} \Delta \mathbf{X}. \tag{1.4}$$

The Cartesian stiffness matrix $\mathbf{K}_c$ and the Cartesian compliance matrix $\mathbf{C}_c$ are therefore

$$\mathbf{K}_c = \mathbf{J}^{-T} \mathbf{K} \mathbf{J}^{-1}, \qquad \mathbf{C}_c = \mathbf{J} \mathbf{K}^{-1} \mathbf{J}^T. \tag{1.5}$$

1.2.2   1.2.2 Literature Review on the Static Force Capabilities Analysis

The force or the wrench capabilities analysis are essential for the design and performance evaluation of parallel manipulators. For a given pose, the end-effector is required to move with a desired force and to sustain a specified wrench. Thus, the information of the joint velocities and joint torques that will produce such conditions could be investigated. These studies are referred to as the inverse velocity and static force problems. An extended problem can be formulated as the analysis of the maximum force or wrench that the end-effector can apply in the force or wrench spaces.

A methodology of using scaling factors to determine the force capabilities of non-redundantly and redundantly-actuated parallel manipulators is presented in [25]. The optimization-based solution generated larger maximum applicable force magnitudes for redundantly-actuated parallel manipulator in comparison to the force magnitudes provided by the pseudo-inverse solution. Using this method, the force-moment capabilities of redundantly-actuated planar parallel manipulator architectures are investigated in [26]. One approach using screw theory for a 3-RPS parallel mechanism is proposed in [27]. It is able to markedly reduce the number of unknowns and even make the number of simultaneous equations to solve not more than six each time, which may be called force decoupling. With this approach, first the main-pair reactions need to be solved, then, the active forces and constraint reactions of all other kinematic pairs can be simultaneously obtained by analyzing the equilibrium of each body one by one. The static force capabilities of the proposed 2S$\underline{\text{P}}$S+$\underline{\text{P}}$RR$\underline{\text{P}}$R parallel manipulator with 3-leg 5-DOF is analyzed in [28]. The R, P, S are used to denote a revolute joint, a prismatic joint and a spherical joint. And the underline means that the joint is an actuated joint. The wrench capabilities of redundantly actuated parallel manipulators are studied in [29–31]. The wrench polytope concept is presented and wrench performance indices are introduced for planar parallel manipulators in [29]. The concept of wrench capabilities is extended to redundant manipulators and the wrench workspace of different planar parallel manipulators is analyzed in [30]. Wrench capabilities represent the maximum forces and moments that can be applied

or sustained by the manipulator. In [29, 30], the wrench capabilities of planar parallel manipulators are determined by a linear mapping of the actuator output capabilities from the joint space to the task space. The analysis is based upon properly adjusting the actuator outputs to their extreme capabilities. The linear mapping results in a wrench polytope. It is shown that for non-redundant planar parallel manipulators, one actuator output capability constrains the maximum wrench that can be applied with a plane in the wrench space yielding a facet of the polytope. Two methods, namely, a numerical, optimization-based scaling factor method and an analytical method, have been proposed for determining the wrench capabilities of redundant actuated planar parallel manipulators. In [31], the methods are extended to redundant 6-DOF spatial manipulators. The results show that the analytical method is more efficient in determining maximum wrench capabilities than the scaling factor method.

In order to have an overall insight about the force capabilities of the mechanisms, the stiffness and the natural frequencies of the manipulators can be investigated [32]. Many different methodologies [33, 34] have been used to obtain the stiffness matrix which relates an applied external wrench to the displacements it produces:

– Jacobian matrix-based methods — [35] analyzes the stiffness of the parallel mechanisms considering only the stiffness of the actuators, while passive joints and links are assumed to be rigid. The Jacobian matrix is used to calculate a stiffness matrix and the analysis is carried out for the entire workspace. In [36, 37], this Jacobian-based method has been extended, the stiffness of the actuators and the links are both taken into account.

– Matrix product method —The stiffness matrix can be produced with several matrices. In [38, 39], a formulation is proposed as a combination of three characteristic matrices so that both numerical and experimental evaluations can identify the entries of the stiffness matrix of a given parallel manipulator.

– Structural or finite element method —In [40, 41], structural matrices of the components are built and assembled including joint stiffness, while in [42], a finite element software package is used to model the links of a decoupled manipulator and stiffness is calculated using the relationship between the tension and deformation.

– Analytical-experimental method —In [43], an analytical procedure combined with finite elements is completed with experimental results to calculate the static stiffness of a 3T1R manipulator and in [38], a tracking system is designed to measure experimental displacements.

1.3 Dynamic Capabilities Analysis for Parallel Mechanisms

1.3.1 1.3.1 Introduction of Dynamics

Dynamics plays an important role in the control of parallel robots for some applications like flight simulators or pick-and-place operations involving fast manipulators. It is therefore necessary to establish the dynamics relations for closed-loop mechanisms before we can establish a control scheme for fast manipulators.

A classical method for establishing the dynamics equations for closed-loop mechanism was suggested in various forms in [44–46]. For a mechanism containing N rigid bodies and L links, the method consists in calculating the dynamics equations of a $t$ree mechanism that is obtained from the original mechanism by opening the loops at certain passive links so that the obtained tree mechanism has as many independent loops $B = L - N$ as the original mechanism.

Simplifying assumptions can also be used in order to obtain approximate dynamic models as it will be done in this thesis.

1.3.2 1.3.2 Literature Review on the Dynamic Capabilities Analysis

Ordinarily, there are two problems of dynamic analysis of parallel mechanisms, namely the inverse and forward dynamics. The former solves the actuation forces of actuators once the trajectories are planned, while the latter deals with the output motion of the parallel mechanisms when the actuation forces are given. The inverse dynamics can be used for the design of a dynamics controller, whereas the forward dynamics can be adopted for dynamic simulation of the parallel mechanisms which can also be conducted by resorting to effective dynamic software packages such as ADAMS, DADS, and RecurDyn, etc. .

As far as the approaches to generate the parallel mechanisms' dynamic model are concerned, most traditional methods are used, such as Newton-Euler formulation, Lagrangian formulation, virtual work principle, and some other methods. Many research works about the dynamic analysis of parallel mechanisms are described in the following.

In [50], the dynamic model and the virtual reality simulation for two 3DOF medical parallel robots are presented. A closed form dynamic model has been set up in the rigid link hypothesis, and an evaluation model from the Matlab/SimMechanics environment was used for the simulation. The dynamic performance comparison of the 8PSS redundant parallel manipulator and the 6PSS parallel manipulator was presented in [49]. The dynamic models of the two parallel manipulators have been formulated by means of the principle of virtual work and the concept of link Jacobian matrices. The research shows that their kinematics characteristics

are equivalent while the dynamic performance of the 8PSS redundant parallel manipulator is better than that of the 6PSS parallel manipulator. In [48], the dynamic model of spherical 2-DOF parallel manipulator with actuation redundancy was established by Lagrangian method, and driving moment was optimized by force optimization method and energy consumption optimization method. In [47], the dynamic model of the proposed asymmetric mechanism, which was successfully obtained for both the lumped mass and distributed mass assumptions. The simulation results showed that although the mechanism has a parallel architecture its actuators influences are quite decoupled, according to its particular asymmetric configuration. In [54], a double parallel manipulator has been designed by combining two parallel mechanisms with a central axis for enlarging workspace and avoiding singularities. The motion of the device is decoupled and constrained by the central axis. With virtual coefficient, a dynamic model is developed for the parallel mechanism possessing one passive and n-active link trains to compute the wrenches acting at the passive joints as well as the active ones including gravity and inertia loads.

In [52], dynamic finite element analysis of a fully parallel planar platform with flexible links has been performed. The method [53] used leads to a set of linear ordinary differential equations of motion. The effect of structure parameters on the dynamic characteristics of a planar PRRRP parallel manipulator is studied in [55], the sensitivity model of the dynamic characteristic to critical structure parameters is proposed. The thickness of column and leg, the radial stiffness of bearing, and the lumped mass on the end-effector are determined based on the natural frequency and sensitivity index. In [56], the dynamic performance of two 3-DOF parallel manipulators, the HALF [57] and the HALF* [58], is compared and a new optimization method for the counterweight masses is proposed for the development of a new hybrid machine tool. The dynamic models of the manipulators are derived via the Lagrangian formulation and the translational and rotational quantities are separated due to the unit inhomogeneity. The proposed dynamic capability indices and counterweight optimization method provide insights into the dynamic models and are very useful to improve the dynamic characteristics, and they can be used for other manipulators, especially for those with both translation and rotation. In [59], using the Lagrange-D'Alembert formulation, a simple and straightforward approach is used to develop the dynamic models of closed-chain manipulators with normal or redundant actuation. It showed the structural properties of the dynamic equations needed for applying the vast control literature developed for serial manipulators. The dynamic modeling and robust control for a three-prismatic-revolute-cylindrical(3-PRC) parallel kinematic machine with translational motion have been investigated in [60]. By introducing a mass distribution factor, the simplified dynamic equations have been derived via the virtual work principle and validated on a virtual prototype with the ADAMS software package.

1.4 Overview of the thesis

This thesis has five chapters. In Chapter 1, there are some introductions about parallel mechanisms and review of some current research about parallel mechanisms. The research for this program are mainly in two part. The first part is about the force capabilities analysis of 2-DOF parallel mechanisms which are equipped with torque limiters and force limiters, it is described in Chapter 2 and Chapter 3. Chapter 4 considers the dynamic capabilities of the tripteron and quadrupteron decoupled parallel manipulators. Then, the conclusions are stated in Chapter 5. More details are given in the following.

In Chapter 1, the development of parallel mechanisms is introduced at first, then the definition and characteristics the parallel mechanisms are given. The applications of parallel mechanisms are mentioned. The force capabilities analysis and dynamic analysis for parallel mechanisms are stated briefly. A literature review on the force capabilities analysis and dynamic analysis for parallel mechanisms is also given in this chapter.

In Chapter 2, the force capabilities of the 2DOF parallel mechanisms equipped with torque limiters are analyzed. First, the structure of the parallel mechanisms is described and the kinematic equations are given. Then, the Jacobian matrices and the static force equation are derived. Although the equations derived are conceptually simple, their component form is rather cumbersome, which makes it difficult to gain useful insight. In order to make the analysis more intuitive, two special designs of the robot are also studied more specifically and the corresponding equations are developed. The force characteristics are analyzed based on the force equations and a performance index referred to as the force effectiveness is proposed. Finally, numerical simulation results for the different special 2DOF parallel mechanisms are presented.

In Chapter 3, two force limiters take the place of the torque limiters of proximal links of the mechanism described in Chapter 2. The two force limiters are mounted on the proximal links on one mechanism, and the force limiters are on the distal links on another mechanism. Two Passive torque limiters are mounted at the actuators of the robot. The structure of the mechanisms are described at first. Then, the Jacobian matrices and the static force equations are derived. The force characteristics are analyzed based on the force equations and a performance index referred to as the force effectiveness is proposed. Finally, numerical simulation results are presented.

In Chapter 4, the external force range of the end-effector for the tripteron and quadrupteron manipulators are found for the given actuating force limit. First, the architecture and kinematics of the tripteron and the quadrupteron are briefly recalled. Then, an approximate dynamic model is obtained based on the Newton-Euler approach, Lagrange equations and the compact dynamic models obtained in [93]. The feasible external force of the end-effector for

the tripteron and quadrupteron manipulators can be found based on these dynamic models. At the end, certain numerical simulation results are given.

Finally, a summary of the results obtained in this thesis and some discussion as well as directions on future research work are given in Chapter 5.

Chapter 2

Force Capabilities of 2-DOF Parallel Mechanisms Equipped with Torque Limiters

In this chapter, the design of intrinsically safe planar 2-DOF parallel mechanisms is addressed. Passive torque limiters are mounted at four points of the structure of the robot. The design problem then consists in finding geometric parameters and maximum allowable torques at the limiters that ensure a safe and effective behaviour of the robot throughout its workspace. The structure of the two variants of the mechanism are described at first. Then, the Jacobian matrices and the static force equation are derived. The force characteristics are analyzed based on the force equations and a performance index referred to as the force effectiveness is proposed. Finally, numerical simulation results are presented.

2.1 Introduction

Collaborating with humans is becoming a major trend in both industrial and non-industrial (such as service or medical) robotics [61–63]. Human safety is one of the most important aspects to be considered for robots working in a human environment.

Different strategies can be used to build safe robots. One way is to develop control algorithms that use sensors to anticipate and avoid potentially harmful contacts. In [64], a system using many different sensors for automatically locating and tracking a human in the vicinity of a robot is described. Another approach consists in developing a flexible robot skin for safe physical human-robot interaction such as the concept developed in [65]. However, active control has several disadvantages, which includes higher cost and lower reliability of the control system and limited absorption capability of the initial collision force due to the response time of a control system [66].

Safe robots can also be realized by detecting a collision with the monitoring of joint torques and by maintaining the contact forces under a certain level. Safe robot arms can be achieved by either a passive or active compliance system. Several types of compliant joints and flexible links of manipulators have been proposed for safety, which can guarantee that the force within the joint cannot exceed a given reference. One approach consists in using springs to realize compliance [67–72]. Alternatively, a double actuator unit composed of two actuators and a planetary gear train is proposed in [73]. In this concept, the torque exerted on the joint can be estimated without the use of a torque or force sensor. A series clutch actuator based on magnetorheological fluid is proposed in [74]. It allows a fast electrical change of the impedance while maintaining good force tracking. However, in all these concepts, the safety features remain dependent on the controller of the robot. Also, the performance and the safety level are configuration dependent and require on-line adaptation [75].

In this context, there is a need for intrinsically mechanically safe robots [76,77] whose safety features are independent from the controller. In [78], a 2-DOF Cartesian Force Limiting Device (CFLD) that can be installed between a suspended robot and its end effector is presented. Such a device is completely passive and does not require controller actions. Similarly, a 3-DOF CFLD using the Delta architecture which is sensitive to collisions occuring in any direction is presented in [79].

In this chapter, the design of intrinsically safe planar 2-DOF parallel mechanisms is addressed. Passive torque limiters are mounted at four points of the structure of the robot. The design problem then consists in finding geometric parameters and maximum allowable torques at the limiters that ensure a safe and effective behaviour of the robot throughout its workspace. The structure of the two variants of the mechanism are described at first. Then, the Jacobian matrices and the static force equations are derived. The force characteristics are analyzed

| (a) symmetric | (b) non-symmetric |
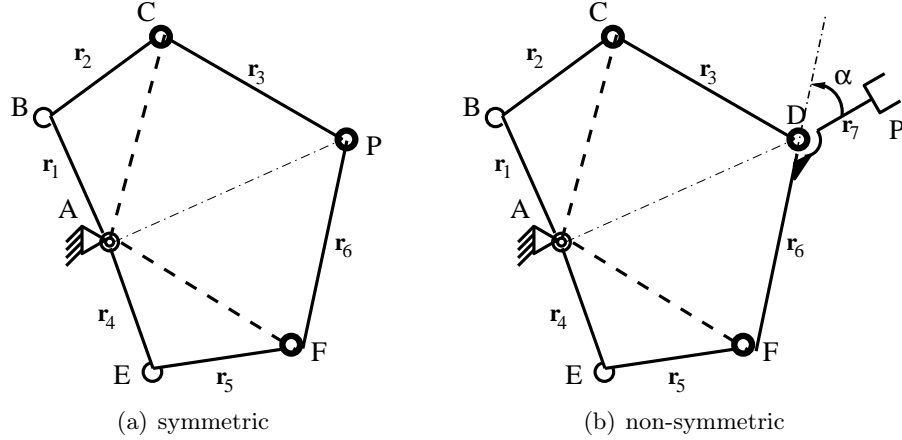
Figure 2.1: The two variants of the planar parallel mechanism.

based on the force equations and a performance index referred to as the force effectiveness is proposed. Finally, numerical simulation results are presented.

2.2   Description of the Mechanisms

The structure of each of the two planar parallel mechanisms analyzed in this chapter is shown in Fig. 2.1. The only difference between the two mechanisms is that the non-symmetric mechanism has a link DP rigidly attached on link DF where the constant angle between DP and FD is defined as α, as shown in the figure. In both mechanisms, there are two actuators located at joint A that independently drive links ABC and AEF respectively. Links ABC and AEF are normally rigid. However, there are two torque limiters placed at points B and E. When the torque at these joints exceeds a prescribed maximum value, the link will dislocate and a message will be sent to the controller (collision or excessive force). Similarly, there are also two torque limiters in series with the actuators at joint A. Finally, joints C, F and P (or D for the non-symmetric mechanism) are free joints which are not actuated and which do not have torque limiters. Globally, the mechanism has two degrees of freedom, two fixed actuators located at A and four torque limiters (two limiters located at A and two others located at B and E respectively). The torque limiters can be considered as rigid joints until the prescribed maximum torque is exceeded, which corresponds to a fault situation.

In order to maximize the workspace of the robot, $ACPF$ forms a parallelogram for the symmetric mechanism while $ACDF$ is a parallelogram for the non-symmetric mechanism. Vector $\mathbf{r}_i$, $i = 1, \ldots, 7$ is defined as the vector connecting consecutive joints, as illustrated in Fig. 2.1. Also, l_i is defined as the length of vector $\mathbf{r}_i$. One then has

$$\mathbf{r}_6 = \mathbf{r}_1 + \mathbf{r}_2, \qquad \mathbf{r}_3 = \mathbf{r}_4 + \mathbf{r}_5.$$

For the symmetric mechanism, one has

$$\mathbf{r}_1 + \mathbf{r}_2 + \mathbf{r}_3 = \mathbf{p} \tag{2.1}$$

$$\mathbf{r}_4 + \mathbf{r}_5 + \mathbf{r}_6 = \mathbf{p} \tag{2.2}$$

while for the non-symmetric mechanism, one has

$$\mathbf{r}_1 + \mathbf{r}_2 + \mathbf{r}_3 + \mathbf{r}_7 = \mathbf{p} \tag{2.3}$$

$$\mathbf{r}_4 + \mathbf{r}_5 + \mathbf{r}_6 + \mathbf{r}_7 = \mathbf{p} \tag{2.4}$$

where $\mathbf{p}$ is the position vector of the end-effector point P with respect to the base (point A) of the mechanism.

2.3 Jacobian Matrices and Force Equations

2.3.1 2.3.1 General Jacobian Matrices

The objective of the force analysis is to determine the relationship between the Cartesian force capabilities at the end-effector (point P) and the joint torques at the torque limiters located at points A, B and E, in order to be able to assess the safety features of the robot. Therefore, in the analysis presented here, it is assumed that joints B and E are moveable 'actuated' joints so that the torque at these joints can then be obtained through the application of the principle of virtual work.

First, Eqn. (2.3) is solved for vector $\mathbf{r}_3$ and its magnitude is taken, leading to

$$\mathbf{r}_3^T\mathbf{r}_3 = (\mathbf{p} - \mathbf{r}_7 - \mathbf{r}_1 - \mathbf{r}_2)^T(\mathbf{p} - \mathbf{r}_7 - \mathbf{r}_1 - \mathbf{r}_2) = l_3^2. \tag{2.5}$$

Derivating Eqn. (2.5) with respect to time and collecting terms, one has

$$\mathbf{r}_3^T\dot{\mathbf{p}} = (\mathbf{p} - \mathbf{r}_2 - \mathbf{r}_7)^T\dot{\mathbf{r}}_1 + (\mathbf{p} - \mathbf{r}_1 - \mathbf{r}_7)^T\dot{\mathbf{r}}_2 + (\mathbf{p} - \mathbf{r}_1 - \mathbf{r}_2)^T\dot{\mathbf{r}}_7,$$

where $\dot{\mathbf{r}}_1 = \dot{\theta}_1\mathbf{E}\mathbf{r}_1$, $\dot{\mathbf{r}}_2 = (\dot{\theta}_1 + \dot{\theta}_2)\mathbf{E}\mathbf{r}_2$, $\dot{\mathbf{r}}_4 = \dot{\theta}_4\mathbf{E}\mathbf{r}_4$, $\dot{\mathbf{r}}_5 = (\dot{\theta}_4 + \dot{\theta}_5)\mathbf{E}\mathbf{r}_5$, and θ_i, $i = 1, 2, 4, 5$, are the joint coordinates of the corresponding joints and

$$\mathbf{E} = \begin{bmatrix} 0 & -1 \\ 1 & 0 \end{bmatrix}.$$

A similar equation can be obtained based on Eqn. (2.4).

Since AC is parallel to FD in the non-symmetric mechanism, then the vector for link DP is $\mathbf{r}_7 = l_7[\cos\theta_7, \sin\theta_7]^T$ where

$$\theta_7 = \arctan\left[\frac{l_1\sin\theta_1 + l_2\sin(\theta_1 + \theta_2)}{l_1\cos\theta_1 + l_2\cos(\theta_1 + \theta_2)}\right] - \alpha.$$

Therefore, the velocity of link 7 is readily computed as a fonction of the joint velocity of joints 1 and 2, namely

$$\dot{\mathbf{r}}_7 = \frac{(\dot{\mathbf{r}}_1 + \dot{\mathbf{r}}_2)^T \mathbf{E}(\mathbf{r}_1 + \mathbf{r}_2)}{(\mathbf{r}_1 + \mathbf{r}_2)^T(\mathbf{r}_1 + \mathbf{r}_2)} \mathbf{Er}_7 = \dot{\theta}_1 \mathbf{Er}_7 + \frac{\dot{\theta}_2 \mathbf{r}_2^T(\mathbf{r}_1 + \mathbf{r}_2)}{(\mathbf{r}_1 + \mathbf{r}_2)^T(\mathbf{r}_1 + \mathbf{r}_2)} \mathbf{Er}_7.$$

Based on the above derivations, the Jacobian matrices can then be constructed. The matrices are first defined as

$$\mathbf{A}\dot{\mathbf{p}} = \mathbf{B}\dot{\boldsymbol{\theta}} \tag{2.6}$$

where $\boldsymbol{\theta} = [\theta_1, \ \theta_2, \ \theta_4, \ \theta_5]^T$ and where $\mathbf{A}$ is a 2×2 matrix while $\mathbf{B}$ is a 2×4 matrix. The Jacobian matrices are written as

$$\mathbf{A} = \begin{bmatrix} \mathbf{r}_3^T \\ \mathbf{r}_6^T \end{bmatrix}, \qquad \mathbf{B} = \begin{bmatrix} \mathbf{b}_1 & \mathbf{b}_2 & \mathbf{b}_3 & \mathbf{b}_4 \end{bmatrix},$$

with

$$\mathbf{b}_1 = \begin{bmatrix} (\mathbf{p} - \mathbf{r}_2 - \mathbf{r}_7)^T \mathbf{Er}_1 + (\mathbf{p} - \mathbf{r}_1 - \mathbf{r}_7)^T \mathbf{Er}_2 + \mathbf{z} \\ (\mathbf{p} - \mathbf{r}_4 - \mathbf{r}_5)^T \mathbf{Er}_7 \end{bmatrix},$$

$$\mathbf{b}_2 = \begin{bmatrix} (\mathbf{p} - \mathbf{r}_1 - \mathbf{r}_7)^T \mathbf{Er}_2 + \frac{\mathbf{r}_2^T(\mathbf{r}_1 + \mathbf{r}_2)\mathbf{z}}{(\mathbf{r}_1 + \mathbf{r}_2)^T(\mathbf{r}_1 + \mathbf{r}_2)} \\ \frac{\mathbf{r}_2^T(\mathbf{r}_1 + \mathbf{r}_2)}{(\mathbf{r}_1 + \mathbf{r}_2)^T(\mathbf{r}_1 + \mathbf{r}_2)}(\mathbf{p} - \mathbf{r}_4 - \mathbf{r}_5)^T \mathbf{Er}_7 \end{bmatrix},$$

$$\mathbf{b}_3 = \begin{bmatrix} 0 \\ (\mathbf{p} - \mathbf{r}_5 - \mathbf{r}_7)^T \mathbf{Er}_4 + (\mathbf{p} - \mathbf{r}_4 - \mathbf{r}_7)^T \mathbf{Er}_5 \end{bmatrix},$$

$$\mathbf{b}_4 = \begin{bmatrix} 0 \\ (\mathbf{p} - \mathbf{r}_4 - \mathbf{r}_7)^T \mathbf{Er}_5 \end{bmatrix},$$

where

$$\mathbf{z} = (\mathbf{p} - \mathbf{r}_1 - \mathbf{r}_2)^T \mathbf{Er}_7. \tag{2.7}$$

The Jacobian matrix $\mathbf{B}$ of the symmetric mechanism is readily obtained by setting $\mathbf{r}_7$ to zero in the above equations.

The principle of virtual work is now applied in order to obtain the static equations. The virtual input power at the actuators is equal to the virtual output power at the end-effector, i.e.,

$$\mathbf{F}^T \dot{\mathbf{p}} = \boldsymbol{\tau}^T \dot{\boldsymbol{\theta}} \tag{2.8}$$

where $\mathbf{F} = F[\cos\phi, \sin\phi]^T$ is the external force at the end-effector and $\boldsymbol{\tau} = [\tau_1, \ \tau_2, \ \tau_3, \ \tau_4]^T$ is the generalized joint torque vector for the actuators and the torque limiters.

Based on Eqn. (2.6), the velocity of the end-effector can be expressed as

$$\dot{\mathbf{p}} = \mathbf{A}^{-1}\mathbf{B}\dot{\boldsymbol{\theta}} \tag{2.9}$$

Substituting Eqn. (2.9) into Eqn. (2.8) and noting that the equation obtained must be valid for any vector $\dot{\boldsymbol{\theta}}$, the force equation can be found as

$$\boldsymbol{\tau} = \mathbf{J}^T \mathbf{F}, \tag{2.10}$$

where $\mathbf{J}^T = \mathbf{B}^T \mathbf{A}^{-T}$ is a 4×2 matrix that maps the Cartesian forces $\mathbf{F}$ into the joint torques $\boldsymbol{\tau}$.

Note that $\mathbf{A}^{-1}$ can be written as

$$\mathbf{A}^{-1} = \frac{1}{\mathbf{r}_3^T \mathbf{E} \mathbf{r}_6} \begin{bmatrix} \mathbf{E} \mathbf{r}_6 & -\mathbf{E} \mathbf{r}_3 \end{bmatrix} \tag{2.11}$$

hence

$$\mathbf{A}^{-T} = \frac{1}{\mathbf{r}_3^T \mathbf{E} \mathbf{r}_6} \begin{bmatrix} -\mathbf{r}_6^T \mathbf{E} \\ \mathbf{r}_3^T \mathbf{E} \end{bmatrix}. \tag{2.12}$$

2.3.2 2.3.2 Simplified Analysis and Special Cases

Referring to the architecture of the robots shown in Fig. 2.1, it can be observed that, since both actuators are located at point A, a rotation of both actuators of a same given angle does not change the force properties of the robot. Indeed, rotating the two input joints by a same angle is equivalent to rotating the base frame of the robot. Therefore, the properties of the Jacobian matrix of the robot — and hence its force capabilities — remain unchanged. As a consequence, in order to analyze the force capabilities of the mechanisms, it suffices to consider a one-dimensional workspace obtained with the following constraint: $\theta_4 = -\theta_1$. In other words, the joint connecting links 3 and 6 is moved radially from point A to the maximum extension of the robot. Moreover, the equations are further simplified by defining the x axis of the fixed frame in the radial direction along which the end-effector is moved.

Although the equations derived in the preceding section are conceptually simple, their component form is rather cumbersome, which makes it difficult to gain useful insight. In order to make the analysis more intuitive, two special designs of the robot are also studied more specifically and the corresponding equations are now developed.

2.3.2.1 Special case 1: points ABC aligned and points AEF aligned

In this case, one has $\theta_2 = \theta_5 = 0$ and it is assumed that $l_1 = l_2 = l_3 = l_4 = l$ and $l_3 = l_6 = 2l$. Therefore one can write

$$\mathbf{r}_1 = \mathbf{r}_2 = \begin{bmatrix} l\cos\theta_1 \\ l\sin\theta_1 \end{bmatrix}, \quad \mathbf{r}_3 = \begin{bmatrix} 2l\cos\theta_1 \\ -2l\sin\theta_1 \end{bmatrix},$$

$$\mathbf{r}_4 = \mathbf{r}_5 = \begin{bmatrix} l\cos\theta_1 \\ -l\sin\theta_1 \end{bmatrix}, \quad \mathbf{r}_6 = \begin{bmatrix} 2l\cos\theta_1 \\ 2l\sin\theta_1 \end{bmatrix},$$

$$\mathbf{r}_7 = \begin{bmatrix} l_7\cos(\psi - \alpha) \\ l_7\sin(\psi - \alpha) \end{bmatrix} = \begin{bmatrix} l_7\cos(\theta_1 - \alpha) \\ l_7\sin(\theta_1 - \alpha) \end{bmatrix},$$

and the Jacobian matrices simplify to

$$\mathbf{A} = \begin{bmatrix} \mathbf{r}_3^T \\ \mathbf{r}_6^T \end{bmatrix} = \begin{bmatrix} 2l\cos\theta_1 & -2l\sin\theta_1 \\ 2l\cos\theta_1 & 2l\sin\theta_1 \end{bmatrix},$$

$$\mathbf{B} = \begin{bmatrix} \mathbf{b}_1 & \mathbf{b}_2 & \mathbf{b}_3 & \mathbf{b}_4 \end{bmatrix},$$

and

$$\mathbf{b}_1 = \begin{bmatrix} -4l^2\sin 2\theta_1 - 2ll_7\sin(2\theta_1 - \alpha) \\ 2ll_7\sin\alpha \end{bmatrix},$$

$$\mathbf{b}_2 = \begin{bmatrix} -2l^2\sin 2\theta_1 - ll_7\sin(2\theta_1 - \alpha) \\ ll_7\sin\alpha \end{bmatrix},$$

$$\mathbf{b}_3 = \begin{bmatrix} 0 \\ 2l^2\sin 2\theta_1 \end{bmatrix}, \quad \mathbf{b}_4 = \begin{bmatrix} 0 \\ l^2\sin 2\theta_1 \end{bmatrix}.$$

2.3.2.2 Special case 2: points ABC and points AEF respectively form a right angle

In this case one has $\theta_2 = \frac{3\pi}{2}$ and $\theta_5 = \frac{\pi}{2}$, and it is assumed that $l_1 = l_2 = l_3 = l_4 = l$ and $l_3 = l_6 = \sqrt{2}l$. Then one has

$$\mathbf{r}_1 = \begin{bmatrix} l\cos\theta_1 \\ l\sin\theta_1 \end{bmatrix}, \quad \mathbf{r}_2 = \begin{bmatrix} l\sin\theta_1 \\ -l\cos\theta_1 \end{bmatrix}, \quad \mathbf{r}_3 = \begin{bmatrix} \sqrt{2}l\sin(\theta_1 + \frac{\pi}{4}) \\ \sqrt{2}l\cos(\theta_1 + \frac{\pi}{4}) \end{bmatrix},$$

$$\mathbf{r}_4 = \begin{bmatrix} l\cos\theta_1 \\ -l\sin\theta_1 \end{bmatrix}, \quad \mathbf{r}_5 = \begin{bmatrix} l\sin\theta_1 \\ l\cos\theta_1 \end{bmatrix}, \quad \mathbf{r}_6 = \begin{bmatrix} \sqrt{2}l\sin(\theta_1 + \frac{\pi}{4}) \\ -\sqrt{2}l\cos(\theta_1 + \frac{\pi}{4}) \end{bmatrix},$$

$$\mathbf{r}_7 = \begin{bmatrix} l_7\cos(\psi - \alpha) \\ l_7\sin(\psi - \alpha) \end{bmatrix} = \begin{bmatrix} l_7\cos(\theta_1 - \alpha - \frac{\pi}{4}) \\ l_7\sin(\theta_1 - \alpha - \frac{\pi}{4}) \end{bmatrix},$$

and the Jacobian matrices can be written as

$$\mathbf{A} = \begin{bmatrix} \mathbf{r}_3^T \\ \mathbf{r}_6^T \end{bmatrix} = \begin{bmatrix} \sqrt{2}l\sin(\theta_1 + \frac{\pi}{4}) & \sqrt{2}l\cos(\theta_1 + \frac{\pi}{4}) \\ \sqrt{2}l\sin(\theta_1 + \frac{\pi}{4}) & -\sqrt{2}l\cos(\theta_1 + \frac{\pi}{4}) \end{bmatrix},$$

$$\mathbf{B} = \begin{bmatrix} \mathbf{b}_1 & \mathbf{b}_2 & \mathbf{b}_3 & \mathbf{b}_4 \end{bmatrix},$$

and

$$\mathbf{b}_1 = \begin{bmatrix} 2l^2\cos 2\theta_1 + \sqrt{2}ll_7\cos(2\theta_1 - \alpha) \\ \sqrt{2}ll_7\sin\alpha \end{bmatrix},$$

$$\mathbf{b}_2 = \begin{bmatrix} \sqrt{2}l^2\sin(2\theta_1 + \frac{\pi}{4}) + \frac{\sqrt{2}}{2}ll_7\cos(2\theta_1 - \alpha) \\ \frac{\sqrt{2}}{2}ll_7\sin\alpha \end{bmatrix},$$

$$\mathbf{b}_3 = \begin{bmatrix} 0 \\ -2l^2\cos 2\theta_1 \end{bmatrix}, \quad \mathbf{b}_4 = \begin{bmatrix} 0 \\ -\sqrt{2}l^2\sin(2\theta_1 + \frac{\pi}{4}) \end{bmatrix}.$$

2.4   Analysis of the Force Capabilities

The analysis of the force capabilities is based on the assumption that the mechanism is working in a static or quasi-static mode. Additionally, it is assumed that the mechanism is operating in a horizontal plane and hence gravity is not considered. Assuming that the limit torque of the ith joint is $\tau_{i,max}$, then the following inequality should be satisfied

$$-\tau_{i,max} \le \tau_i \le \tau_{i,max}. \tag{2.13}$$

Hence, the external static force $\mathbf{F} = F\mathbf{e} = F[\cos\phi, \sin\phi]^T$ that can be applied at the end-effector must satisfy the following relationship

$$-\frac{\tau_{i,max}}{F} \le \mathbf{j}_i^T \mathbf{e} \le \frac{\tau_{i,max}}{F}. \tag{2.14}$$

where $\mathbf{j}_i$ is the ith column of matrix $\mathbf{J}$. Letting $\mathbf{j}_i = [j_{ix}, j_{iy}]^T$, inequality (2.14) can be written as

$$-\frac{\tau_{i,max}}{F} \le S_i\sin(\phi - \varphi_i) \le \frac{\tau_{i,max}}{F} \tag{2.15}$$

where $S_i = ||\mathbf{j}_i|| = \sqrt{j_{ix}^2 + j_{iy}^2}$ and $\varphi_i = \arctan(-\frac{j_{ix}}{j_{iy}})$.

Based on inequality (2.15), the two boundary lines in the Cartesian force space (shown in Fig. 2.2) can be found. The inequality reaches the extreme values when

$$\sin(\phi - \varphi_i) = \pm 1.$$

And the extreme value should satisfy

$$\frac{\tau_{i,max}}{S_i F} = 1.$$
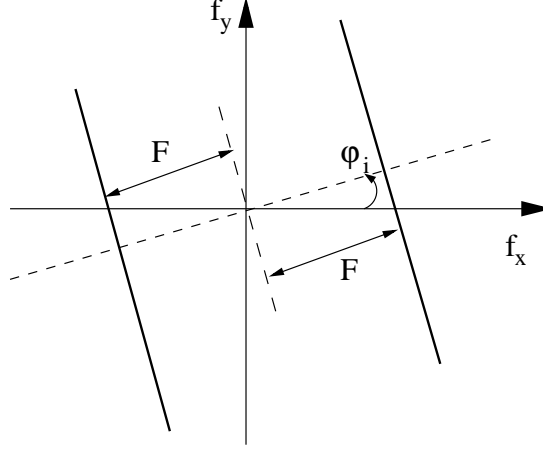
Figure 2.2: The lines defined by the inequality associated with the ith torque limiter in the Cartesian force space.

Then, the angle giving the direction of the boundary lines in the force space is

$$\phi_i = \varphi_i \pm \frac{\pi}{2},$$

and the slope of the boundary lines is $-\cot\phi_i$, the equation for the boundary line can be written as

$$f_y = \frac{j_{iy}}{j_{ix}} f_x + b \tag{2.16}$$

where b is the intercept which can be found with a given point on the boundary line. The line which passes through the origin of the force plane and which is perpendicular to the boundary lines can be expressed as

$$f_y = \tan\varphi_i f_x.$$

The distance between the origin and the intersection point of this line with the force boundary line can be written as

$$\sqrt{f_y^2 + f_x^2} = \sqrt{\tan^2\varphi_i f_x^2 + f_x^2} = F = \frac{\tau_{i,max}}{S_i},$$

The intersection points can be found as $\left[\pm\frac{\tau_{i,max}}{S_i}\cos\varphi_i, \ \pm\frac{\tau_{i,max}}{S_i}\sin\varphi_i\right]$. Substituting them into Eqn. (2.16), the intercept can be obtained and the two boundary lines defined by inequality (2.15) are

$$f_y = \frac{j_{iy}}{j_{ix}} f_x \pm \frac{\tau_{i,max}}{j_{ix}}. \tag{2.17}$$

With the force boundary lines determined by the actuators and the torque limiters, the force polygons in the Cartesian force space can be found. Similarly to what was done in [75], the maximum force that can be applied in any direction at the end-effector while guaranteeing that no torque limit is exceeded is defined as F_{min} (maximum isotropic force) while the maximum force that can be applied by the mechanism, noted F_{max}, can be obtained based on the force
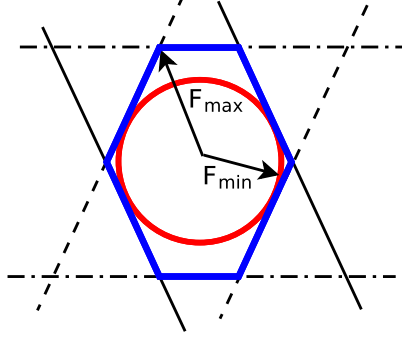
Figure 2.3: Example of a force polygon.

polygons. Then, the performance-to-safety index, referred to as the force effectiveness, is proposed as

$$\mu = \frac{F_{min}}{F_{max}}. \tag{2.18}$$

In order to give an example, a force polygon is shown in Fig. 2.3. There are three pairs of force boundary lines which are illustrated with the solid lines, dashed lines and dash point lines. A hexagon force polygon is determined by the six lines. The maximum value of the distances between the centre to the vertics of the force polygon is F_{max}. The redius of the hexagon inscribed circle is F_{min}, which is the maximum force that can be applied in any direction at the end-effector.

2.4.1 2.4.1 Symmetric Mechanisms

For the symmetric mechanism, when $\theta_2 = \theta_5 = 0$, the Jacobian matrix $\mathbf{J}$ can be written as

$$\mathbf{J}_{s,0} = \mathbf{A}^{-1}\mathbf{B} = \begin{bmatrix} -2l\sin\theta_1 & -l\sin\theta_1 & 2l\sin\theta_1 & l\sin\theta_1 \\ 2l\cos\theta_1 & l\cos\theta_1 & 2l\cos\theta_1 & l\cos\theta_1 \end{bmatrix}.$$

while when $\theta_2 = \frac{3\pi}{2}$ and $\theta_5 = \frac{\pi}{2}$, the Jacobian matrix is written as

$$\mathbf{J}_{s,\pi} = \begin{bmatrix} l(\cos\theta_1 - \sin\theta_1) & \frac{l(\cos 2\theta_1 + \sin 2\theta_1)}{2(\cos\theta_1 + \sin\theta_1)} & l(\sin\theta_1 - \cos\theta_1) & -\frac{l(\cos 2\theta_1 + \sin 2\theta_1)}{2(\cos\theta_1 + \sin\theta_1)} \\ l(\cos\theta_1 + \sin\theta_1) & \frac{l(\cos 2\theta_1 + \sin 2\theta_1)}{2(\cos\theta_1 - \sin\theta_1)} & l(\cos\theta_1 + \sin\theta_1) & \frac{l(\cos 2\theta_1 + \sin 2\theta_1)}{2(\cos\theta_1 - \sin\theta_1)} \end{bmatrix}.$$

It can be readily observed that for these two Jacobian matrices, one has

$$\frac{j_{1y}}{j_{1x}} = \frac{j_{2y}}{j_{2x}} = -\frac{j_{3y}}{j_{3x}} = -\frac{j_{4y}}{j_{4x}}. \tag{2.19}$$

These relationships are satisfied for any values of the angles ABC and AEF. Indeed, the Jacobian matrices $\mathbf{A}$ and $\mathbf{B}$ for the symmetric mechanisms can always be written in the following form

$$\mathbf{A}_s = \begin{bmatrix} r_{3x} & r_{3y} \\ r_{3x} & -r_{3y} \end{bmatrix}, \qquad \mathbf{B}_s = \begin{bmatrix} b_1 & b_2 & 0 & 0 \\ 0 & 0 & b_3 & b_4 \end{bmatrix}$$

and then, the Jacobian matrix $\mathbf{J}$ is written as

$$\mathbf{J}_s = \frac{1}{-2r_{3x}r_{3y}} \begin{bmatrix} -r_{3y}b_1 & -r_{3y}b_2 & -r_{3y}b_3 & -r_{3y}b_4 \\ -r_{3x}b_1 & -r_{3x}b_2 & r_{3x}b_3 & r_{3x}b_4 \end{bmatrix}. \tag{2.20}$$

It can be noted that the relationships shown in Eqn. (2.19) are always satisfied for the Jacobian matrix $\mathbf{J}_s$. This means that the force polygons in the Cartesian force space are composed of two groups of four parallel lines, for all configurations of the symmetric parallel mechanisms. On one hand, this situation simplifies the analysis. On the other hand, it reduces the ability of the mechanism to produce well balanced force polygons since the force polygons always have only four edges.

The maximum external force that can be applied from all directions is

$$F_{min} = \min\left(\left[\frac{\tau_{i,max}}{||\mathbf{j}_i||}\right]\right), \quad i = 1, 2, 3, 4. \tag{2.21}$$

Considering the structure of the two symmetric mechanisms, the range of values of θ_1 that should be considered are different. For the symmetric mechanism for which $\theta_2 = \theta_5 = 0$, if the maximum torque of the torque limiters are $\tau_{1,max} = 2\tau_{2,max} = \tau_{3,max} = 2\tau_{4,max} = 2\tau_{max}$, the maximum force is

$$F_{max} = \begin{cases} \dfrac{\tau_{max}}{l\sin\theta_1}, & \text{when} \quad \theta_1 \in (0, \dfrac{\pi}{4}], \\ \dfrac{\tau_{max}}{l\cos\theta_1}, & \text{when} \quad \theta_1 \in [\dfrac{\pi}{4}, \dfrac{\pi}{2}). \end{cases} \tag{2.22}$$

and $F_{min} = \frac{\tau_{max}}{l}$. The force effectiveness can then be written as

$$\mu = \frac{F_{min}}{F_{max}} = \begin{cases} \sin\theta_1, & \text{when} \quad \theta_1 \in (0, \dfrac{\pi}{4}], \\ \cos\theta_1, & \text{when} \quad \theta_1 \in [\dfrac{\pi}{4}, \dfrac{\pi}{2}). \end{cases} \tag{2.23}$$

For the symmetric mechanism with $\theta_2 = \frac{3\pi}{2}$ and $\theta_5 = \frac{\pi}{2}$, if $\tau_{1,max} = \tau_{3,max}$ and $\tau_{2,max} = \tau_{4,max}$, then one has

$$F_{min} = \min\left(\left[\frac{\tau_{1,max}}{\sqrt{2}l}, \frac{2\cos^2(2\theta_1)\tau_{2,max}}{(\sin 4\theta_1 + 1)l}\right]\right). \tag{2.24}$$

and

$$F_{max} = \begin{cases} \min\left(\dfrac{\tau_{1,max}}{l(\sin\theta_1 + \cos\theta_1)}, \left|\dfrac{(\cos\theta_1 - \sin\theta_1)\tau_{2,max}}{l(\cos 2\theta_1 + \sin 2\theta_1)}\right|\right), \\ \quad \text{when} \quad \theta_1 \in (\dfrac{\pi}{4}, \dfrac{\pi}{2}], \\ \min\left(\dfrac{\tau_{1,max}}{l(\sin\theta_1 - \cos\theta_1)}, -\dfrac{(\cos\theta_1 + \sin\theta_1)\tau_{2,max}}{l(\cos 2\theta_1 + \sin 2\theta_1)}\right), \\ \quad \text{when} \quad \theta_1 \in [\dfrac{\pi}{2}, \dfrac{3\pi}{4}). \end{cases} \tag{2.25}$$

2.4.2 2.4.2 Non-Symmetric Mechanisms

The case for which $\alpha = 0$ is first considered. Suppose $l_1 = l_4$, $l_2 = l_5$, $\theta_4 = -\theta_1$ and $\theta_5 = 2\pi - \theta_2$, the Jacobian matrix $\mathbf{J}$ for such mechanisms can be found as

$$\mathbf{J}_{n,0} = \left[\ \mathbf{j}_{1,n,0}\ \ \mathbf{j}_{2,n,0}\ \ \mathbf{j}_{3,n,0}\ \ \mathbf{j}_{4,n,0}\ \right], \tag{2.26}$$

where

$$\mathbf{j}_{1,n,0} = \begin{bmatrix} [\sin\theta_1 + \sin(\theta_1 + \theta_2)]\left[-l - 2l_7\frac{1}{\sqrt{2+2\cos\theta_2}}\right] \\ [\cos\theta_1 + \cos(\theta_1 + \theta_2)]\left[-l - 2l_7\frac{1}{\sqrt{2+2\cos\theta_2}}\right] \end{bmatrix},$$

$$\mathbf{j}_{2,n,0} = \begin{bmatrix} \frac{1}{\cos\theta_1 + \cos(\theta_1+\theta_2)}d_{j2} \\ \frac{1}{\sin\theta_1 + \sin(\theta_1+\theta_2)}d_{j2} \end{bmatrix},$$

$$\mathbf{j}_{3,n,0} = \begin{bmatrix} l[\sin\theta_1 + \sin(\theta_1 + \theta_2)] \\ -l[\cos\theta_1 + \cos(\theta_1 + \theta_2)] \end{bmatrix},$$

$$\mathbf{j}_{4,n,0} = \begin{bmatrix} \frac{l}{\cos\theta_1 + \cos(\theta_1+\theta_2)}[\sin(2\theta_1 + \theta_2) + \sin(2\theta_1 + 2\theta_2)] \\ \frac{-l}{\sin\theta_1 + \sin(\theta_1+\theta_2)}[\sin(2\theta_1 + \theta_2) + \sin(2\theta_1 + 2\theta_2)] \end{bmatrix},$$

and

$$d_{j2} = -l[\sin\theta_1 + \sin(\theta_1 + \theta_2)] - \frac{1}{2}l_7\frac{\sin 2\theta_1 + \sin(2\theta_1 + 2\theta_2) + 2\sin(2\theta_1 + \theta_2)}{\sqrt{2 + 2\cos\theta_2}}.$$

It can be observed that the relationships shown in Eqn. (2.19) are satisfied for this mechanism. That is to say, the force polygons for the non-symmetric mechanisms with $\alpha = 0$ are always composed of two groups of four parallel lines, like in the case of the symmetric mechanisms.

Next, the case for which $\alpha \neq 0$ is considered. Two situations are investigated, namely $\theta_2 = \theta_5 = 0$ or $\theta_2 = \frac{3\pi}{2}$ and $\theta_5 = \frac{\pi}{2}$.

When $\theta_2 = \theta_5 = 0$, assuming that $l_1 = l_2 = l_4 = l_5 = l$ and $l_3 = l_6 = 2l$, the Jacobian matrix $\mathbf{J}$ can be found as

$$\mathbf{J}_{\alpha,0} = \mathbf{J}_{s,0} + \begin{bmatrix} -l_7\sin(\theta_1 - \alpha) & -\frac{1}{2}l_7\sin(\theta_1 - \alpha) & 0 & 0 \\ l_7\cos(\theta_1 - \alpha) & \frac{1}{2}l_7\cos(\theta_1 - \alpha) & 0 & 0 \end{bmatrix}$$

It can be seen that

$$\frac{j_{1x,\alpha,0}}{j_{1y,\alpha,0}} = \frac{j_{2x,\alpha,0}}{j_{2y,\alpha,0}}, \qquad \frac{j_{3x,\alpha,0}}{j_{3y,\alpha,0}} = \frac{j_{4x,\alpha,0}}{j_{4y,\alpha,0}}, \qquad \frac{j_{1x,\alpha,0}}{j_{1y,\alpha,0}} \neq \frac{j_{3x,\alpha,0}}{j_{3y,\alpha,0}}.$$

Hence, the force polygon formed by the force boundary lines determined by this Jacobian matrix is a parallelogram with four edges but not necessarily a diamond shaped polygon like in the previous cases.

If $\tau_{1,max} = 2\tau_{2,max}$ and $\tau_{3,max} = 2\tau_{4,max}$, there are four force boundary lines, given by

$$f_y = \frac{2l\cos\theta_1 + l_7\cos(\theta_1 - \alpha)}{-2l\sin\theta_1 - l_7\sin(\theta_1 - \alpha)}f_x \pm \frac{\tau_{1,max}}{2l\sin\theta_1 + l_7\sin(\theta_1 - \alpha)},$$

$$f_y = \cot\theta_1 f_x \pm \frac{\tau_{3,max}}{2l\sin\theta_1}.$$

and F_{min} can be found as

$$F_{min} = \min\left[\frac{\tau_{1,max}}{\sqrt{4l^2 + l_7^2 + 4ll_7\cos\alpha}},\ \frac{\tau_{3,max}}{2l}\right]. \tag{2.27}$$

The maximum force that can be applied at the end-effector is obtained by computing the intersection of all the lines associated with the torque limiters and determining the intersection point that is the furthest from the origin while satisfying all torque limit constraints.

When $\theta_2 = \frac{3\pi}{2}$ and $\theta_5 = \frac{\pi}{2}$, assuming $l_1 = l_2 = l_4 = l_5 = l$ and $l_3 = l_6 = \sqrt{2}l$, the Jacobian matrix $\mathbf{J}$ can be found as

$$\mathbf{J}_{\alpha,\pi} = \mathbf{J}_{s,\pi} + \begin{bmatrix} -l_7\sin(\theta_1 - \frac{\pi}{4}\alpha) & -\frac{1}{2}l_7\sin(\theta_1 - \frac{\pi}{4} - \alpha) & 0 & 0 \\ l_7\cos(\theta_1 - \frac{\pi}{4} - \alpha) & \frac{1}{2}l_7\cos(\theta_1 - \frac{\pi}{4} - \alpha) & 0 & 0 \end{bmatrix}$$

Matrix $\mathbf{J}_{\alpha,\pi}$ is such that only the following relationship is satisfied, namely

$$\frac{\dot{j}_{3x,\alpha,0}}{\dot{j}_{3y,\alpha,0}} = \frac{\dot{j}_{4x,\alpha,0}}{\dot{j}_{4y,\alpha,0}}.$$

Therefore, there may be three pairs of parallel lines to form the force polygon, which may now have more than four edges. The lines can be defined as

$$a_1 f_x - b_1 f_y = \pm c_1 \tag{2.28}$$

$$a_2 f_x - b_2 f_y = \pm c_2 \tag{2.29}$$

$$a_3 f_x - b_3 f_y = \pm c_3 \tag{2.30}$$

where

$$\begin{aligned}
a_1 &= l(\cos\theta_1 + \sin\theta_1) + l_7\cos(\theta_1 - \frac{\pi}{4} - \alpha), \\
b_1 &= l(\cos\theta_1 - \sin\theta_1) - l_7\sin(\theta_1 - \frac{\pi}{4} - \alpha),\quad c_1 = \tau_{1,max}, \\
a_2 &= l(\cos\theta_1 + \sin 3\theta_1) + l_7\cos 2\theta_1\cos(\theta_1 - \frac{\pi}{4} - \alpha), \\
b_2 &= l(\cos 3\theta_1 + \sin\theta_1) - l_7\cos 2\theta_1\sin(\theta_1 - \frac{\pi}{4} - \alpha), \\
c_2 &= 2\cos 2\theta_1\tau_{2,max},\quad a_3 = \cos\theta_1 + \sin\theta_1,\quad b_3 = \sin\theta_1 - \cos\theta_1, \\
c_3 &= \min\left[\left|\frac{\tau_{3,max}}{l}\right|,\ \left|\frac{-2\tau_{4,max}\cos 2\theta_1}{l(\cos 2\theta_1 + \sin 2\theta_1)}\right|\right].
\end{aligned}$$

The maximum external force that can be applied from all directions can be found with Eqn. (2.21). The maximum applicable force can be found by calculating the intersection

of all the lines associated with the torque limiters and determining the intersection point that is the furthest from the origin while satisfying all torque limit constraints.

First, calculating the intersection points of Eqn. (2.28) and Eqn. (2.29),

$$
\mathbf{f}_1 = \begin{bmatrix} f_{1x} \\ f_{1y} \end{bmatrix} = \begin{bmatrix} a_1 & -b_1 \\ a_2 & -b_2 \end{bmatrix}^{-1} \begin{bmatrix} c_1 \\ c_2 \end{bmatrix},
$$

$$
\mathbf{f}_2 = \begin{bmatrix} f_{2x} \\ f_{2y} \end{bmatrix} = \begin{bmatrix} a_1 & -b_1 \\ a_2 & -b_2 \end{bmatrix}^{-1} \begin{bmatrix} -c_1 \\ c_2 \end{bmatrix},
$$

$$
\mathbf{f}_3 = \begin{bmatrix} f_{3x} \\ f_{3y} \end{bmatrix} = \begin{bmatrix} a_1 & -b_1 \\ a_2 & -b_2 \end{bmatrix}^{-1} \begin{bmatrix} -c_1 \\ -c_2 \end{bmatrix},
$$

$$
\mathbf{f}_4 = \begin{bmatrix} f_{4x} \\ f_{4y} \end{bmatrix} = \begin{bmatrix} a_1 & -b_1 \\ a_2 & -b_2 \end{bmatrix}^{-1} \begin{bmatrix} c_1 \\ -c_2 \end{bmatrix}.
$$

Substituting the coordinates of these points into the third pair of equations,

- if $(a_3 f_{xi} - b_3 f_{yi} - c_3)(a_3 f_{xi} - b_3 f_{yi} + c_3) < 0$, it means that point $\mathbf{f}_i$ is located between the two lines, this point is one vertex of the force polygon;
- if $(a_3 f_{xi} - b_3 f_{yi} - c_3)(a_3 f_{xi} - b_3 f_{yi} + c_3) = 0$, it means that point $\mathbf{f}_i$ is located at one of the two lines, this point is one vertex of the force polygon;
- if $(a_3 f_{xi} - b_3 f_{yi} - c_3)(a_3 f_{xi} - b_3 f_{yi} + c_3) > 0$, it means that point $\mathbf{f}_i$ is located at one side of the two lines, this point is not one vertex of the force polygon;

We should select the points which are located between the two lines or at one of the two lines as the vertices of the force polygon.

Similarly, we can find the intersection points of Eqn. (2.28) and Eqn. (2.30) which are located between the lines determined by Eqn. (2.29) and the intersection points of Eqn. (2.29) and lines determined by Eqn. (2.28).

After all the vertices of the force polygon $\mathbf{v}_i$ have been found, the maximum isotropic force is determined using

$$
F_{max} = \max([||\mathbf{v}_i||]). \tag{2.31}
$$

The force effectiveness is given as

$$
\mu = \frac{F_{min}}{F_{max}}. \tag{2.32}
$$

There is an interesting configuration for such mechanisms. When $\theta_1 = \frac{\pi}{2}$, Eqn. (2.28) and Eqn. (2.29) can be modified as

$$
f_y = -\frac{l + l_7 \cos(\frac{\pi}{4} - \alpha)}{l + l_7 \sin(\frac{\pi}{4} - \alpha)} f_x \pm \frac{\tau_{1,max}}{l + l_7 \sin(\frac{\pi}{4} - \alpha)}, \tag{2.33}
$$

$$
f_y = -\frac{l + l_7 \cos(\frac{\pi}{4} - \alpha)}{l + l_7 \sin(\frac{\pi}{4} - \alpha)} f_x \pm \frac{2\tau_{2,max}}{l + l_7 \sin(\frac{\pi}{4} - \alpha)}. \tag{2.34}
$$

Hence, the force boundary lines defined by the four torque limiters are two pairs of parallel lines at the configuration of $\theta_1 = \frac{\pi}{2}$ when $\tau_{1,max} = 2\tau_{2,max}$.

The angle between the two pairs of the force boundary lines determined by joint 1 and 2 can be found as

$$
\begin{aligned}
\gamma = {} & \arctan\left[\frac{l(\cos\theta_1 + \sin\theta_1) + l_7\cos(\theta_1 - \frac{\pi}{4} - \alpha)}{l(\cos\theta_1 - \sin\theta_1) - l_7\sin(\theta_1 - \frac{\pi}{4} - \alpha)}\right] \\
& - \arctan\left[\frac{l(\cos\theta_1 + \sin 3\theta_1) + l_7\cos 2\theta_1\cos(\theta_1 - \frac{\pi}{4} - \alpha)}{l(\cos 3\theta_1 + \sin\theta_1) - l_7\cos 2\theta_1\sin(\theta_1 - \frac{\pi}{4} - \alpha)}\right].
\end{aligned}
$$

2.5 Numerical Examples

Numerical results are given in this section in order to provide insight on the use of the force effectiveness index μ.

2.5.1 2.5.1 Symmetric Mechanisms

The link lengths of the mechanism are normalized as $l = 1$. For the mechanism with $\theta_2 = \theta_5 = 0$, the maximum torques at the torque limiters are chosen as $\tau_{max} = 1$ and the maximum isotropic force F_{min} can be easily found as $F_{min} = 1$. The maximum force F_{max} and the force effectiveness μ are plotted in Fig. 2.4.

It can be seen that the force effectiveness goes to 0 when the mechanism is in a singular configuration ($\theta_1 = 0$ and $\theta_1 = \frac{\pi}{2}$). Since the force polygon is a diamond, the maximum value of μ is $\frac{\sqrt{2}}{2}$ when the diamond is a square and it occurs at the configuration for which $\theta_1 = \frac{\pi}{4}$. This configuration is noted with a square point in Fig. 2.4(b).

Since the Jacobian matrices of all the symmetric mechanisms with different given θ_2, θ_5 and the non-symmetric mechanisms with $\alpha = 0$ satisfy the relationships shown in Eqn. (2.19), the shape of the force effectiveness plots for these mechanisms are similar to that of Fig. 2.4(b), possibly with a shift along the θ_1 axis.

2.5.2 2.5.2 Non-Symmetric Mechanisms

Non-symmetric mechanisms with $\theta_2 = \theta_5 = 0$ are first considered. Assuming $\alpha = \frac{\pi}{4}$ and $l_i = 1$, $i = 1, 2, \ldots, 7$, $\tau_{1,max} = 2\tau_{2,max} = \sqrt{4l^2 + l_7^2 + 4ll_7\cos\alpha} = \sqrt{5 + 2\sqrt{2}}$, $\tau_{3,max} = 2\tau_{4,max} = 2$. The force polygons for different configurations ($\theta_1 = \frac{\pi}{6}$, $\theta_1 = \frac{\pi}{3}$) are shown in Fig. 2.5.
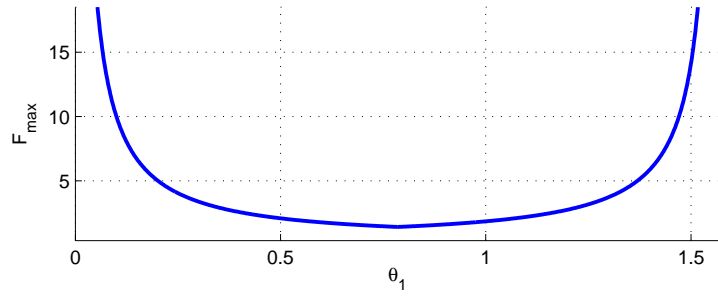
(a) maximum force
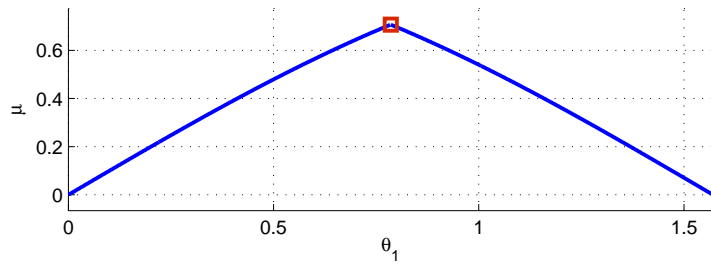
(b) force effectiveness

Figure 2.4: F_{max} and μ for the symmetric mechanism with $\theta_2 = \theta_5 = 0$.
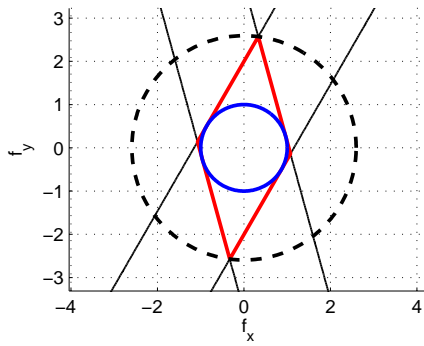
(a) $\theta_1 = \frac{\pi}{6}$, $\mu = 0.3856$
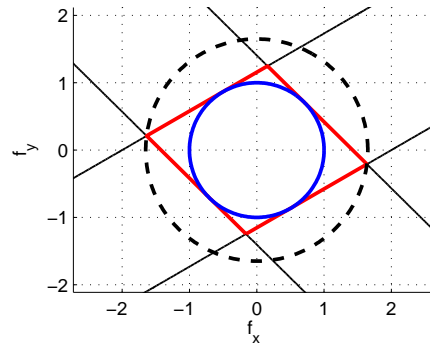
(b) $\theta_1 = \frac{\pi}{3}$, $\mu = 0.6063$

Figure 2.5: Force polygons of the non-symmetric mechanism with $\theta_2 = \theta_5 = 0$ and $\alpha = \frac{\pi}{4}$.
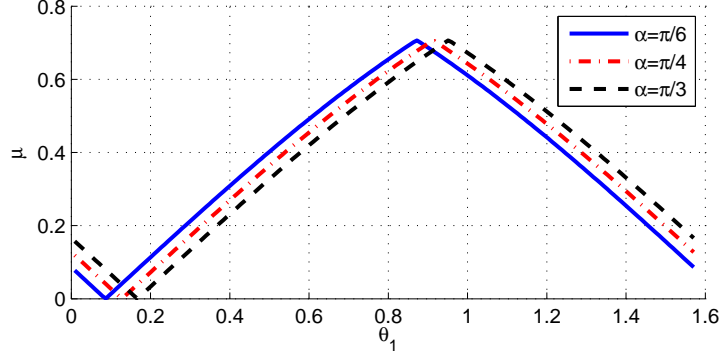
Figure 2.6: The force effectiveness of the non-symmetric mechanisms with different values of α.

The plots of the force effectiveness for the non-symmetric mechanisms with $\theta_2 = \theta_5 = 0$ and different values of α are shown in Fig. 2.6. Since the force polygons are parallelograms, the maximum force effectiveness μ is still equal to $\frac{\sqrt{2}}{2}$.

Non-symmetric mechanisms with $\theta_2 = \frac{3\pi}{2}$, $\theta_5 = \frac{\pi}{2}$ and $\alpha = \frac{\pi}{4}$ are now considered. The link lengths are chosen as $l_1 = l_2 = l_4 = l_5 = 1$ and $l_3 = l_6 = l_7 = \sqrt{2}l$ and the maximum torques of the torque limiters are determined as $\tau_{i,max} = ||\mathbf{j}_i||$, $i = 1, 2, 3, 4$, with $\theta_1 = \frac{\pi}{2}$. That is to say, $\tau_{1,max} = \sqrt{2l^2 + l_7^2 + 2\sqrt{2}ll_7 \cos\alpha} = \sqrt{4 + 2\sqrt{2}}$, $\tau_{2,max} = \sqrt{1 + \frac{\sqrt{2}}{2}}$, $\tau_{3,max} = \sqrt{2}$ and $\tau_{4,max} = \frac{\sqrt{2}}{2}$.

The force polygons for different configurations ($\theta_1 = \frac{5\pi}{12}$, $\theta_1 = \frac{\pi}{2}$, $\theta_1 = \frac{7\pi}{12}$) are shown in Fig. 2.7.

The angle between the two pairs of the force boundary lines determined by the joints in the distal part of the linkage is shown in Fig. 2.8.

For the mechanisms with different values of α ($\alpha = \frac{\pi}{6}$, $\alpha = \frac{\pi}{4}$ and $\alpha = \frac{\pi}{3}$), if the maximum torques at the torque limiters are set to $||\mathbf{j}_i||$ with $\theta_1 = \frac{\pi}{2}$, the plot of the force effectiveness is shown in Fig. 2.9.

For the mechanism with $\alpha = \frac{\pi}{4}$, the maximum torques at the torque limiters are set to the value of $||\mathbf{j}_i||$ with $\theta_1 = 100°$ or $\theta_1 = 120°$ and the plots of the force effectiveness are shown in Fig. 2.10. The dashed curves are for the maximum torques with the value of $||\mathbf{j}_i||$ when $\theta_1 = 100°$ while the solid curves are for the maximum torques with the value of $||\mathbf{j}_i||$ when $\theta_1 = 120°$.

It can be observed from Fig. 2.9 that the force effectiveness is generally smaller than $\frac{\sqrt{2}}{2}$. However, the smallest force effectiveness of the non-symmetric mechanisms with $\theta_2 = \frac{3\pi}{2}$ and $\theta_5 = \frac{\pi}{2}$ is larger than the smallest force effectiveness of the symmetric mechanisms and the non-symmetric mechanisms with $\theta_2 = \theta_5 = 0$.
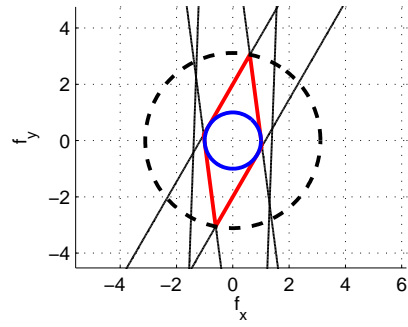
(a) $\theta_1 = \frac{5\pi}{12}$, $\mu = 0.3214$
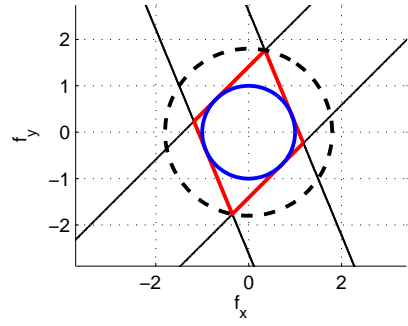
(b) $\theta_1 = \frac{6\pi}{12} = \frac{\pi}{2}$, $\mu = 0.5556$
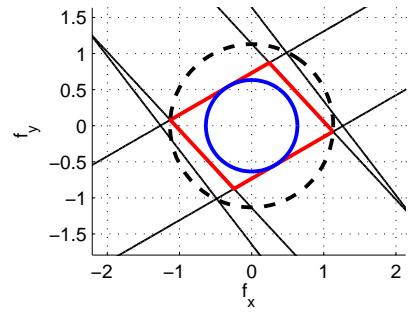
(c) $\theta_1 = \frac{7\pi}{12}$, $\mu = 0.5606$

Figure 2.7: Force polygons for the non-symmetric mechanism with $\theta_2 = \frac{3\pi}{2}$, $\theta_5 = \frac{\pi}{2}$ and $\alpha = \frac{\pi}{4}$.
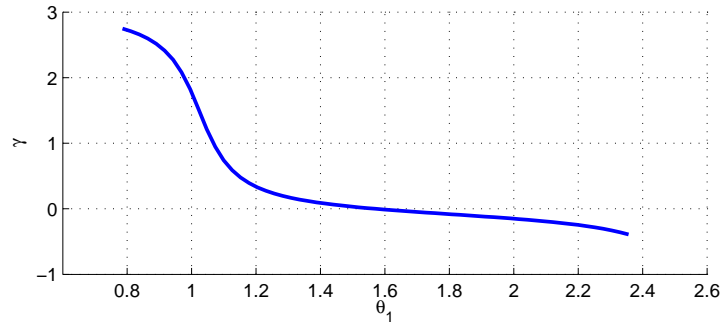
Figure 2.8: The angle between the two pairs of the force boundary lines determined by Eqn. (2.28) and Eqn. (2.29).
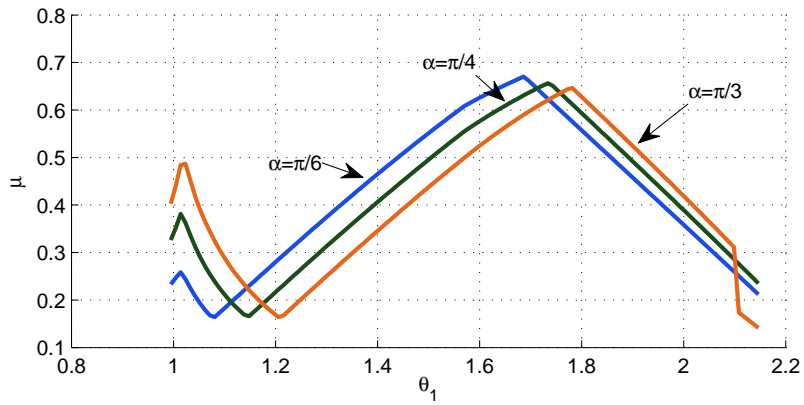
Figure 2.9: The force effectiveness for different values of α with the maximum torque as $||\mathbf{j}_i||$ when $\theta_1 = \frac{\pi}{2}$.
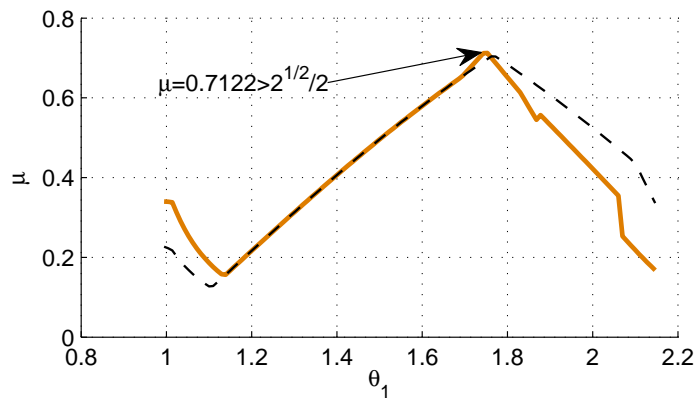
Figure 2.10: Force effectiveness for different values of $\tau_{i,max}$.

Although the examples presented in this section are chosen rather arbitrarily and are only illustrative, they demonstrate that the force capabilities of the mechanisms can be modulated by choosing the geometric parameters and the torque limits.

2.6   Conclusion

The force characteristics of symmetric and non-symmetric planar 2-DOF parallel mechanisms are analyzed in this chapter. Four torque limiters (clutches) are mounted on the mechanism in order to produce a feasible force polygon at the end-effector. The most favorable force polygon that can be achieved is a square for the symmetric mechanisms, the non-symmetric mechanisms with linkage FDP as a straight link and the non-symmetric mechanisms with ABC and AEF as straight links. This result arises from the observation that only two pairs of parallel lines form the force polygon in these cases.

For the non-symmetric mechanisms with ABC and AEF as triangular links, three pairs of parallel lines form the force polygon. If the torque limiters are set properly, it is expected that this kind of mechanism can lead to more balanced force polygons. Further work is required in order to develop a synthesis procedure that would allow a designer to select the geometric parameters and the torque limits based on a prescribed desirable force polygon.

Chapter 3

Force Capabilities of 2-DOF Parallel Mechanisms Equipped with Torque Limiters and Force Limiters

This chapter is similar to the preceding chapter. Two force limiters now replace the torque limiters of the proximal links of the mechanism. The two force limiters are mounted on the proximal links on one mechanism, and the force limiters are on the distal links on another mechanism. Two passive torque limiters are mounted at the actuators of the robot. The structure of the mechanisms are described at first. Then, the Jacobian matrices and the static force equations are derived. The force characteristics are analyzed based on the force equations and a performance index referred to as the force effectiveness is proposed. Finally, numerical simulation results are presented.

(a) Force limiters on the proximal links   (b) Force limiters on the distal links
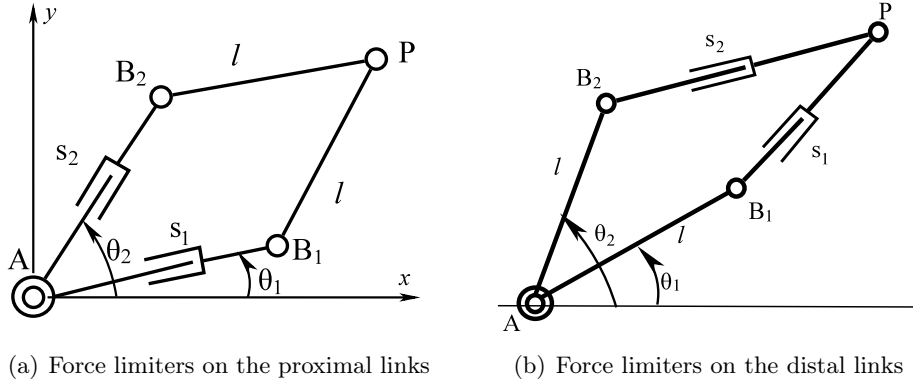
Figure 3.1: The structure of the mechanisms.

3.1 Introduction

Similarly to the analysis performed in Chapter 2, the force capabilities of the planar 2-DOF planar mechanisms with two torque limiters and two force limiters is analyzed in this chapter. At first, the structure and the kinematics of the mechanism are described. Then, the static force equations are derived with the Jacobian matrices. The force characteristics are then analyzed based on the force equations and numerical simulations are presented in the end.

3.2 Structure and Kinematics of the Mechanism

The architecture of the 2-DOF planar parallel mechanisms studied in this chapter is shown in Fig. 3.1. There are two revolute actuators located at joint A that independently drive links AB_1 and AB_2 respectively. The four links AB_1, AB_2 B_1P and B_2P are normally rigid. However, there are two force limiters placed at the proximal links AB_1 and AB_2 of the mechanism shown in Fig. 3.1(a), while the mechanism shown in Fig. 3.1(b) has two force limiters placed at the distal links B_1P and B_2P. The torque limiters and the force limiters will dislocate and a message will be sent to the controller when one of their limits has been reached. Joints B_1 and B_2 are free joints which are not actuated and do not have torque limiters.

For the mechanism with force limiters on the proximal links, the geometric relationship can be found as follows. As shown in Fig. 3.2, one has

$$\mathbf{p} = \mathbf{b_1} + l \begin{bmatrix} \cos(\pi - \theta_l - \theta_x) \\ \sin(\pi - \theta_l - \theta_x) \end{bmatrix} = \mathbf{b_2} + l \begin{bmatrix} \cos\theta_y \\ \sin\theta_y \end{bmatrix} \tag{3.1}$$

and $\theta_l = \theta_x + \theta_y$. The values of θ_x and θ_y can be found using the following method.
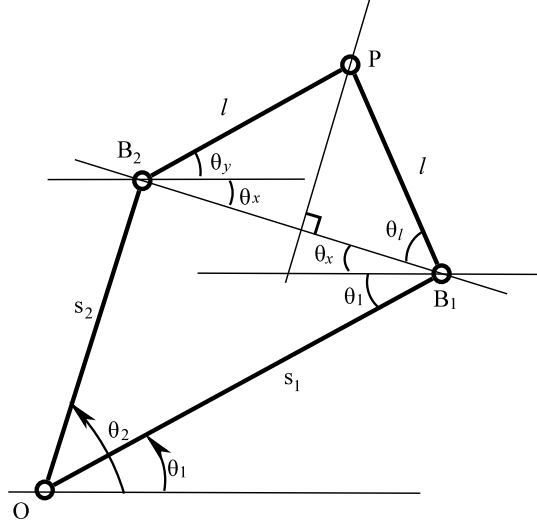
Figure 3.2: The geometry of the mechanism.

According to the law of cosines and sines, one has

$$\overline{B_1B_2}^2 = s_1^2 + s_2^2 - 2s_1s_2\cos(\theta_2 - \theta_1), \quad \frac{\overline{B_1B_1}}{\sin(\theta_2 - \theta_1)} = \frac{s_2}{\sin(\theta_1 + \theta_x)}.$$

Then, the value of θ_x can be found as

$$\theta_x = \arcsin\left(\frac{s_2\sin(\theta_2 - \theta_1)}{\sqrt{s_1^2 + s_2^2 - 2s_1s_2\cos(\theta_2 - \theta_1)}}\right) - \theta_1. \tag{3.2}$$

Since PB_1B_2 is an isosceles triangle, one has

$$\cos\theta_l = \frac{\frac{\overline{B_1B_2}}{2}}{l}, \tag{3.3}$$

leading to

$$\theta_l = \arccos\left(\frac{\sqrt{s_1^2 + s_2^2 - 2s_1s_2\cos(\theta_2 - \theta_1)}}{2l}\right), \tag{3.4}$$

then, the value of θ_y can be found as

$$\theta_y = \theta_l - \theta_x = \arccos\left(\frac{\sqrt{s_1^2 + s_2^2 - 2s_1s_2\cos(\theta_2 - \theta_1)}}{2l}\right)$$
$$- \arcsin\left(\frac{s_2\sin(\theta_2 - \theta_1)}{\sqrt{s_1^2 + s_2^2 - 2s_1s_2\cos(\theta_2 - \theta_1)}}\right) + \theta_1. \tag{3.5}$$

For the mechanism with force limiters on the distal links, the position of the end-effector can be found with the following equations when the angles of the actuators and the length of distal links are given.

$$s_i^2 = (\mathbf{p} - \mathbf{b}_i)^T(\mathbf{p} - \mathbf{b}_i), \qquad i = 1, 2. \tag{3.6}$$

3.3 Jacobian Matrices and Force Equations

The Jacobian matrices and the force equations are established in this section.

3.3.1 3.3.1 Mechanism with Force Limiters on the Proximal Links

Based on the structure of the mechanism, one obtains

$$(\mathbf{p} - \mathbf{b}_i)^T(\mathbf{p} - \mathbf{b}_i) = l^2, \qquad i = 1, 2 \tag{3.7}$$

where

$$\mathbf{b}_i = \begin{bmatrix} s_i \cos \theta_i \\ s_i \sin \theta_i \end{bmatrix}, \qquad i = 1, 2$$

Derivating the above equation, we obtain

$$(\mathbf{p} - \mathbf{b}_i)^T(\dot{\mathbf{p}} - \dot{\mathbf{b}}_i) = 0 \tag{3.8}$$

where $\dot{\mathbf{b}}_i = \dot{s}_i \mathbf{e}_i + s_i \dot{\theta}_i \mathbf{E} \mathbf{e}_i$, $\mathbf{e}_i = [\cos \theta_i, \ \sin \theta_i]^T$, and

$$\mathbf{E} = \begin{bmatrix} 0 & -1 \\ 1 & 0 \end{bmatrix}.$$

Equation (3.8) can be written in matrix form as

$$\mathbf{A}\dot{\mathbf{p}} = \mathbf{B}\dot{\boldsymbol{\theta}} \tag{3.9}$$

where

$$\mathbf{A} = \begin{bmatrix} (\mathbf{p} - \mathbf{b}_1)^T \\ (\mathbf{p} - \mathbf{b}_2)^T \end{bmatrix},$$

$$\mathbf{B} = \begin{bmatrix} s_1(\mathbf{p} - \mathbf{b}_1)^T \mathbf{E} \mathbf{e}_1 & 0 & (\mathbf{p} - \mathbf{b}_1)^T \mathbf{e}_1 & 0 \\ 0 & s_2(\mathbf{p} - \mathbf{b}_2)^T \mathbf{E} \mathbf{e}_2 & 0 & (\mathbf{p} - \mathbf{b}_2)^T \mathbf{e}_2 \end{bmatrix},$$

and $\dot{\boldsymbol{\theta}} = [\dot{\theta}_1, \ \dot{\theta}_2, \ \dot{s}_1, \ \dot{s}_2]^T$. The velocity of the end-effector can be expressed as

$$\dot{\mathbf{p}} = \mathbf{A}^{-1}\mathbf{B}\dot{\boldsymbol{\theta}}. \tag{3.10}$$

Based on the principle of virtual work, the static equations can be established as

$$\boldsymbol{\tau} = \mathbf{J}^T \mathbf{F} \tag{3.11}$$

where $\mathbf{J}^T = \mathbf{B}^T \mathbf{A}^{-T}$ is a 4×2 matrix and $\boldsymbol{\tau} = [\tau_1, \ \tau_2, \ f_1, \ f_2]^T$.

3.3.2   3.3.2 Mechanism with Force Limiters on the Distal Links

Differenting Eqn. (3.6), one has

$$(\mathbf{p} - \mathbf{b}_i)^T (\dot{\mathbf{p}} - \dot{\mathbf{b}}_i) = s_i \dot{s}_i, \qquad i = 1, 2 \tag{3.12}$$

and $\dot{\mathbf{b}}_i = l\dot{\theta}_i \mathbf{E} \mathbf{e}_i$. Combining these two equations and written in matrix form, we have

$$\mathbf{A}\dot{\mathbf{p}} = \mathbf{B}\dot{\boldsymbol{\theta}} \tag{3.13}$$

where

$$\mathbf{A} = \begin{bmatrix} (\mathbf{p} - \mathbf{b}_1)^T \\ (\mathbf{p} - \mathbf{b}_2)^T \end{bmatrix}, \quad \mathbf{B} = \begin{bmatrix} l(\mathbf{p} - \mathbf{b}_1)^T \mathbf{E} \mathbf{e}_1 & 0 & s_1 & 0 \\ 0 & l(\mathbf{p} - \mathbf{b}_2)^T \mathbf{E} \mathbf{e}_2 & 0 & s_2 \end{bmatrix}.$$

The velocity equations and the static equations can be established as

$$\dot{\mathbf{p}} = \mathbf{J}\dot{\boldsymbol{\theta}}, \quad \boldsymbol{\tau} = \mathbf{J}^T \mathbf{F}. \tag{3.14}$$

where $\mathbf{J} = \mathbf{A}^{-1}\mathbf{B}$ and $\boldsymbol{\tau} = [\tau_1, \ \tau_2, \ f_1, \ f_2]^T$.

For both of the mechanisms, note that $\mathbf{A}^{-1}$ can be calculated as

$$\mathbf{A}^{-1} = \frac{1}{-(\mathbf{p} - \mathbf{b}_1)^T \mathbf{E}(\mathbf{p} - \mathbf{b}_2)} \begin{bmatrix} -\mathbf{E}(\mathbf{p} - \mathbf{b}_2) & \mathbf{E}(\mathbf{p} - \mathbf{b}_1) \end{bmatrix} \tag{3.15}$$

hence

$$\mathbf{A}^{-T} = \frac{1}{-(\mathbf{p} - \mathbf{b}_1)^T \mathbf{E}(\mathbf{p} - \mathbf{b}_2)} \begin{bmatrix} -(\mathbf{E}(\mathbf{p} - \mathbf{b}_2))^T \\ (\mathbf{E}(\mathbf{p} - \mathbf{b}_1))^T \end{bmatrix}. \tag{3.16}$$

3.4   Analysis of the Force Capabilities

The force capability analysis can be performed using the method described in Chapter 2. The force boundaries equations, the maximum isotropic force F_{min} and the maximum force that can be applied by the mechanism F_{max} for both of the planar mechanisms will be found.

3.4.1   3.4.1 General Case

3.4.1.1 Mechanism with Force Limiters on the Proximal Links

The Jacobian matrix can be calculated as

$$\mathbf{J}^T = \frac{-1}{(\mathbf{p} - \mathbf{b}_1)^T \mathbf{E}(\mathbf{p} - \mathbf{b}_2)} \begin{bmatrix} (y - s_2 \sin\theta_2)s_1(\mathbf{p} - \mathbf{b}_1)^T \mathbf{E} \mathbf{e}_1 & (-x + s_2 \cos\theta_2)s_1(\mathbf{p} - \mathbf{b}_1)^T \mathbf{E} \mathbf{e}_1 \\ (-y + s_1 \sin\theta_1)s_2(\mathbf{p} - \mathbf{b}_2)^T \mathbf{E} \mathbf{e}_2 & (x - s_1 \cos\theta_1)s_2(\mathbf{p} - \mathbf{b}_2)^T \mathbf{E} \mathbf{e}_2 \\ (y - s_2 \sin\theta_2)(\mathbf{p} - \mathbf{b}_1)^T \mathbf{e}_1 & (-x + s_2 \cos\theta_2)(\mathbf{p} - \mathbf{b}_1)^T \mathbf{e}_1 \\ (-y + s_1 \sin\theta_1)(\mathbf{p} - \mathbf{b}_2)^T \mathbf{e}_2 & (x - s_1 \cos\theta_1)(\mathbf{p} - \mathbf{b}_2)^T \mathbf{e}_2 \end{bmatrix}.$$

It can be observed that

$$\frac{j_{1x}}{j_{1y}} = \frac{j_{3x}}{j_{3y}} = \frac{y - s_2 \sin\theta_2}{-x + s_2 \cos\theta_2} \quad \text{and} \quad \frac{j_{2x}}{j_{2y}} = \frac{j_{4x}}{j_{4y}} = \frac{-y + s_1 \sin\theta_1}{x - s_1 \cos\theta_1}$$

which means that two of the four pairs of force boundary lines are parallel and the other two are parallel to each other.

If the external force is represented with $\mathbf{F} = F[\cos\phi, \ \sin\phi]^T$, the joint forces and torques can be found as

$$\tau = \frac{-F}{(\mathbf{p}-\mathbf{b}_1)^T\mathbf{E}(\mathbf{p}-\mathbf{b}_2)} \begin{bmatrix} s_1(\mathbf{p}-\mathbf{b}_1)^T\mathbf{E}\mathbf{e}_1[\cos\phi(y-s_2\sin\theta_2)+\sin\phi(-x+s_2\cos\theta_2)] \\ s_2(\mathbf{p}-\mathbf{b}_2)^T\mathbf{E}\mathbf{e}_2[\cos\phi(-y+s_1\sin\theta_1)+\sin\phi(x-s_1\cos\theta_1)] \\ (\mathbf{p}-\mathbf{b}_1)^T\mathbf{e}_1[\cos\phi(y-s_2\sin\theta_2)+\sin\phi(-x+s_2\cos\theta_2)] \\ (\mathbf{p}-\mathbf{b}_2)^T\mathbf{e}_2[\cos\phi(-y+s_1\sin\theta_1)+\sin\phi(x-s_1\cos\theta_1)] \end{bmatrix}$$

Suppose the limit torque and force of the revolute actuators and the linear force limiters are $\tau_{i,max}$ and $f_{i,max}$, $i = 1, 2$, respectively, then the following inequalities should be satisfied

$$\frac{\tau_{1,max}(\mathbf{p}-\mathbf{b}_1)^T\mathbf{E}(\mathbf{p}-\mathbf{b}_2)}{Fs_1(\mathbf{p}-\mathbf{b}_1)^T\mathbf{E}\mathbf{e}_1} \le a_1\sin(\phi-\psi_1) \le \frac{-\tau_{1,max}(\mathbf{p}-\mathbf{b}_1)^T\mathbf{E}(\mathbf{p}-\mathbf{b}_2)}{Fs_1(\mathbf{p}-\mathbf{b}_1)^T\mathbf{E}\mathbf{e}_1} \tag{3.17}$$

$$\frac{\tau_{2,max}(\mathbf{p}-\mathbf{b}_1)^T\mathbf{E}(\mathbf{p}-\mathbf{b}_2)}{Fs_2(\mathbf{p}-\mathbf{b}_2)^T\mathbf{E}\mathbf{e}_2} \le a_2\sin(\phi-\psi_2) \le \frac{-\tau_{2,max}(\mathbf{p}-\mathbf{b}_1)^T\mathbf{E}(\mathbf{p}-\mathbf{b}_2)}{Fs_2(\mathbf{p}-\mathbf{b}_2)^T\mathbf{E}\mathbf{e}_2} \tag{3.18}$$

$$\frac{f_{1,max}(\mathbf{p}-\mathbf{b}_1)^T\mathbf{E}(\mathbf{p}-\mathbf{b}_2)}{F(\mathbf{p}-\mathbf{b}_1)^T\mathbf{e}_1} \le a_1\sin(\phi-\psi_1) \le \frac{-f_{1,max}(\mathbf{p}-\mathbf{b}_1)^T\mathbf{E}(\mathbf{p}-\mathbf{b}_2)}{F(\mathbf{p}-\mathbf{b}_1)^T\mathbf{e}_1} \tag{3.19}$$

$$\frac{f_{2,max}(\mathbf{p}-\mathbf{b}_1)^T\mathbf{E}(\mathbf{p}-\mathbf{b}_2)}{F(\mathbf{p}-\mathbf{b}_2)^T\mathbf{e}_2} \le a_2\sin(\phi-\psi_2) \le \frac{-f_{2,max}(\mathbf{p}-\mathbf{b}_1)^T\mathbf{E}(\mathbf{p}-\mathbf{b}_2)}{F(\mathbf{p}-\mathbf{b}_2)^T\mathbf{e}_2} \tag{3.20}$$

where

$$a_1 = \sqrt{(y-s_2\sin\theta_2)^2 + (-x+s_2\cos\theta_2)^2}, \qquad \psi_1 = \arctan\left(\frac{y-s_2\sin\theta_2}{x-s_2\cos\theta_2}\right)$$

$$a_2 = \sqrt{(-y+s_1\sin\theta_1)^2 + (x-s_1\cos\theta_1)^2}, \qquad \psi_2 = \arctan\left(\frac{y-s_1\sin\theta_1}{x-s_1\cos\theta_1}\right)$$

The force boundary lines determined by these inequalities are

$$f_y = \frac{-x+s_2\cos\theta_2}{y-s_2\sin\theta_2}f_x \pm \frac{\tau_{1,max}(\mathbf{p}-\mathbf{b}_1)^T\mathbf{E}(\mathbf{p}-\mathbf{b}_2)}{(y-s_2\sin\theta_2)s_1(\mathbf{p}-\mathbf{b}_1)^T\mathbf{E}\mathbf{e}_1} \tag{3.21}$$

$$f_y = \frac{x-s_1\cos\theta_1}{-y+s_1\sin\theta_1}f_x \pm \frac{\tau_{2,max}(\mathbf{p}-\mathbf{b}_1)^T\mathbf{E}(\mathbf{p}-\mathbf{b}_2)}{(-y+s_1\sin\theta_1)s_2(\mathbf{p}-\mathbf{b}_2)^T\mathbf{E}\mathbf{e}_2} \tag{3.22}$$

$$f_y = \frac{-x+s_2\cos\theta_2}{y-s_2\sin\theta_2}f_x \pm \frac{f_{1,max}(\mathbf{p}-\mathbf{b}_1)^T\mathbf{E}(\mathbf{p}-\mathbf{b}_2)}{(y-s_2\sin\theta_2)(\mathbf{p}-\mathbf{b}_1)^T\mathbf{e}_1} \tag{3.23}$$

$$f_y = \frac{x-s_1\cos\theta_1}{-y+s_1\sin\theta_1}f_x \pm \frac{f_{2,max}(\mathbf{p}-\mathbf{b}_1)^T\mathbf{E}(\mathbf{p}-\mathbf{b}_2)}{(-y+s_1\sin\theta_1)(\mathbf{p}-\mathbf{b}_2)^T\mathbf{e}_2} \tag{3.24}$$

The maximum isotropic force F_{min} can be found as

$$F_{min} = \min\left(\begin{bmatrix} \frac{\tau_{1,max}}{\|\mathbf{j}_1\|}, & \frac{\tau_{2,max}}{\|\mathbf{j}_2\|}, & \frac{f_{1,max}}{\|\mathbf{j}_3\|}, & \frac{f_{2,max}}{\|\mathbf{j}_4\|} \end{bmatrix}\right) \tag{3.25}$$

where

$$\|\mathbf{j}_1\| = \left| \frac{s_1(\mathbf{p} - \mathbf{b}_1)^T \mathbf{E} \mathbf{e}_1}{(\mathbf{p} - \mathbf{b}_1)^T \mathbf{E}(\mathbf{p} - \mathbf{b}_2)} \right| a_1, \quad \|\mathbf{j}_2\| = \left| \frac{s_2(\mathbf{p} - \mathbf{b}_2)^T \mathbf{E} \mathbf{e}_2}{(\mathbf{p} - \mathbf{b}_1)^T \mathbf{E}(\mathbf{p} - \mathbf{b}_2)} \right| a_2,$$

$$\|\mathbf{j}_3\| = \left| \frac{(\mathbf{p} - \mathbf{b}_1)^T \mathbf{e}_1}{(\mathbf{p} - \mathbf{b}_1)^T \mathbf{E}(\mathbf{p} - \mathbf{b}_2)} \right| a_1, \quad \|\mathbf{j}_4\| = \left| \frac{(\mathbf{p} - \mathbf{b}_2)^T \mathbf{e}_2}{(\mathbf{p} - \mathbf{b}_1)^T \mathbf{E}(\mathbf{p} - \mathbf{b}_2)} \right| a_2.$$

Let

$$b_{min,1} = \min \left[\left| \frac{\tau_{1,max}(\mathbf{p} - \mathbf{b}_1)^T \mathbf{E}(\mathbf{p} - \mathbf{b}_2)}{(y - s_2 \sin \theta_2) s_1 (\mathbf{p} - \mathbf{b}_1)^T \mathbf{E} \mathbf{e}_1} \right|, \quad \left| \frac{f_{1,max}(\mathbf{p} - \mathbf{b}_1)^T \mathbf{E}(\mathbf{p} - \mathbf{b}_2)}{(y - s_2 \sin \theta_2)(\mathbf{p} - \mathbf{b}_1)^T \mathbf{e}_1} \right| \right] \tag{3.26}$$

$$b_{min,2} = \min \left[\left| \frac{\tau_{2,max}(\mathbf{p} - \mathbf{b}_1)^T \mathbf{E}(\mathbf{p} - \mathbf{b}_2)}{(-y + s_1 \sin \theta_1) s_2 (\mathbf{p} - \mathbf{b}_2)^T \mathbf{E} \mathbf{e}_2} \right|, \quad \left| \frac{f_{2,max}(\mathbf{p} - \mathbf{b}_1)^T \mathbf{E}(\mathbf{p} - \mathbf{b}_2)}{(-y + s_1 \sin \theta_1)(\mathbf{p} - \mathbf{b}_2)^T \mathbf{e}_2} \right| \right] \tag{3.27}$$

The force polygon formed by the four following equations

$$f_y = \frac{-x + s_2 \cos \theta_2}{y - s_2 \sin \theta_2} f_x \pm b_{min,1}, \tag{3.28}$$

$$f_y = \frac{x - s_1 \cos \theta_1}{-y + s_1 \sin \theta_1} f_x \pm b_{min,2}. \tag{3.29}$$

The coordinates of the intersection points of these lines can be found as

$$\mathbf{f}_1 = \begin{bmatrix} \dfrac{b_{min,2} - b_{min,1}}{\frac{-x+s_2\cos\theta_2}{y-s_2\sin\theta_2} - \frac{x-s_1\cos\theta_1}{-y+s_1\sin\theta_1}} \\[2ex] \dfrac{-x+s_2\cos\theta_2}{y-s_2\sin\theta_2} \dfrac{b_{min,2} - b_{min,1}}{\frac{-x+s_2\cos\theta_2}{y-s_2\sin\theta_2} - \frac{x-s_1\cos\theta_1}{-y+s_1\sin\theta_1}} + b_{min,1} \end{bmatrix}$$

$$\mathbf{f}_2 = \begin{bmatrix} \dfrac{b_{min,2} + b_{min,1}}{\frac{-x+s_2\cos\theta_2}{y-s_2\sin\theta_2} - \frac{x-s_1\cos\theta_1}{-y+s_1\sin\theta_1}} \\[2ex] \dfrac{-x+s_2\cos\theta_2}{y-s_2\sin\theta_2} \dfrac{b_{min,2} + b_{min,1}}{\frac{-x+s_2\cos\theta_2}{y-s_2\sin\theta_2} - \frac{x-s_1\cos\theta_1}{-y+s_1\sin\theta_1}} - b_{min,1} \end{bmatrix}$$

$$\mathbf{f}_3 = \begin{bmatrix} \dfrac{-b_{min,2} + b_{min,1}}{\frac{-x+s_2\cos\theta_2}{y-s_2\sin\theta_2} - \frac{x-s_1\cos\theta_1}{-y+s_1\sin\theta_1}} \\[2ex] \dfrac{-x+s_2\cos\theta_2}{y-s_2\sin\theta_2} \dfrac{-b_{min,2} + b_{min,1}}{\frac{-x+s_2\cos\theta_2}{y-s_2\sin\theta_2} - \frac{x-s_1\cos\theta_1}{-y+s_1\sin\theta_1}} - b_{min,1} \end{bmatrix}$$

$$\mathbf{f}_4 = \begin{bmatrix} \dfrac{-b_{min,2} - b_{min,1}}{\frac{-x+s_2\cos\theta_2}{y-s_2\sin\theta_2} - \frac{x-s_1\cos\theta_1}{-y+s_1\sin\theta_1}} \\[2ex] \dfrac{-x+s_2\cos\theta_2}{y-s_2\sin\theta_2} \dfrac{-b_{min,2} - b_{min,1}}{\frac{-x+s_2\cos\theta_2}{y-s_2\sin\theta_2} - \frac{x-s_1\cos\theta_1}{-y+s_1\sin\theta_1}} + b_{min,1} \end{bmatrix}$$

and it can be seen that

$$\|\mathbf{f}_1\| = \|\mathbf{f}_3\|, \qquad \|\mathbf{f}_2\| = \|\mathbf{f}_4\| \tag{3.30}$$

Then, the maximum applicable force F_{max} is the norm of coordinates of the intersection point having the largest norm.

$$F_{max} = \max \left[\|\mathbf{f}_1\|, \quad \|\mathbf{f}_2\| \right] \tag{3.31}$$

The performance-to-safety index, μ, can be calculated by the ratio of F_{min} and F_{max}.

3.4.1.2 Mechanism with Force Limiters on the Distal Links

For this architecture, one has

$$\mathbf{J}^T = \frac{-1}{(\mathbf{p}-\mathbf{b}_1)^T\mathbf{E}(\mathbf{p}-\mathbf{b}_2)}\begin{bmatrix} l(\mathbf{p}-\mathbf{b}_1)^T\mathbf{E}\mathbf{e}_1(y-l\sin\theta_2) & l(\mathbf{p}-\mathbf{b}_1)^T\mathbf{E}\mathbf{e}_1(-x+l\cos\theta_1) \\ l(\mathbf{p}-\mathbf{b}_2)^T\mathbf{E}\mathbf{e}_2(-y+l\sin\theta_1) & l(\mathbf{p}-\mathbf{b}_2)^T\mathbf{E}\mathbf{e}_2(x-l\cos\theta_1) \\ s_1(y-l\sin\theta_2) & s_1(-x+l\cos\theta_2) \\ s_2(-y+l\sin\theta_1) & s_2(x-l\cos\theta_2) \end{bmatrix}$$

It can be seen that

$$\frac{j_{1x}}{j_{1y}}=\frac{j_{3x}}{j_{3y}}=\frac{y-l\sin\theta_2}{-x+l\cos\theta_2} \quad \text{and} \quad \frac{j_{2x}}{j_{2y}}=\frac{j_{4x}}{j_{4y}}=\frac{-y+l\sin\theta_1}{x-l\cos\theta_1}$$

which means that the four pairs of force boundary lines of the mechanism with force limiters on distal links are also parallel two by two.

The equations of force boundary lines, the maximum isotropic force F_{min} and the maximum applicable force F_{max} can be found with the same method that has been applied on the mechanism with force limiters on the proximal links.

3.4.2   3.4.2 Simplified Analysis for Singular Configurations

The force analysis for mechanisms with two torque limiters and two force limiters, one-dimensional workspace obtained with the constraint $\theta_1 = -\theta_2$ will be analyzed for degenerate situations. Indeed, in some cases the above defined force polygon can degenerate.

3.4.2.1 Mechanism with Force Limiters on the Proximal Links

From the above derivations, the force boundary equations can be written as

$$s_1(\mathbf{p}-\mathbf{b}_1)^T\mathbf{E}\mathbf{e}_1(y-s_2\sin\theta_2)f_y - s_1(\mathbf{p}-\mathbf{b}_1)^T\mathbf{E}\mathbf{e}_1(-x+s_2\cos\theta_2)f_x$$
$$\pm\tau_{1,max}(\mathbf{p}-\mathbf{b}_1)^T\mathbf{E}(\mathbf{p}-\mathbf{b}_2)=0 \tag{3.32}$$

$$s_2(\mathbf{p}-\mathbf{b}_2)^T\mathbf{E}\mathbf{e}_2(-y+s_1\sin\theta_1)f_y - s_2(\mathbf{p}-\mathbf{b}_2)^T\mathbf{E}\mathbf{e}_2(x-s_1\cos\theta_1)f_x$$
$$\pm\tau_{2,max}(\mathbf{p}-\mathbf{b}_1)^T\mathbf{E}(\mathbf{p}-\mathbf{b}_2)=0 \tag{3.33}$$

$$(\mathbf{p}-\mathbf{b}_1)^T\mathbf{e}_1(y-s_2\sin\theta_2)f_y - (\mathbf{p}-\mathbf{b}_1)^T\mathbf{e}_1(-x+s_2\cos\theta_2)f_x$$
$$\pm f_{1,max}(\mathbf{p}-\mathbf{b}_1)^T\mathbf{E}(\mathbf{p}-\mathbf{b}_2)=0 \tag{3.34}$$

$$(\mathbf{p}-\mathbf{b}_2)^T\mathbf{e}_2(-y+s_1\sin\theta_1)f_y - (\mathbf{p}-\mathbf{b}_1)^T\mathbf{e}_1(x-s_1\cos\theta_1)f_x$$
$$\pm f_{2,max}(\mathbf{p}-\mathbf{b}_1)^T\mathbf{E}(\mathbf{p}-\mathbf{b}_2)=0 \tag{3.35}$$

These four equations define the lines that constitute the boundaries of the force polygon.

Suppose $s_1 = s_2 = s$ and $\theta_1 = -\theta_2$, we have

$$\theta_y = \arccos\left(\frac{s\sin\theta_2}{l}\right) - \frac{\pi}{2} \tag{3.36}$$

and

$$\mathbf{p} = \begin{bmatrix} s\cos\theta_2 + l\cos\theta_y \\ s\sin\theta_2 + l\sin\theta_y \end{bmatrix} = \begin{bmatrix} s\cos\theta_2 + \sqrt{l^2 - s^2\sin^2\theta_2} \\ 0 \end{bmatrix} \tag{3.37}$$

– In Eqn. (3.32), the common factor of f_y and f_x can be simplified as

$$s_1(\mathbf{p} - \mathbf{b}_1)^T\mathbf{E}\mathbf{e}_1 = s_1(y\cos\theta_1 - x\sin\theta_1)$$
$$= s_1 x\sin\theta_2$$
$$= s(s\sin\theta_2\cos\theta_2 + \sin\theta_2\sqrt{l^2 - s^2\sin^2\theta_2})$$

When 1) $\theta_2 = 0$ or 2) $s = l$ and $\theta_2 = \frac{\pi}{2}$, the above expression is equal to 0.
1) When $\theta_2 = 0$, $\mathbf{p} = [s + l,\ 0]^T$, and

$$\begin{aligned}(\mathbf{p} - \mathbf{b}_1)^T\mathbf{E}(\mathbf{p} - \mathbf{b}_2) &= \begin{bmatrix} l & 0 \end{bmatrix}\begin{bmatrix} 0 & -1 \\ 1 & 0 \end{bmatrix}\begin{bmatrix} l \\ 0 \end{bmatrix} \\ &= \begin{bmatrix} 0 & -l \end{bmatrix}\begin{bmatrix} l \\ 0 \end{bmatrix} \\ &= 0\end{aligned} \tag{3.38}$$

2) When $s = l$ and $\theta_2 = \frac{\pi}{2}$, $\mathbf{p} = [0,\ 0]^T$, and

$$\begin{aligned}(\mathbf{p} - \mathbf{b}_1)^T\mathbf{E}(\mathbf{p} - \mathbf{b}_2) &= \begin{bmatrix} -s\cos\theta_1 & -s\sin\theta_1 \end{bmatrix}\begin{bmatrix} 0 & -1 \\ 1 & 0 \end{bmatrix}\begin{bmatrix} -s\cos\theta_2 \\ -s\sin\theta_2 \end{bmatrix} \\ &= \begin{bmatrix} s\sin\theta_2 & s\cos\theta_2 \end{bmatrix}\begin{bmatrix} -s\cos\theta_2 \\ -s\sin\theta_2 \end{bmatrix} \\ &= -2s^2\cos\theta_2\sin\theta_2 \\ &= 0\end{aligned} \tag{3.39}$$

– Similarly, in Eqn. (3.33), the common factor of f_y and f_x can be simplified as

$$s_2(\mathbf{p} - \mathbf{b}_2)^T\mathbf{E}\mathbf{e}_2 = s_2(y\cos\theta_2 - x\sin\theta_2)$$
$$= s(-s\sin^2\theta_2 - \sin\theta_2\sqrt{l^2 - s^2\sin^2\theta_2})$$

When 1) $\theta_2 = 0$ and $s = -l$ and $\theta_2 = \frac{\pi}{4}$, the above expression equals to 0.
1) When $\theta_2 = 0$, the analysis is the same as Eqn. (3.32).
2) When $s = -l$ and $\theta_2 = \frac{\pi}{4}$, $\mathbf{p} = \mathbf{0}$ so we have $(\mathbf{p} - \mathbf{b}_1)^T\mathbf{E}(\mathbf{p} - \mathbf{b}_2) = 0$
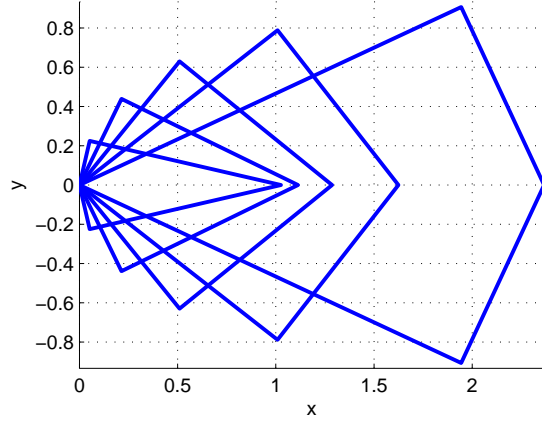
Figure 3.3: One kind of singularities.

– In Eqn. (3.34) and Eqn. (3.35), the common factors of f_y and f_x are

$$(\mathbf{p} - \mathbf{b}_1)^T \mathbf{e}_1 = (\mathbf{p} - \mathbf{b}_2)^T \mathbf{e}_2$$
$$= \cos\theta_2 \sqrt{l^2 - s^2 \sin^2\theta_2} - s\sin^2\theta_2 \tag{3.40}$$

when $s = l\cot\theta_2$, $(\mathbf{p} - \mathbf{b}_1)^T \mathbf{e}_1 = (\mathbf{p} - \mathbf{b}_2)^T \mathbf{e}_2 = 0$ and $\mathbf{p} = \left[\frac{l}{\sin\theta_2},\ 0\right]^T$. And

$$(\mathbf{p} - \mathbf{b}_1)^T \mathbf{E}(\mathbf{p} - \mathbf{b}_2) = 2l^2 \cos\theta_2 \sin\theta_2 \tag{3.41}$$

Equations (3.34) and (3.35) degenerate and they cannot be used as the force boundary. The corresponding degenerate configuration is represented in Fig. 3.3. This situation occurs when $OB_2 \perp B_2P$ and $OB_1 \perp B_1P$.

3.4.2.2 Mechanism with Force Limiters on the Distal Links

For the mechanism with force limiter on the distal links, the analysis is similar.
– Torques τ_1 and τ_2 cannot give out the boundary equations when $(\mathbf{p} - \mathbf{b}_1)^T \mathbf{E}\mathbf{e}_1 = 0$ or $(\mathbf{p} - \mathbf{b}_2)^T \mathbf{E}\mathbf{e}_2 = 0$ which means $OB_1 \perp B_1P$ or $OB_2 \perp B_2P$ respectively.
– Forces f_1 and f_2 cannot give out the boundary equations when $s_1 = 0$ or $s_2 = 0$.

3.4.3   3.4.3 Simplified Analysis of the Force Capabilities

The one-dimensional workspace obtained with the constraint $\theta_1 = -\theta_2$ will now be analyzed for the special case for which it is assumed that the quadrilateral AB_1PB_2 is a parallelogram which means that $s_1 = s_2 = l$. The force capabilities of the two mechanisms are found in the following.

3.4.3.1 Mechanism with Force Limiters on the Proximal Links

For the mechanism with force limiters on the proximal links, when $\theta_2 = -\theta_1 = \theta$ and $s_1 = s_2 = l$, the position of joints B_1, B_2 and the position of the end-effector are

$$\mathbf{b}_1 = \begin{bmatrix} l\cos\theta \\ -l\sin\theta \end{bmatrix}, \quad \mathbf{b}_2 = \begin{bmatrix} l\cos\theta \\ l\sin\theta \end{bmatrix}, \quad \mathbf{p} = \begin{bmatrix} 2l\cos\theta \\ 0 \end{bmatrix}.$$

Then, the Jacobian matrices can be calculated as

$$\mathbf{A}^{-1} = \begin{bmatrix} \frac{1}{2l\cos\theta} & \frac{1}{2l\cos\theta} \\ \frac{1}{2l\sin\theta} & -\frac{1}{2l\sin\theta} \end{bmatrix}, \quad \mathbf{B} = \begin{bmatrix} l^2\sin 2\theta & 0 & l\cos 2\theta & 0 \\ 0 & -l^2\sin 2\theta & 0 & l\cos 2\theta \end{bmatrix},$$

and

$$\mathbf{J} = \mathbf{A}^{-1}\mathbf{B} = \begin{bmatrix} l\sin\theta & -l\sin\theta & \frac{\cos 2\theta}{2\cos\theta} & \frac{\cos 2\theta}{2\cos\theta} \\ l\cos\theta & l\cos\theta & \frac{\cos 2\theta}{2\sin\theta} & -\frac{\cos 2\theta}{2\sin\theta} \end{bmatrix} \tag{3.42}$$

It can be seen that

$$\frac{j_{1x}}{j_{1y}} = \frac{j_{3x}}{j_{3y}} = -\frac{j_{2x}}{j_{2y}} = -\frac{j_{4x}}{j_{4y}} = \frac{\sin\theta}{\cos\theta} \tag{3.43}$$

which means that the force polygon is a diamond.

If the external force is represented with $\mathbf{F} = F[\cos\phi, \quad \sin\phi]^T$, the vector of joint forces and torques can be found as

$$\boldsymbol{\tau} = F \begin{bmatrix} l\sin(\phi+\theta) \\ l\sin(\phi-\theta) \\ \cot 2\theta\sin(\phi+\theta) \\ -\cot 2\theta\sin(\phi-\theta) \end{bmatrix} \tag{3.44}$$

The force boundary equations are

$$f_y = \frac{\cos\theta}{\sin\theta}f_x \pm \frac{\tau_{1,max}}{l\sin\theta} \tag{3.45}$$

$$f_y = -\frac{\cos\theta}{\sin\theta}f_x \pm \frac{\tau_{2,max}}{l\sin\theta} \tag{3.46}$$

$$f_y = \frac{\cos\theta}{\sin\theta}f_x \pm \frac{2\cos\theta f_{1,max}}{\cos 2\theta} \tag{3.47}$$

$$f_y = -\frac{\cos\theta}{\sin\theta}f_x \pm \frac{2\cos\theta f_{2,max}}{\cos 2\theta} \tag{3.48}$$

where $\tau_{i,max}$, $f_{i,max}$, $i = 1, 2$ are the limit torque or limit force of the ith revolute or prismatic joint.

The maximum external force which can be applied from all directions is

$$F_{min} = \min\left(\begin{bmatrix} \frac{\tau_{1,max}}{l}, & \frac{\tau_{2,max}}{l}, & |\frac{f_{1,max}\sin 2\theta}{\cos 2\theta}|, & |\frac{f_{2,max}\sin 2\theta}{\cos 2\theta}| \end{bmatrix} \right). \tag{3.49}$$

If $\tau_{1,max} = \tau_{2,max} = \tau_{max}$ and $f_{1,max} = f_{2,max} = f_{max}$, the pitch of the lines which form the force polygon is

$$b_{min} = \min \left(\left[\begin{array}{cc} \frac{\tau_{max}}{l \sin \theta}, & \frac{2 \cos \theta f_{max}}{\cos 2\theta} \end{array} \right] \right). \tag{3.50}$$

The coordinates of the vertices of the force polygon is

$$(0, \ \pm b_{min}), \qquad (\pm \tan \theta b_{min}, 0) \tag{3.51}$$

The maximum force which can applied at the end-effector is

$$F_{max} = \begin{cases} b_{min} = \min \left(\left[\begin{array}{cc} \frac{\tau_{max}}{l \sin \theta}, & \frac{2 \cos \theta f_{max}}{\cos 2\theta} \end{array} \right] \right), & \text{when} \quad \theta_1 \in (0, \frac{\pi}{4}], \\[3mm] \tan \theta b_{min} = \min \left(\left[\begin{array}{cc} \frac{\tau_{max}}{l \cos \theta}, & -\frac{2 \sin \theta f_{max}}{\cos 2\theta} \end{array} \right] \right), & \text{when} \quad \theta_1 \in [\frac{\pi}{4}, \frac{\pi}{2}). \end{cases} \tag{3.52}$$

Then, the force effectiveness μ can then be found with the ratio of F_{min} and F_{max}.

$$\mu = \frac{F_{min}}{F_{max}} \tag{3.53}$$

3.4.3.2 Mechanism with Force Limiters on the Distal Links

For the mechanism with force limiters on the distal links, when $\theta_2 = -\theta_1 = \theta$ and $s_1 = s_2 = l$, the expression for the position of the joints B_1, B_2 and the position of the end-effector are the same as these obtained with the mechanism with force limiters on the proximal links. The Jacobian matrices are

$$\mathbf{A}^{-1} = \left[\begin{array}{cc} \frac{1}{2l \cos \theta} & \frac{1}{2l \cos \theta} \\[2mm] \frac{1}{2l \sin \theta} & -\frac{1}{2l \sin \theta} \end{array} \right], \quad \mathbf{B} = \left[\begin{array}{cccc} l^2 \sin 2\theta & 0 & l & 0 \\[2mm] 0 & -l^2 \sin 2\theta & 0 & l \end{array} \right],$$

$$\mathbf{J} = \mathbf{A}^{-1}\mathbf{B} = \left[\begin{array}{cccc} l \sin \theta & -l \sin \theta & \frac{1}{2 \cos \theta} & \frac{1}{2 \cos \theta} \\[2mm] l \cos \theta & l \cos \theta & \frac{1}{2 \sin \theta} & -\frac{1}{2 \sin \theta} \end{array} \right] \tag{3.54}$$

It can be seen that the Jacobian matrix $\mathbf{J}$ for the mechanism with force limiters on the distal links and the Jacobian matrix $\mathbf{J}$ for the mechanism with force limiters on the proximal links only have a factor difference on the third and fourth columns. The force boundary equations, the maximum isotropic force F_{min} and the maximum applicable force F_{max} can be found out easily. Then, the force effectiveness μ can be obtained.

3.5   Numerical Examples

The force boundary lines for the mechanism with force limiters both on proximal links and on distal links are four pairs of parallel straight lines. Since two of the four pairs are parallel to

each other, the other two pairs are also parallel to each other. Examples are now provided to illustrate these results. Consider a mechanism with force limiters on the proximal links.

Suppose $l_1 = l_2 = 1$, $\tau_{1,max} = \tau_{2,max} = 1$, $f_{1,max} = f_{2,max} = 1$, and $s_1 = s_2 = s = 1$, $-\theta_1 = \theta_2 = \theta$, the force polygons for $\theta = \frac{\pi}{3}$, $\theta = \frac{\pi}{4}$ and $\theta = \frac{\pi}{6}$ are shown in Fig. 3.4.

Suppose $l_1 = l_2 = 1$, $\tau_{1,max} = \tau_{2,max} = 1$, $f_{1,max} = f_{2,max} = 1$, $s_1 = s_2 = s = 1$, and $-\theta_1 = \theta_2 = \theta$, for different values of θ_2, the maximum isotropic force F_{min}, the maximum applicable force F_{max} and the index μ are ploted in Fig. 3.5.

Suppose $l_1 = l_2 = 1$, $\tau_{1,max} = \tau_{2,max} = 1$, $f_{1,max} = f_{2,max} = 1$, $-\theta_1 = \theta_2 = \frac{pi}{4}$, and $s_1 = s_2 = s$, for different values of s, the minimum force, the maximum force and the index μ are ploted in Fig. 3.6.

3.6   Conclusion

The force characteristics of the planar 2-DOF mechanism with force limiters in the proximal links and the mechanism with force limiters in the distal links are analyzed in this chapter. Two torque limiters are mounted on the actuators and two force limiters are located on the links in order to produce a feasible force polygon at the end-effector. Similarly to the symmetric mechanism analyzed in the preceding chapter, the most favorable force polygon that can be achieved is square for both of these mechanisms with force limiters. That is because the force polygon is formed by only two pairs of parallel lines.
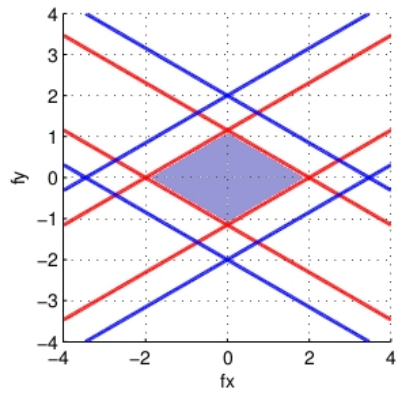
(a) $\theta = \frac{\pi}{3}$
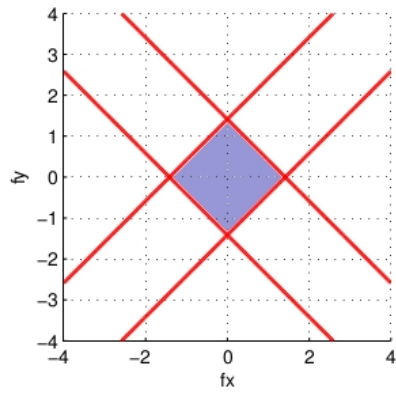
(b) $\theta = \frac{\pi}{4}$
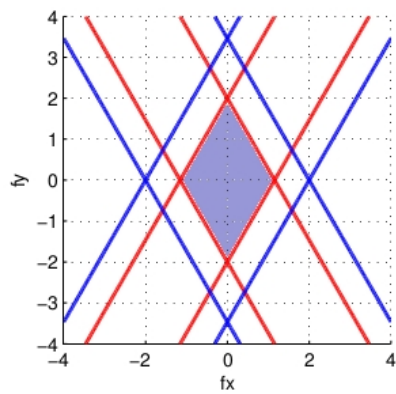
(c) $\theta = \frac{\pi}{6}$

Figure 3.4: Force polygons for different configurations.
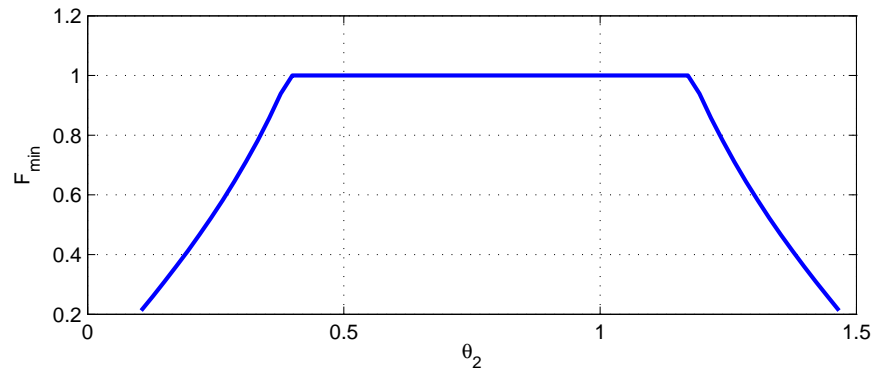
(a) maximum isotropic force F_{min}
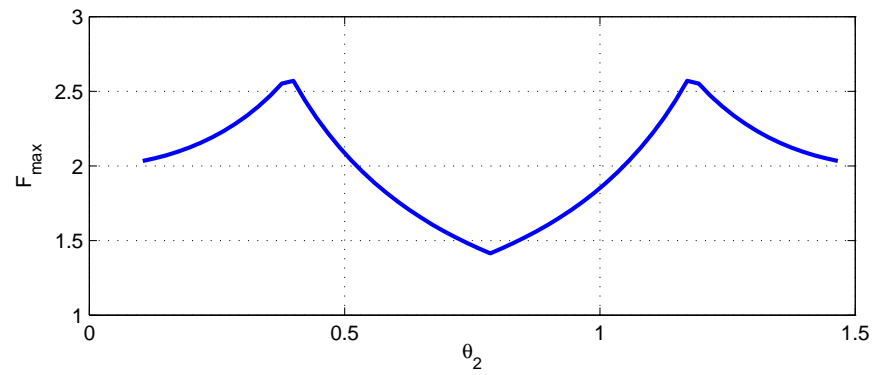
(b) maximum applicable force F_{max}
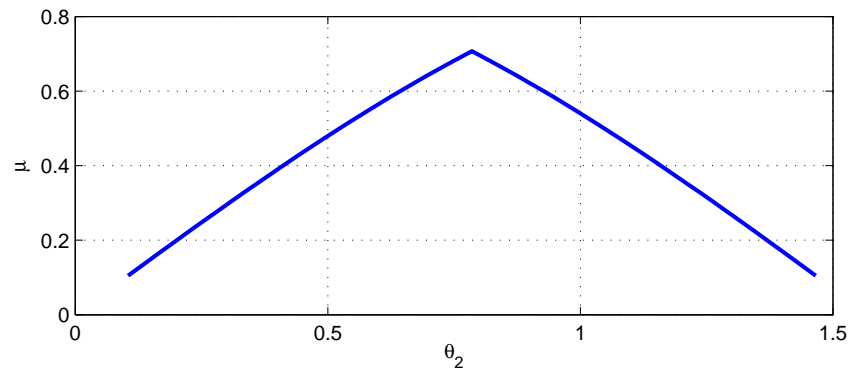
(c) index μ

Figure 3.5: The minimum force, the maximum force and the index μ as a function of θ_2.
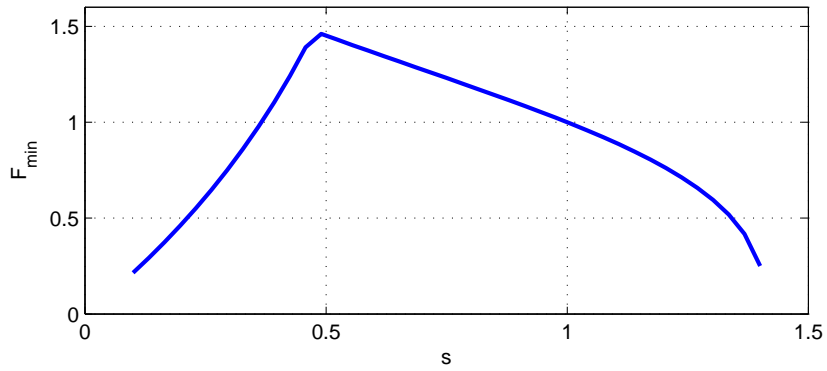
(a) maximum isotropic force F_{min}
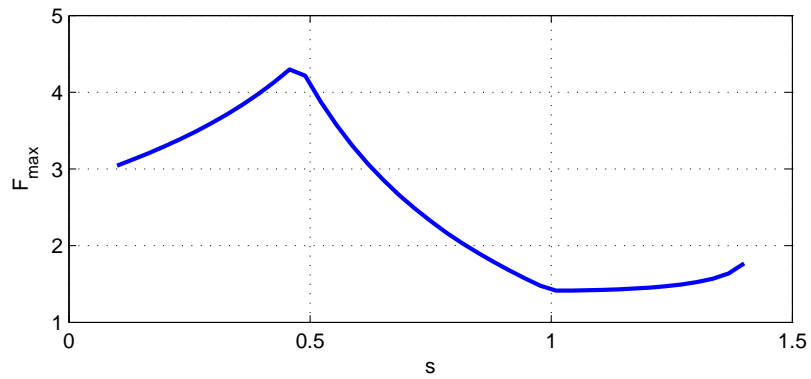
(b) maximum applicable force F_{max}
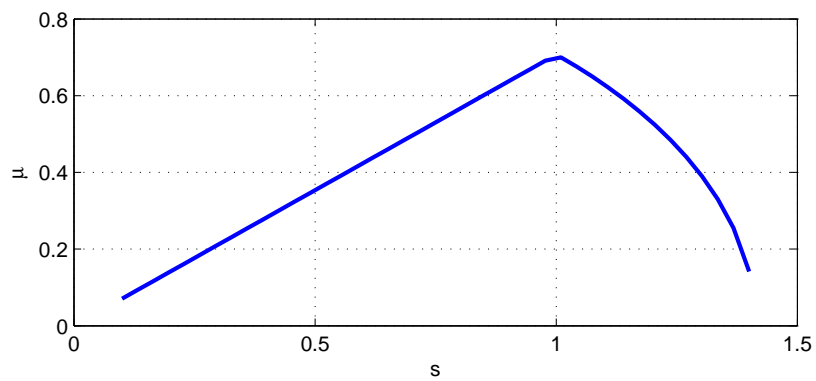
(c) index μ

Figure 3.6: The minimum force, the maximum force and the index μ as a function of s.

Chapter 4

Dynamic Capabilities of the Tripteron and Quadrupteron Parallel Manipulators

Based on the dynamic models for the tripteron, a three-degree-of-freedom (DOF) translational parallel manipulator and the quadrupteron, a 4-DOF Schönflies-motion parallel manipulator, this chapter determines the acceleration range or the external force range of the end-effector for given security considerations. The architecture and kinematics of the tripteron and quadrupteron are briefly recalled at first. Considering each link and slider system as a single body, approximate dynamic models are derived based on the Newton-Euler approach and Lagrange equations. For a given range of actuating forces, the range of the acceleration of the end effector and the feasible external force can be found. Numerical examples are provided in the end.

4.1 Introduction

The tripteron is a 3-DOF translational parallel robot with fully-decoupled input-output equations [80] while the quadrupteron is a partially decoupled robot with Schöenflies motions [81, 82]. Other works have also targeted the development of decoupled parallel manipulators [83–85].

For the traditional parallel manipulators, the dynamic analysis is a complex task due to the numerous constraints imposed by the closed kinematic loops. Still, many works can be found on the dynamics of parallel manipulators [86–88]. Several approaches have been applied to the dynamic analysis of parallel manipulators. They can be classified mainly into four categories: Newton-Euler method [89,93], Lagrange method [90], Kane's method [91] and the virtual work principle [92].

The dynamic model for the multipteron manipulators might be simpler than the traditional manipulators due to the compactness of the architectures. Reference [93] proposed compact dynamic models for the tripteron and the quadrupteron manipulators. The dynamic model is obtained by applying the Newton-Euler approach on each of the moving bodies composing the manipulator. It is shown that, by a judicious choice of the solution strategy, the model can be made computationally inexpensive and conceptually simple. However, the dynamic models can be approximated simply due to the decoupling characteristics of the manipulators. It is intended to obtain an approximate dynamic model by considering each leg and the corresponding actuator of the manipulators as a single body. Then, simplified and more compact but reasonably accurate dynamic models can be established. The relationships between the accelerations, the actuating forces and the external forces can then be established simply.

In this chapter, the external force range of the end effector of the tripteron and quadrupteron manipulators are found for a given actuating force limit. First, the architecture and kinematics of the tripteron and the quadrupteron are briefly recalled. Then, the dynamic model is obtained based on the Newton-Euler approach and Lagrange equations. The feasible external force of the end effector for the tripteron and quadrupteron manipulators can be found based on these dynamic models.

4.2 Architecture and Kinematics of the Manipulators

4.2.1 4.2.1 Tripteron Manipulator

The tripteron is a parallel mechanism composed of three legs, each consisting of a 4-DOF serial mechanism whose links are connected by, from base to platform, an actuated prismatic
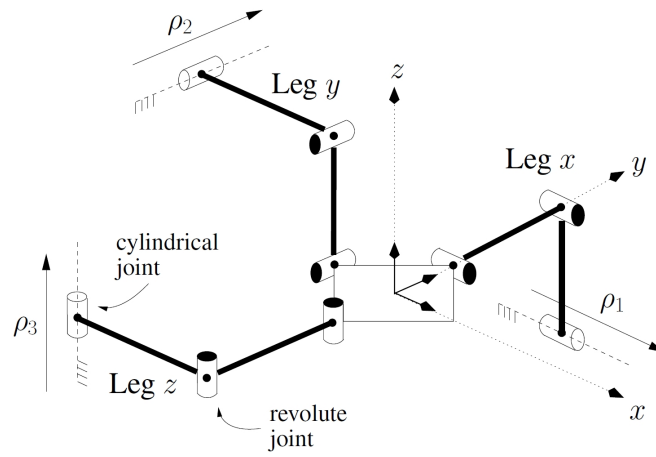
(a) Schematic representation

(b) The phototype

Figure 4.1: The tripteron: a 3-DOF translational parallel mechanism, taken from [93].

joint fixed to the base, and three revolute joints whose axes are parallel to each other but not orthogonal to the direction of the prismatic joint. The terminal revolute joints of the three legs are connected to the mobile platform in such a manner that their axes are orthogonal. Although several versions of the tripteron are possible [80], the most notable is the orthogonal tripteron, shown in Fig. 4.1. In this version, the axes of the actuated prismatic joints are orthogonal to each other and the axes of the passive revolute joints on a given leg are parallel to the direction of the prismatic joint of the leg. Each of the actuators controls the motion of the platform in one of the Cartesian directions. The manipulator is singularity-free and completely decoupled: its Jacobian matrix is equal to the identity matrix, it is globally isotropic and, with a proper geometric design of the legs, its workspace is a parallelepiped. Its kinematics is equivalent to that of a serial so-called Cartesian manipulator which consists of three orthogonal prismatic sliders mounted in series. The inverse and direct kinematic problem of

the (orthogonal) tripteron can be written as

$$\rho_1 = x, \quad \rho_2 = y, \quad \rho_3 = z, \tag{4.1}$$

where ρ_1, ρ_2 and ρ_3 denote the actuated joint coordinates, that is to say the linear displacement of the actuators, while x, y and z are the Cartesian coordinates of the moving platform.

4.2.2 4.2.2 Quadrupteron Manipulator

The general architecture of the 4-PRRU mechanism on which the quadrupteron manipulator is based consists of a platform connected to a fixed base by four legs each having five joints namely, from base to platform, a P joint and four R joints. The axes of the last two revolute joints intersect, and the latter can thereby be replaced by a universal or Hooke joint, noted U. The P joints, mounted directly on the base, are the only actuated joints. The joints in one leg are numbered from 1 to 5 from the actuator to the moving platform. In order to produce the Schönflies motions and to be drivable by the prismatic actuators, the following geometric constraints must be satisfied: (i) the axes of the four R joints attached to the moving platform are all parallel; (ii) the axes of joints 2, 3, and 4 within a given leg are all parallel; (iii) the axes of joints 1 and 2 within a same leg are not orthogonal to each other; (iv) the axes of joints 2 of the four legs are not all parallel to a plane; (v) the axes of joints 2 and 5 are not orthogonal to each other in at least one of the legs.

Several versions of the quadrupteron are possible [81]. Arguably the most interesting architecture is the one in which the linear actuators are mounted orthogonally (similarly to the orthogonal tripteron). This geometric arrangement, represented in Fig. 4.2, leads to a partial decoupling of the motion. The inverse kinematics simplifies to

$$\rho_1 = x + s_{x1}\cos\phi - s_{y1}\sin\phi - r_{x1}, \tag{4.2}$$
$$\rho_2 = y + s_{x2}\sin\phi + s_{y2}\cos\phi - r_{y2}, \tag{4.3}$$
$$\rho_3 = z + s_{z3} - r_{z3}, \tag{4.4}$$
$$\rho_4 = y + s_{x4}\sin\phi + s_{y4}\cos\phi - r_{y4}, \tag{4.5}$$

where $\mathbf{s}_i = [s_{xi}, \ s_{yi}, \ s_{zi}]^T$, $i = 1, 2, 3, 4$, is the vector connecting the origin of the moving frame attached to the platform to the intersection of the axes of the last two R joints of leg i and $\mathbf{r}_i = [r_{xi}, \ r_{yi}, \ r_{zi}]^T$ is the vector connecting the origin of the fixed frame located on the base to the reference point ($\rho_i = 0$) on the axis of the prismatic joint of the ith leg. Variables ρ_1 to ρ_4 are the actuated joint variables, vector $\mathbf{p} = [x, \ y, \ z]^T$ is the position vector of the origin of the moving frame with respect to the origin of the fixed frame and ϕ is the angle representing the rotation of the platform with respect to the base.

The velocity equations of the quadrupteron can be written as

$$\mathbf{Jt} = \mathbf{K}\dot{\rho}, \tag{4.6}$$
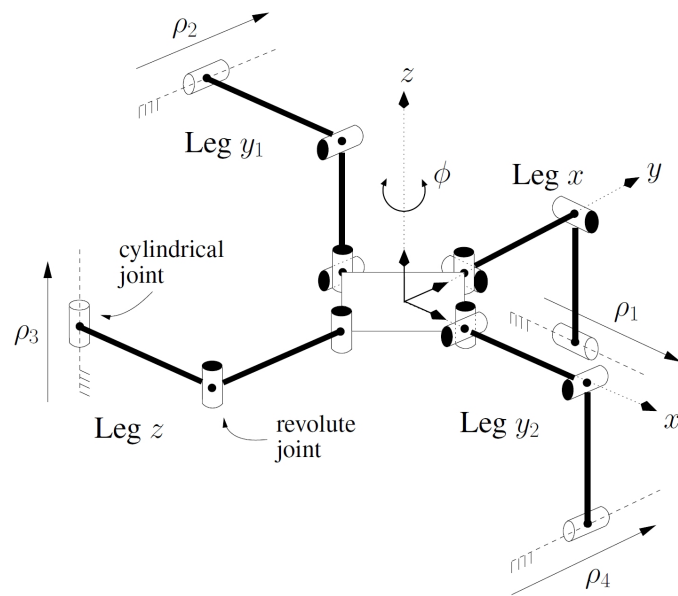
(a) Schematic representation
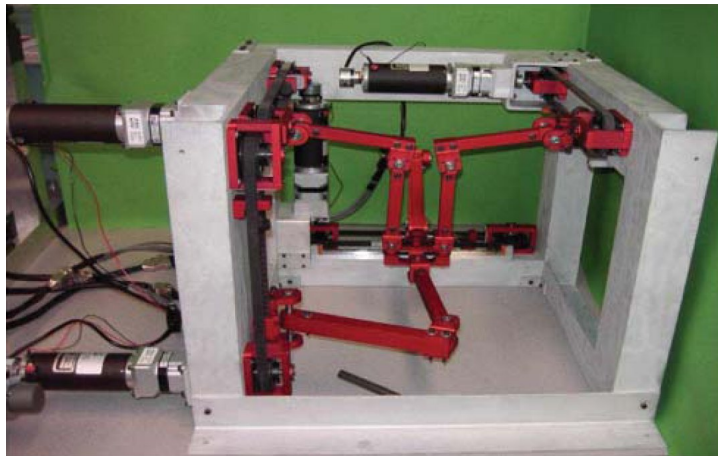
(b) The phototype

Figure 4.2: The quadrupteron: a 4-DOF Schönflies-motion parallel mechanism, taken from [93].

where $\mathbf{t} = [\dot{\mathbf{p}}^T, \dot{\phi}]^T$ is the four-dimensional vector of Cartesian velocities, $\dot{\boldsymbol{\rho}} = [\dot{\rho}_1, \dot{\rho}_2, \dot{\rho}_3, \dot{\rho}_4]^T$ is the vector of actuated joint velocities and $\mathbf{J}$ and $\mathbf{K}$ are 4×4 Jacobian matrices. With the orthogonal geometry, matrix $\mathbf{K}$ becomes the identity matrix while matrix $\mathbf{J}$ simplifies to

$$\mathbf{J} = \begin{bmatrix} 1 & 0 & 0 & (-s_{x1}\sin\phi - s_{y1}\cos\phi) \\ 0 & 1 & 0 & (s_{x2}\cos\phi - s_{y2}\sin\phi) \\ 0 & 0 & 1 & 0 \\ 0 & 1 & 0 & (s_{x4}\cos\phi - s_{y4}\sin\phi) \end{bmatrix},$$

and Jacobian matrix $\mathbf{J}$ becomes singular for only two orientations, that is those for which

$$\tan\phi = \frac{s_{x2} - s_{x4}}{s_{y2} - s_{y4}}. \tag{4.7}$$

With the velocity equations Eqn. (4.6), the acceleration equations can be found as

$$\mathbf{K}\ddot{\boldsymbol{\rho}} = \mathbf{J}\dot{\mathbf{t}} + \dot{\mathbf{J}}\mathbf{t}, \tag{4.8}$$

where

$$\dot{\mathbf{J}} = \begin{bmatrix} 0 & 0 & 0 & (-s_{x1}\cos\phi + s_{y1}\sin\phi)\dot{\phi} \\ 0 & 0 & 0 & (-s_{x2}\sin\phi - s_{y2}\cos\phi)\dot{\phi} \\ 0 & 0 & 0 & 0 \\ 0 & 0 & 0 & (-s_{x4}\sin\phi - s_{y4}\cos\phi)\dot{\phi} \end{bmatrix}.$$

4.3   Approximate Dynamic Models and Force Analysis

4.3.1   4.3.1 Tripteron

Since each leg of the tripteron mechanism is constrained to be moving in a plane that translates along the actuated prismatic joint, it is possible to directly write Newton's equations for the entire leg in the direction of the prismatic joint. Strictly speaking, Newton's second law can only be applied on a single rigid body. However, because of the specific arrangement of the leg, it can be applied here to the entire leg, although only in the direction of the prismatic joint. Thus, it can be written as

$$\mathbf{f}_a = (m_p\mathbf{K} + \mathbf{M}_d)(\mathbf{a}_p - \mathbf{g}) + \mathbf{f}_e, \tag{4.9}$$

where $\mathbf{f}_a = [f_{ax}, f_{ay}, f_{az}]^T$ is the actuating force, $\mathbf{f}_e = [f_{ex}, f_{ey}, f_{ez}]^T$ is the external force, $\mathbf{K}$ is a 3×3 unit matrix, $\mathbf{M}_d = \mathrm{diag}[m_x, m_y, m_z]$ is the mass matrix for the legs, including the mass of the slider, the proximal link and the distal link, m_p and $\mathbf{a}_p$ are the mass and the acceleration of the end effector, and $\mathbf{g}$ is defined as $[0, 0, g]^T$ with g representing the gravitational acceleration.

This model is an approximation because it does not consider the motion of the intermediate links of leg induced by the motion of the other legs. However, in practice this effect is likely to be small because the intermediate links are small and light. The advantage of this approximation is that it makes the model very simple.

4.3.2 4.3.2 Quadrupteron

For the quadrupteron manipulator, Lagrange method and Newton-Euler approach are used to build the dynamic model. Similarly to the tripteron, the legs of the quadrupteron are also constrained to be moving in a plane that translates along the actuated prismatic joints. As an approximation, it is reasonable to consider the legs as a mass moving with the prismatic joints.

4.3.2.1 Lagrange Method

First, Lagrange method is used to establish the dynamic model. The kinetic energy and the gravitational potential energy of the manipulator can be expressed as

$$T = \frac{1}{2}m_p\dot{\mathbf{p}}^T\dot{\mathbf{p}} + \frac{1}{2}I\dot{\phi}^2 + \sum_{i=1}^{4}\frac{1}{2}m_i\dot{\rho_i}^2, \tag{4.10}$$

$$V = m_pgz + m_3g(\rho_3 + r_{z3}), \tag{4.11}$$

where m_p is the mass of the moving platform, I is the moment of inertia of the platform in the direction of the allowed rotation, m_i, $i = 1, 2, 3, 4$, is the mass of the ith leg.

Suppose the actuating force of the prismatic joints are $\mathbf{f}_a = [f_{\rho1},\ f_{\rho2},\ f_{\rho3},\ f_{\rho4}]^T$, according to the Lagrange equations, we have

$$\frac{d}{dt}\left(\frac{\partial L}{\partial\dot{\rho_i}}\right) - \frac{\partial L}{\partial\rho_i} = f_{\rho i}, \qquad i = 1, 2, 3, 4. \tag{4.12}$$

where $L = T - V$.

Observing the kinematic equations for the quadrupteron, it can be noticed that ϕ is related with ρ_1, ρ_2 and ρ_4, but it is independent from ρ_3, so one has

$$\frac{\partial L}{\partial\rho_3} = -(m_p + m_3)g, \tag{4.13}$$

and

$$\frac{\partial L}{\partial\rho_i} = \frac{\partial L}{\partial\phi}\frac{\partial\phi}{\partial\rho_i}, \qquad i = 1, 2, 4. \tag{4.14}$$

Calculating the partial derivative of Eqn. (4.2), Eqn. (4.3) and Eqn. (4.5) with respect to ρ_i, $i = 1, 2, 4$, one has

$$\mathbf{A} \begin{bmatrix} \frac{\partial x}{\partial \rho_1} \\ \frac{\partial y}{\partial \rho_1} \\ \frac{\partial \phi}{\partial \rho_1} \end{bmatrix} = \begin{bmatrix} 1 \\ 0 \\ 0 \end{bmatrix}, \quad \mathbf{A} \begin{bmatrix} \frac{\partial x}{\partial \rho_2} \\ \frac{\partial y}{\partial \rho_2} \\ \frac{\partial \phi}{\partial \rho_2} \end{bmatrix} = \begin{bmatrix} 0 \\ 1 \\ 0 \end{bmatrix}, \quad \mathbf{A} \begin{bmatrix} \frac{\partial x}{\partial \rho_4} \\ \frac{\partial y}{\partial \rho_4} \\ \frac{\partial \phi}{\partial \rho_4} \end{bmatrix} = \begin{bmatrix} 0 \\ 0 \\ 1 \end{bmatrix},$$

where

$$\mathbf{A} = \begin{bmatrix} 1 & 0 & (-s_{x1} \sin \phi - s_{y1} \cos \phi) \\ 0 & 1 & (s_{x2} \cos \phi - s_{y2} \sin \phi) \\ 0 & 1 & (s_{x4} \cos \phi - s_{y4} \sin \phi) \end{bmatrix}.$$

Then, the partial derivative of ϕ with respect to ρ_i, $i = 1, 2, 4$, can be calculated as

$$\frac{\partial \phi}{\partial \rho_1} = 0, \qquad \frac{\partial \phi}{\partial \rho_2} = \frac{1}{\Delta}, \qquad \frac{\partial \phi}{\partial \rho_4} = -\frac{1}{\Delta},$$

where $\Delta = (s_{x2} - s_{x4}) \cos \phi - (s_{y2} - s_{y4}) \sin \phi$. Calculating the partial derivative of L with respect to ϕ and substituting the expressions of $\dot{\rho}_i$ and $\ddot{\rho}_i$ to simplifiy the formula, one has

$$\frac{\partial L}{\partial \phi} = m_p \left[\frac{s_{x1}(s_{x2} - s_{x4}) + s_{y1}(s_{y2} - s_{y4})}{\Delta} \dot{x}\dot{\phi} + \frac{s_{x2}s_{y4} - s_{x4}s_{y2}}{\Delta} \dot{y}\dot{\phi} \right]$$
$$+ I \frac{(s_{x2} - s_{x4}) \sin \phi + (s_{y2} - s_{y4}) \cos \phi}{\Delta} \dot{\phi}^2.$$

Then, the partial derivative of L with respect to ρ_i, $i = 1, 2, 4$, can be found as

$$\frac{\partial L}{\partial \rho_1} = 0,$$
$$\frac{\partial L}{\partial \rho_2} = -\frac{\partial L}{\partial \rho_4} = m_p \left[\frac{s_{x1}(s_{x2} - s_{x4}) + s_{y1}(s_{y2} - s_{y4})}{\Delta^2} \dot{x}\dot{\phi} + \frac{s_{x2}s_{y4} - s_{x4}s_{y2}}{\Delta^2} \dot{y}\dot{\phi} \right]$$
$$+ I \frac{(s_{x2} - s_{x4}) \sin \phi + (s_{y2} - s_{y4}) \cos \phi}{\Delta^2} \dot{\phi}^2.$$

The expressions of the partial derivative of L with respect to $\dot{\rho}_i$ are deduced as

$$\frac{d}{dt} \left(\frac{\partial L}{\partial \dot{\rho}_1} \right) = (m_p + m_1)\ddot{x} - m_1(s_{x1} \sin \phi + s_{y1} \cos \phi)\ddot{\phi}$$
$$+ m_1(-s_{x1} \cos \phi + s_{y1} \sin \phi)\dot{\phi}^2$$

$$\frac{d}{dt} \left(\frac{\partial L}{\partial \dot{\rho}_2} \right) = \left[m_2(s_{x2} \cos \phi - s_{y2} \sin \phi) + \frac{I}{\Delta} \right] \ddot{\phi}$$
$$+ \frac{m_p}{\Delta}(s_{x1} \sin \phi + s_{y1} \cos \phi)\ddot{x} + \left[m_2 + \frac{m_p}{\Delta}(-s_{x4} \cos \phi + s_{y4} \sin \phi) \right] \ddot{y}$$
$$+ \frac{m_p}{\Delta^2} \left\{ [s_{x1}(s_{x2} - s_{x4}) + s_{y1}(s_{y2} - s_{y4})] \dot{x} + (s_{x2}s_{y4} - s_{x4}s_{y2})\dot{y} \right\} \dot{\phi} + \dot{\phi}^2$$
$$\left\{ \frac{I}{\Delta^2}[(s_{x2} - s_{x4}) \sin \phi + (s_{y2} - s_{y4}) \cos \phi] - m_2(s_{x2} \sin \phi + s_{y2} \cos \phi) \right\}$$

$$\frac{d}{dt}\left(\frac{\partial L}{\partial \dot{\rho}_3}\right) = (m_p + m_3)\ddot{z},$$

$$\frac{d}{dt}\left(\frac{\partial L}{\partial \dot{\rho}_4}\right) = \left[m_4(s_{x4}\cos\phi - s_{y4}\sin\phi) - \frac{I}{\Delta}\right]\ddot{\phi}$$
$$- \frac{m}{\Delta}(s_{x1}\sin\phi + s_{y1}\cos\phi)\ddot{x} + \left[m_4 + \frac{m}{\Delta}(s_{x2}\cos\phi - s_{y2}\sin\phi)\right]\ddot{y}$$
$$- \frac{m}{\Delta^2}\left\{[s_{x1}(s_{x2} - s_{x4}) + s_{y1}(s_{y2} - s_{y4})]\dot{x} + (s_{x2}s_{y4} - s_{x4}s_{y2})\dot{y}\right\}\dot{\phi} - \dot{\phi}^2$$
$$\left\{\frac{I}{\Delta^2}[(s_{x2} - s_{x4})\sin\phi + (s_{y2} - s_{y4})\cos\phi] + m_4(s_{x4}\sin\phi + s_{y4}\cos\phi)\right\}$$

Collecting the above terms, the expressions of actuating forces can be found with Eqn. (4.12).

4.3.2.2 Newton-Euler Approach

In the Lagrange method, the external force is not considered. Here, it is intended to find the dynamic model while considering the external force $\mathbf{f}_e = [f_{ex}, \ f_{ey}, \ f_{ez}, \tau_e]^T$. For the four moving directions, based on the Newton-Euler method, the dynamic equations can be established as

$$x: \qquad\qquad\qquad f_{\rho 1} = m_1\ddot{\rho}_1 + m_p\ddot{x} + f_{ex}, \qquad\qquad\qquad (4.15)$$

$$y: \qquad\qquad f_{\rho 2} + f_{\rho 4} = m_2\ddot{\rho}_2 + m_4\ddot{\rho}_4 + m_p\ddot{y} + f_{ey}, \qquad\qquad (4.16)$$

$$z: \qquad\qquad f_{\rho 3} = m_3\ddot{\rho}_3 + m_p\ddot{z} + f_{ez} + (m_p + m_3)g, \qquad\qquad (4.17)$$

$$\phi: \quad (f_{\rho 2} - m_2\ddot{\rho}_2)d_{y1} + (f_{\rho 4} - m_4\ddot{\rho}_4)d_{y2} - (f_{\rho 1} - m_1\ddot{\rho}_1)d_x = I\ddot{\phi} + \tau_e. \qquad (4.18)$$

where d_{y1} and d_{y2} are the moment arm applied by the links y_2 and y_4 to the end effector and they are the distances between the end of the link to the y axis. d_x is the moment arm applied by link x to the end effector and it is the distance between the end of the link to the x axis, and

$$d_{y1} = s_{x2}\cos\phi - s_{y2}\sin\phi,$$
$$d_{y2} = s_{x4}\cos\phi - s_{y4}\sin\phi,$$
$$d_x = s_{x1}\sin\phi + s_{y1}\cos\phi.$$

The above equations can be modified as

$$x: \quad f_{\rho 1} = (m_p + m_1)\ddot{x} - m_1(s_{x1}\sin\phi + s_{y1}\cos\phi)\ddot{\phi}$$
$$+ m_1(-s_{x1}\cos\phi + s_{y1}\sin\phi)\dot{\phi}^2 + f_{ex}, \quad (4.19)$$

$$y: f_{\rho 2} + f_{\rho 4} = (m_p + m_2 + m_4)\ddot{y} + [m_2(s_{x2}\cos\phi - s_{y2}\sin\phi)$$
$$+ m_4(s_{x4}\cos\phi - s_{y4}\sin\phi)]\ddot{\phi} - [m_2(s_{x2}\sin\phi + s_{y2}\cos\phi) \quad (4.20)$$
$$+ m_4(s_{x4}\sin\phi + s_{y4}\cos\phi)]\dot{\phi}^2 + f_{ey},$$

$$z: \quad f_{\rho 3} = (m_p + m_3)\ddot{z} + (m_p + m_3)g + f_{ez}, \quad (4.21)$$

$$\phi: \quad -d_x f_{\rho 1} + d_{y1} f_{\rho 2} + d_{y2} f_{\rho 4} = I\ddot{\phi} + m_1\ddot{\rho}_1 d_x + m_2\ddot{\rho}_2 d_{y1} + m_4\ddot{\rho}_4 d_{y2} + \tau_e. \quad (4.22)$$

Forces $f_{\rho 2}$ and $f_{\rho 4}$ can be solved for using Eqn. (4.20) and Eqn. (4.22) as

$$f_{\rho 2} = \left[\frac{I}{\Delta} + m_2(s_{x2}\cos\phi - s_{y2}\sin\phi)\right]\ddot{\phi} + \frac{m_p}{\Delta}(s_{x1}\sin\phi + s_{y1}\cos\phi)\ddot{x}$$
$$+ \left[m_2 - \frac{m_p}{\Delta}(s_{x4}\cos\phi - s_{y4}\sin\phi)\right]\ddot{y} - m_2(s_{x2}\sin\phi + s_{y2}\cos\phi)\dot{\phi}^2$$
$$+ \frac{\tau_e}{\Delta} - \frac{f_{ey}}{\Delta}(s_{x4}\cos\phi - s_{y4}\sin\phi) + \frac{f_{ex}}{\Delta}(s_{x1}\sin\phi + s_{y1}\cos\phi),$$

$$f_{\rho 4} = \left[-\frac{I}{\Delta} + m_4(s_{x4}\cos\phi - s_{y4}\sin\phi)\right]\ddot{\phi} - \frac{m}{\Delta}(s_{x1}\sin\phi + s_{y1}\cos\phi)\ddot{x}$$
$$+ \left[m_4 + \frac{m}{\Delta}(s_{x2}\cos\phi - s_{y2}\sin\phi)\right]\ddot{y} - m_4(s_{x4}\sin\phi + s_{y4}\cos\phi)\dot{\phi}^2$$
$$- \frac{\tau_e}{\Delta} + \frac{f_{ey}}{\Delta}(s_{x2}\cos\phi - s_{y2}\sin\phi) - \frac{f_{ex}}{\Delta}(s_{x1}\sin\phi + s_{y1}\cos\phi).$$

Using the above equations, the actuating forces which are required to support the acceleration and the external forces can be found. It has been verified that the expressions of the actuating forces obtained with the Newton-Euler approach with zero external force are the same as those obtained with the expressions obtained with the Lagrange method.

4.3.2.3 Compact Dynamic Model

The dynamic model for the platform of the quadrupteron obtained in [93] can be expressed as

$$\mathbf{t}_1\mathbf{d}_1 + \mathbf{t}_2\mathbf{d}_2 + \mathbf{t}_3\mathbf{d}_3 + \mathbf{t}_4\mathbf{d}_4 + \mathbf{w}_3 = \mathbf{I}_f\dot{\boldsymbol{\omega}} + \boldsymbol{\omega} \times \mathbf{I}_f\boldsymbol{\omega} + \boldsymbol{\tau}_e \quad (4.23)$$

where $\mathbf{I}_f$ is the inertia tensor of the platform, $\boldsymbol{\omega}$ is the angular velocity of the platform, $\dot{\boldsymbol{\omega}}$ is the angular acceleration of the platform, and $\mathbf{t}_i$ is the vector connecting the platform mass centre to the attachment point (centre of the spherical joint) of the ith leg,

$$\mathbf{t}_i = \begin{bmatrix} s_{xi}\cos\phi - s_{yi}\sin\phi \\ s_{xi}\sin\phi + s_{yi}\cos\phi \\ 0 \end{bmatrix}, \quad i = 1, 2, 3, 4.$$

Also the interaction forces between the legs and the platform — forces $\mathbf{d}_i$ — can be found as

$$\mathbf{d}_1 = \begin{bmatrix} f_{\rho 1} - m_1 \ddot{\rho}_1 \\ 0 \\ 0 \end{bmatrix}, \quad \mathbf{d}_2 = \begin{bmatrix} 0 \\ f_{\rho 2} - m_2 \ddot{\rho}_2 \\ 0 \end{bmatrix},$$

$$\mathbf{d}_3 = \begin{bmatrix} 0 \\ 0 \\ f_{\rho 3} - m_3 \ddot{\rho}_3 - m_3 g \end{bmatrix}, \quad \mathbf{d}_4 = \begin{bmatrix} 0 \\ f_{\rho 4} - m_4 \ddot{\rho}_4 \\ 0 \end{bmatrix}.$$

$\mathbf{w}_3$ has two non zero components, $\mathbf{w}_3 = [w_{3x}, w_{3y}, 0]^T$ and $\boldsymbol{\tau}_e = [0, 0, \tau_{ez}]^T$.

Suppose the moving platform is a regular shape plane (square), $\mathbf{I}_f$ has the forms like

$$\mathbf{I}_f = \begin{bmatrix} I_{xx} & I_{xy} & I_{xz} \\ I_{yx} & I_{yy} & I_{yz} \\ I_{zx} & I_{zy} & I_{zz} \end{bmatrix} = \begin{bmatrix} I_{xx} & 0 & 0 \\ 0 & I_{yy} & 0 \\ 0 & 0 & I_{zz} \end{bmatrix} \tag{4.24}$$

and

$$\boldsymbol{\omega} = \begin{bmatrix} 0 \\ 0 \\ \dot{\phi} \end{bmatrix} \tag{4.25}$$

For example, if the moving platform is a square with $\sqrt{2}s$ side length. As shown in Fig. 4.3, the inertia matrix for the $o - x'y'$ coordinate is

$$\mathbf{I}_{x'y'z'} = m \begin{bmatrix} \frac{(\sqrt{2}s)^2}{12} & 0 & 0 \\ 0 & \frac{(\sqrt{2}s)^2}{12} & 0 \\ 0 & 0 & \frac{2(\sqrt{2}s)^2}{12} \end{bmatrix} = m \begin{bmatrix} \frac{s^2}{6} & 0 & 0 \\ 0 & \frac{s^2}{6} & 0 \\ 0 & 0 & \frac{s^2}{3} \end{bmatrix} \tag{4.26}$$

Since the vectors expressed in $o - x'y'$ coordinate and in $o - xy$ coordinate has the relationship as

$$\mathbf{v} = \begin{bmatrix} x \\ y \\ z \end{bmatrix} = \begin{bmatrix} \cos \frac{\pi}{4} & \sin \frac{\pi}{4} & 0 \\ -\sin \frac{\pi}{4} & \cos \frac{\pi}{4} & 0 \\ 0 & 0 & 1 \end{bmatrix} \begin{bmatrix} x' \\ y' \\ z' \end{bmatrix} = \mathbf{T}\mathbf{v}' \tag{4.27}$$

Then, the inertial matrix with respect to coordinates $o - xy$ is

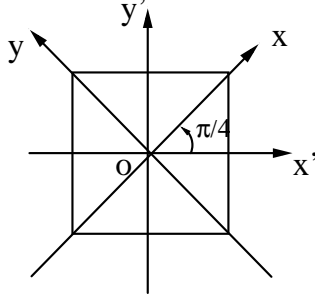$$\mathbf{I}_{xyz} = \mathbf{T}\mathbf{I}_{x'y'z'}\mathbf{T}^T = \mathbf{I}_{x'y'z'} \tag{4.28}$$

Figure 4.3: Transfer of the inertia matrix.

We have

$$
\mathbf{t}_1\mathbf{d}_1 = \begin{bmatrix} 0 \\ 0 \\ -(f_{\rho 1} - m_1\ddot{\rho}_1)(s_{x1}\cos\phi + s_{y1}\sin\phi) \end{bmatrix},
$$

$$
\mathbf{t}_2\mathbf{d}_2 = \begin{bmatrix} 0 \\ 0 \\ (f_{\rho 2} - m_2\ddot{\rho}_2)(s_{x2}\cos\phi - s_{y2}\sin\phi) \end{bmatrix},
$$

$$
\mathbf{t}_3\mathbf{d}_3 = \begin{bmatrix} (f_{\rho 3} - m_3\ddot{\rho}_3 - m_3 g)(s_{x3}\sin\phi + s_{y3}\cos\phi) \\ -(f_{\rho 3} - m_3\ddot{\rho}_3 - m_3 g)(s_{x3}\cos\phi - s_{y3}\sin\phi) \\ 0 \end{bmatrix},
$$

$$
\mathbf{t}_4\mathbf{d}_4 = \begin{bmatrix} 0 \\ 0 \\ (f_{\rho 4} - m_4\ddot{\rho}_4)(s_{x4}\cos\phi - s_{y4}\sin\phi) \end{bmatrix}.
$$

Then, Eqn. (4.23) can be written as three equations as

$$
(f_{\rho 3} - m_3\ddot{\rho}_3 - m_3 g)(s_{x3}\sin\phi + s_{y3}\cos\phi) + \omega_{3x} = 0 \tag{4.29}
$$

$$
-(f_{\rho 3} - m_3\ddot{\rho}_3 - m_3 g)(s_{x3}\cos\phi - s_{y3}\sin\phi) + \omega_{3y} = 0 \tag{4.30}
$$

$$
\begin{aligned}
&-(f_{\rho 1} - m_1\ddot{\rho}_1)(s_{x1}\cos\phi + s_{y1}\sin\phi) + (f_{\rho 2} - m_2\ddot{\rho}_2)(s_{x2}\cos\phi - s_{y2}\sin\phi) \\
&+ (f_{\rho 4} - m_4\ddot{\rho}_4)(s_{x4}\cos\phi - s_{y4}\sin\phi) = I_{zz}\ddot{\phi} + \tau_{ez}
\end{aligned} \tag{4.31}
$$

For the rotation direction, we get the same dynamic equation as the one obtained in the above section. If $\mathbf{I}_f$ is not a diagonal matrix, we have

$$
\mathbf{I}_f\dot{\boldsymbol{\omega}} + \boldsymbol{\omega} \times \mathbf{I}_f\boldsymbol{\omega} = \begin{bmatrix} I_{xz}\ddot{\phi} - I_{yz}\dot{\phi}^2 \\ I_{yz}\ddot{\phi} + I_{xz}\dot{\phi}^2 \\ I_{zz}\ddot{\phi} \end{bmatrix} \tag{4.32}
$$

Then, Eqn. (4.29) to Eqn. (4.31) become

$$
(f_{\rho 3} - m_3\ddot{\rho}_3 - m_3 g)(s_{x3}\sin\phi + s_{y3}\cos\phi) + \omega_{3x} + I_{xz}\ddot{\phi} - I_{yz}\dot{\phi}^2 = 0 \tag{4.33}
$$

$$- (f_{\rho 3} - m_3 \ddot{\rho}_3 - m_3 g)(s_{x3} \cos \phi - s_{y3} \sin \phi) + \omega_{3y} + I_{yz} \ddot{\phi} + I_{xz} \dot{\phi}^2 = 0 \qquad (4.34)$$

$$- (f_{\rho 1} - m_1 \ddot{\rho}_1)(s_{x1} \cos \phi + s_{y1} \sin \phi) + (f_{\rho 2} - m_2 \ddot{\rho}_2)(s_{x2} \cos \phi - s_{y2} \sin \phi)$$
$$+ (f_{\rho 4} - m_4 \ddot{\rho}_4)(s_{x4} \cos \phi - s_{y4} \sin \phi) = I_{zz} \ddot{\phi} + \tau_{ez} \qquad (4.35)$$

We still have the same dynamic model for the rotation direction. Combining the dynamic equations for the x, y, and z directions which have been expressed in the above section as Eqn. (4.15), Eqn. (4.16) and Eqn. (4.17), we can get the same expressions for the driving forces $f_{\rho i}$, $i = 1, 2, 3, 4$.

4.4 Force Capability Analysis

In this section, it is intended to analyze the force capabilities of the manipulators. Based on the dynamic models, the external force boundaries can be obtained with the given range of actuating forces.

4.4.1 4.4.1 Tripteron

Suppose the maximum and minimum force which can be provided by the actuators are $\mathbf{f}_{\rho,max} = [f_{\rho 1,max}, \ f_{\rho 2,max}, \ f_{\rho 3,max}]^T$ and $\mathbf{f}_{\rho,min} = [f_{\rho 1,min}, \ f_{\rho 2,min}, \ f_{\rho 3,min}]^T$, then the following relationships should be satisfied

$$\mathbf{f}_{\rho,min} \preceq \mathbf{f}_a \preceq \mathbf{f}_{\rho,max} \qquad (4.36)$$

where $\preceq$ means that the corresponding components should satisfy the relationship (componentwise inequality). Inequality (4.36) can be written as

$$\begin{aligned}
f_{\rho 1,min} - (m_p + m_x)a_x \ &\leq f_{ex} \leq \ f_{\rho 1,max} - (m_p + m_x)a_x, \\
f_{\rho 2,min} - (m_p + m_y)a_y \ &\leq f_{ey} \leq \ f_{\rho 2,max} - (m_p + m_y)a_y, \\
f_{\rho 3,min} - (m_p + m_z)(a_z - g) \ &\leq f_{ez} \leq \ f_{\rho 3,max} - (m_p + m_z)(a_z - g).
\end{aligned}$$

Suppose the legs have the same mass ($m_x = m_y = m_z$), in order to have the same force range for every direction of the external force while the end effector has the same acceleration in each direction, that is to say $a_x = a_y = a_z$, one has

$$\begin{aligned}
f_{\rho 1,min} &= f_{\rho 2,min} = f_{\rho 3,min} + (m_p + m_z)g, \\
f_{\rho 1,max} &= f_{\rho 2,max} = f_{\rho 3,max} + (m_p + m_z)g.
\end{aligned}$$

4.4.2   4.4.2 Quadrupteron

If the boundary of the actuating forces are

$$f_{\rho i,min} \le f_{\rho i} \le f_{\rho i,max}, \qquad i = 1, 2, 3, 4 \tag{4.37}$$

Based on Eqn. (4.15) to Eqn. (4.18), the following relationships should be satisfied

$$f_{\rho 1,min} - c_x \le f_{ex} \le f_{\rho 1,max} - c_x, \tag{4.38}$$

$$f_{\rho 2,min} + f_{\rho 4,min} - c_y \le f_{ey} \le f_{\rho 2,max} + f_{\rho 4,max} - c_y, \tag{4.39}$$

$$f_{\rho 3,min} - c_z \le f_{ez} \le f_{\rho 3,max} - c_z, \tag{4.40}$$

$$\min(F_\rho) - c_\tau \le \tau_e \le \max(F_\rho) - c_\tau \tag{4.41}$$

where

$$
\begin{aligned}
F_\rho &= -d_x f_{\rho 1} + d_{y1} f_{\rho 2} + d_{y2} f_{\rho 4}, \\
c_x &= m_1 \ddot{\rho}_1 + m\ddot{x}, \\
c_y &= m_2 \ddot{\rho}_2 + m_4 \ddot{\rho}_4 + m\ddot{y}, \\
c_z &= m_3 \ddot{\rho}_3 + m\ddot{z} + (m + m_3)g, \\
c_\tau &= I\ddot{\phi} + m_1 \ddot{\rho}_1 d_x + m_2 \ddot{\rho}_2 d_{y1} + m_4 \ddot{\rho}_4 d_{y2}.
\end{aligned}
$$

and

$$
\begin{aligned}
\ddot{\rho}_1 &= \ddot{x} + (-s_{x1}\sin\phi - s_{y1}\cos\phi)\ddot{\phi} + (-s_{x1}\cos\phi + s_{y1}\sin\phi)\dot{\phi}^2, \\
\ddot{\rho}_2 &= \ddot{y} + (s_{x2}\cos\phi - s_{y2}\sin\phi)\ddot{\phi} + (-s_{x2}\sin\phi - s_{y2}\cos\phi)\dot{\phi}^2, \\
\ddot{\rho}_3 &= \ddot{z}, \\
\ddot{\rho}_4 &= \ddot{y} + (s_{x4}\cos\phi - s_{y4}\sin\phi)\ddot{\phi} + (-s_{x4}\sin\phi - s_{y4}\cos\phi)\dot{\phi}^2,
\end{aligned}
$$

The extreme values of F_ρ depend on the configuration and the actuating force range of the three prismatic joints, where $\min(F_\rho)$ and $\max(F_\rho)$ are the minimum and maximum values of the expression $-d_x f_{\rho 1} + d_{y1} f_{\rho 2} + d_{y2} f_{\rho 4}$.

When the required acceleration are given for certain tasks, and the safety range of acceptable external force are proposed, then, the required actuating forces can be found.

4.5   Numerical Examples

For the tripteron manipulator, suppose the mass of the end effector is $m_p = 1$kg, the force boundaries of the force limiters in the x and y directions are -10N to 10N, the force boundaries of the force limiters in the z directions are $-10 - m_p g = -19.81$N to $10 - m_p g = 0.19$N, the
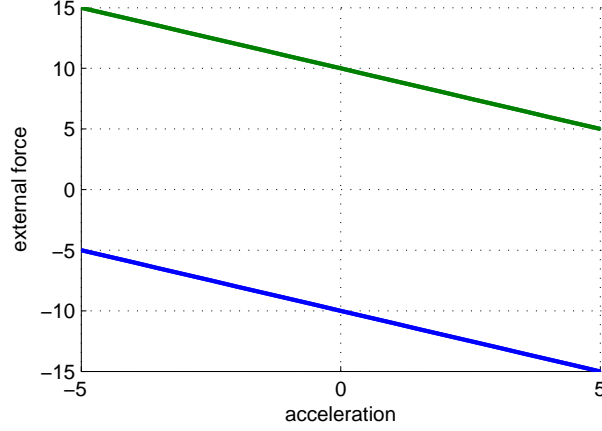
Figure 4.4: The range of the external force for the x, y and z directions.

range of the acceleration in the x, y and z directions are $a_x, a_y, a_z \in [-5, 5]\text{m/s}^2$, the range of the external force f_x, f_y and f_z can be found as Fig. 4.4.

For the quadrupteron, suppose the trajectory of the end effector is

$$
\begin{bmatrix} x \\ y \\ z \\ \phi \end{bmatrix} = \begin{bmatrix} a\cos(\omega_1 t) \\ a\sin(\omega_1 t) \\ b\cos(\omega_2 t) \\ c\cos(\omega_3 t) \end{bmatrix}, \quad \begin{bmatrix} \dot{x} \\ \dot{y} \\ \dot{z} \\ \dot{\phi} \end{bmatrix} = \begin{bmatrix} -a\omega_1 \sin(\omega_1 t) \\ a\omega_1 \cos(\omega_1 t) \\ -b\omega_2 \sin(\omega_2 t) \\ -c\omega_3 \sin(\omega_3 t) \end{bmatrix}, \quad \begin{bmatrix} \ddot{x} \\ \ddot{y} \\ \ddot{z} \\ \ddot{\phi} \end{bmatrix} = \begin{bmatrix} -a\omega_1^2 \cos(\omega_1 t) \\ -a\omega_1^2 \sin(\omega_1 t) \\ -b\omega_2^2 \cos(\omega_2 t) \\ -c\omega_3^2 \cos(\omega_3 t) \end{bmatrix}.
$$

and the actuating forces boundaries are $-F_{\rho 1,min} = F_{\rho 1,max} = 50$, $-F_{\rho 2,min} = F_{\rho 2,max} = -F_{\rho 4,min} = F_{\rho 4,max} = 50$, $-F_{\rho 3,min} = -50 + (10+1)g$, $F_{\rho 3,max} = 50 + (10+1)g$ When $s = 0.1$, $m = 10m_i = 1$, $I = \frac{1}{6}ms^2 = \frac{1}{600}$ and $a = b = 1$, $c = \frac{\pi}{2}$, $\omega_1 = \omega_2 = \omega_3 = \frac{\pi}{2}$, the external force range can be plotted as shown in Fig. 4.5.

4.6 Conclusion

Compact simplified and approximate dynamic models for the tripteron and quadrupteron manipulators are established in this chapter. The Newton-Euler method and Lagrange approach are used to find the dynamic models. Due to the compact architecture of the tripteron, the dynamic model can be used both in the inverse and forward problems. The dynamic force capabilities of the manipulators are analyzed based on the dynamic models. Given the actuating forces and the accelerations of the moving platform, the feasible external forces can be found.
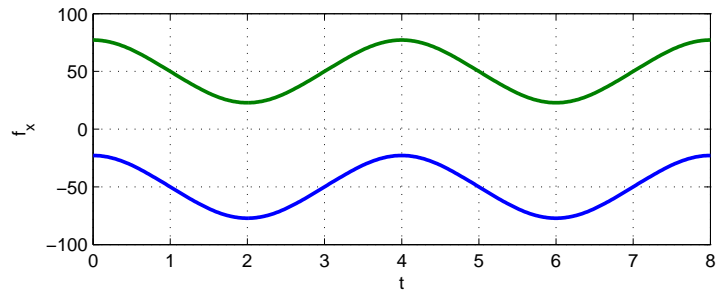
(a) external force boundary in x direction
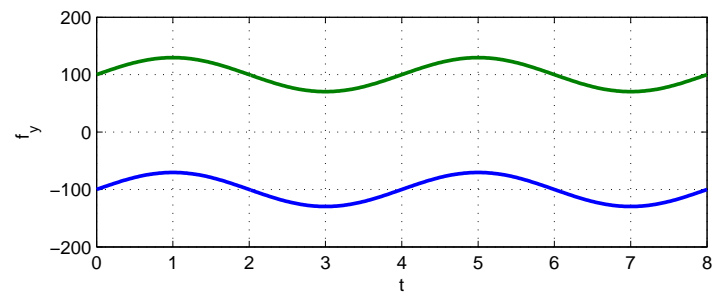
(b) external force boundary in y direction
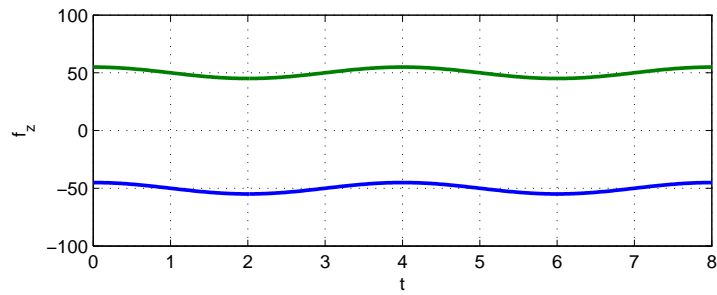
(c) external force boundary in z direction
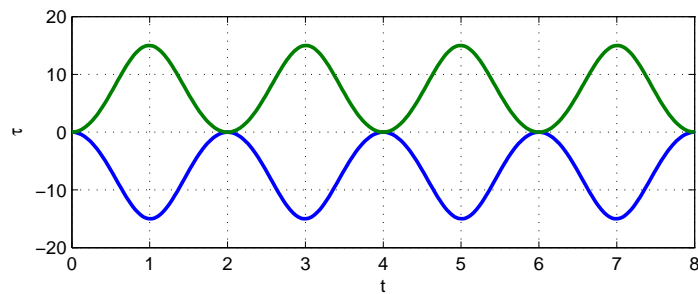
(d) external force boundary in τ direction

Figure 4.5: Force boundaries for the quadrupteron.

Chapter 5

Conclusions

The force characteristics of the symmetric and non-symmetric planar parallel mechanisms with four torque limiters and the parallel mechanisms with two torque limiters and two force limiters are analyzed. For the mechanisms with force limiters, the symmetric mechanisms, the non-symmetric mechanism with linkage FDP as a straight link and the non-symmetric mechanism with ABC and AEF as straight links, it can be seen that the best possible force polygon of the end effector is a square. Indeed, it is shown that there are two pairs of parallel lines form the force polygon.

For the non-symmetric mechanism with ABC and AEF as folding links, there are three pairs of parallel lines to form the force polygon. If the torque limiters are set properly, it is expected that this kind of mechanism can be designed to improve safety.

Compact simplified and approximate dynamic models for the tripteron and quadrupteron manipulators are also established in this thesis. The Newton-Euler method and Lagrange approach are used to find the dynamic models. Due to the compact architecture of the tripteron, the dynamic model can be used both for inverse and forward problems. The dynamic force capabilities of the manipulators are analyzed based on the dynamic models. Given the actuating forces and the accelerations of the moving platform, the feasible external forces can be found.

Future work concerns the mechanical design of the mechanisms in order to test the proposed approach. It is expected that the mechanisms proposed in this thesis can be used to improve the safety of robotic mechanisms in a context of human/robot cooperation.

Bibliography

[1] Gough, V.E., 1956-1957, "Contribution to discussion of papers on research in automobile stability, control and tyre performance", Proc. Auto Div. Inst. Mech. Eng.. 2

[2] Gough, V.E. and Whitehall, S.G., 1962, "Universal tire test machine", In Proceedings 9th Int. Technical Congress F.I.S.I.T.A., Vol. 117, pp. 117-137, May 1962. 2, 3

[3] Stewart, D., 1965-66, "A platform with six degrees of freedom", Proc. Instn. Mech. Engrs., Vol. 180, Pt. 1, No. 15, pp. 371-386. 3

[4] Merlet, J.P., 2000, "Parallel robots", Kluwer Academic Publishers, AH Dordreche, The Netherlands. 3, 4

[5] Bonev, I., 2001, "Delta parallel robot - the story of success", http://www.parallemic.org/Reviews/Review002.html. 4

[6] Birglen, L., 2003, "Haptic devices based on parallel mechanisms. State of the art", http://www.parallemic.org/Reviews/Review003.html . 4

[7] Gosselin, M.C. and Hamel, J.-F., 1994, "The agile eye: a high-performance three-degree-of-freedom camera-orienting device", in Proceedings of IEEE Interaction Conference on Robotics and Automation, 08 May - 13 May, San Diego, CA, Vol. 1, pp. 781-786. 4

[8] Kong, X. and Gosselin, M.C., 2010, "A formula that produces a unique solutions to the forward displacement analysis of a quadratic spherical parallel manipulator: the agile eye", Journal of Mechanisms and Robotics, Vol. 2, 044501. 4, 7

[9] Birglen, L., Gosselin, C., Pouliot, N., Monsarrat, B. and Laliberté, T., 2002, "SHaDe, a new 3-DOF haptic device", IEEE Transactions on Robotics and Automation, Vol. 18, No. 2, pp. 166-175. 4, 7

[10] Ferre, M., Galiana, I., Wirz, R. and Tuttle, N., 2011, "Haptic device for capturing and simulating hand manipulation rehabilitation", IEEE/ASME Transactions on Mechatronics, Vol. 16, No. 5, pp. 808-815. 5, 8

[11] Yu, A., Bonev, I.A. and Zsombor-Murray, P., 2008, "Geometric approach to the accuracy analysis of a class of 3-DOF planar parallel robots", Journal of Mechanism and Machine Theory, Vol. 43, pp. 364-375. 5

[12] Joubair, A., Slamani, M. and Bonev, I.A., 2012, "A novel XY-Theta precision table and a geometric procedure for its kinematic calibration", Robotics and Computer-Integrated Manufacturing, Vol. 28, pp. 57-65. 5, 8

[13] Koseki, Y., Tanikawa, T., KoYachi, N., and Arai, T., 2000, "Kinematic analysis of tranditional 3-DOF micro parallel mechanism using matrix method", in Proceedings of IEEE/RSJ International Conference on Intelligent Robots and Systems, pp. 786-792. 5, 9

[14] Tanikawa, T., Ukiana, M., Koseki, Y., Ohba, K., Fujii, K., and Arai, T., 2002, "Design of 3DOF parallel mechanism with thin plate for micro finger module in micro manipulation", in Proceedings of the IEEE/RSJ International Conference on Intelligent Robots and Systems, pp. 1778-1783. 5

[15] Yi, B.-J., Chung, G. B., Na, H. Y., Kim, W. K., and Suh, I. H., 2003, "Design and experiment of a 3-DOF parallel micromechanism utilizing flexure hinges", IEEE Transactions on Robotics and Automation, Vol. 19, No. 4, pp. 604-612. 5, 9

[16] Li, Y., and Xu, Q., 2009, "Design and analysis of a totally decoupled flexure-based XY parallel micromanipulator", IEEE Transactions on Robotics, Vol. 25, No. 3, pp. 645-657. 5, 10

[17] Li, Y., and Xu, Q., 2009, "Design and optimization of an XYZ parallel micromanipulator with flexure hinges", J Intell Robot Syst, Vol. 55, pp. 377-402. 5, 10

[18] Li, Y., and Xu, Q., 2010, "Adaptive sliding mode control with perturbation estimation and PID sliding surface for mation tracking of a piezo-driven micromanipulator", IEEE Transactions on Control Systems Technology, Vol. 18, No. 4, pp. 798-810. 5

[19] Jensen, K. A., Lusk, C. P., and Howell, L. L., 2006, "An XYZ micromanipulator with three translational degrees of freedom", Robotica, Vol. 24, pp. 305-314. 5, 11

[20] Culpepper, M. L., and Anderson, G., 2004, "Design of a low-cost nano-manipulator which utilizes a monolithic, spatial compliant mechanism", Precision Engineering, Vol. 28, pp. 469-482. 5, 12

[21] Yao, Q., Dong, J., and Ferreira, P. M., 2008, "A novel parallel-kinematics mechanisms for integrated, multi-axis nanopositioning Part 1. Kinematics and design for fabrication", Precision Engineering, Vol. 32, pp. 7-19. 5, 12

[22] Dong, J. Y., Q. Yao, and Placid, M. F., 2008, "Dynamics, control and performance analysis of a novel parallel-kinematics mechanism for integrated, multi-axis nano-positioning", Precision Engineering, Vol. 32, No. 1, pp. 20-33. 5

[23] Rees, Jones J., 1979, "Cross-coordinates control of a robot manipulator", in Int. Workshop on Nuclear Robotics Technologies and Applications: Present and Future, University of Lancaster, pp. 1-10. 12

[24] Berthomieu, T., 1989, "Étude d'un micro-manipulateur parallèle et de son couplage avec un robot proteur", Ph.D. Thesis, ENSTAE, Toulouse, January 24. 12

[25] Nokleby, S. B., Fisher, R., Podhorodeski, R. P., and Firmani, F., 2005, "Force capabilities of redundantly-actuated parallel manipulators", Mechanism and Machine Theory, Vol. 40, pp. 578-599. 13

[26] Nokleby, S. B., Firmani, F., Zibil, A., and Podhorodeski, R. P., 2007, "Force-moment capabilities of redundantly-actuated planar-parallel architectures", 12th IFToMM World Congress, Besançon, June 18-21. 13

[27] Zhao, Y., Liu, J.F., and Huang, Z., 2011, "A force analysis of a 3-RPS parallel mechanism by using screw theory", Robotica, Vol. 29, pp. 959-965. 13

[28] Lu, Y., Hu, B., Li, S.-H., and Tian, X.-B., 2008, "Kinematics/statics analysis of a novel 2SPS+PRRPR parallel manipulator", Mechanism and Machine Theory, Vol. 43, pp. 1099-1111. 13

[29] Firmani, F., Zibil, A., Nokleby, S. B., and Podhorodeski, R. P., 2008, "Wrench capabilities of planar parallel manipulators. Part I: wrench polytopes and performance indices", Robotica, Vol. 26, No. 06, pp. 791-802. 13, 14

[30] Firmani, F., Zibil, A., Nokleby, S. B., and Podhorodeski, R. P., 2008, "Wrench capabilities of planar parallel manipulators. Part II: Redundancy and wrench workspace analysis", Robotica, Vol. 26, No. 06, pp. 803-815. 13, 14

[31] Garg, V., Nokleby, S. B., and Carretero, J. A., 2009, "Wrench capability analysis of redundantly actuated spatial parallel manipulators", Mechanism and Machine Theory, Vol. 44, pp. 1070-1081. 13, 14

[32] Wu, J., Li, T., Wang, J., and Wang, L., 2013, "Stiffness and natural frequency of a 3-DOF parallel manipulator with consideration of additional leg candidates", Robotics and Autonomous Systems, Vol. 61, pp. 868-875. 14

[33] Wu, J., Wang, J., Wang, L., Li, T., and You, Z., 2009, "Study on the stiffness of a 5-DOF hybrid machine tool with actuation redundancy", Mechanism and Machine Theory, Vol. 44, pp. 289-305. 14

[34] Aginaga, J., Zabalza, I., Altuzarra, O., and Nájera, J., 2012, "Improving static stiffness of the 6-RUS parallel manipulator using inverse singularities", Robotics and Computer-Integrated Manufacturing, Vol. 28, pp. 458-471. 14

[35] Gosselin, C. M., 1990, "Stiffness mapping for parallel manipulators", IEEE Transactions on Robotics and Automation, Vol. 6, No. 3, pp. 377-382. 14

[36] Gosselin, C. M., and Zhang, D., 2002, "Stiffness analysis of parallel mechanisms using a lumped model", International Journal of Robotics and Automation, Vol. 17, No. 1, pp. 17-27. 14

[37] Majou, F., Gosselin, C., Wenger, P., and Chablat, D., 2007, "Parametric stiffness analysis of the Orthoglide", Mechanism and Machine Theory, Vol. 42, pp. 296-311. 14

[38] Ceccarellli, M., and Carbone, G., 2005, "Numerical and experimental analysis of the stiffness performances of parallel manipulators", 2nd International Colloquium "Collaborative Research Centre 562″, Braunschweig. 14

[39] Ceccarellli, M., and Carbone, G., 2002, "A stiffness analysis for CaPaMan (CassinoParallel Manipulator)", Mechanism and Machine Theory, Vol. 37, pp. 427-439. 14

[40] Deblaise, D., Hernot, X., and Maurine, P., 2006, "A systematic analytical method for PKM stiffness matrix calculation", in Proceedings of the 2006 IEEE International Conference on Robotics and Automation, Orlando, USA, pp. 4213-4219. 14

[41] Sales, R., and Mendes, J. C., 2008, "Stiffness analysis of a parallel manipulator using matrix structural analysis", in Proceedings of EUCOMES 08, Cassino, Italy, pp. 255-262. 14

[42] Bouzgarrou, B. C., Fauroux, J. C., Gogu, G., and Heerah, Y., 2004, "Rigidity analysis of T3R1 parallel robot with uncoupled kinematics", in Proceedings of the 35th International Symposium on Robotics, Paris, France. 14

[43] Pinto, C., Corral, J., Altuzarra, O., and Hernández, A., 2010, "A methodology for static stiffness mapping in lower mobility parallel manipulators with decoupled motions", Robotica, Vol. 28, No. 5, pp.719-735. 14

[44] Nakamura, Y., and Ghodoussi, M., 1989, "Dynamics computation of closed-link robot mechanisms with nonredundant and redundant actuators", IEEE Transactions on Robotics and Automation, Vol. 5, No. 3, pp. 294-302. 15

[45] Gosselin, C.M., 1996, "Parallel computation algorithms for the kinematics and dynamics of planar and spatial parallel manipulators", Journal of Dynamic Systems, Measurement, and control, Vol. 118, pp. 22-28. 15

[46] Dasgupta, B., and Choudhury, P., 1999, "A general strategy based on the Newton-Euler approach for the dynamic formulation of parallel manipulators", Mechanism and Machine Theory, Vol. 34, pp. 801-824. 15

[47] Almeida, R. Z. H., Hess-Coelho, T. A., 2011, "Structural synthesis, dynamic modeling and analysis of a 3-DOF asymmetric parallel mechanism", 13th World Congress in Mechanism and Machine Science, Guanajuato, México, June 19-25, A12-466. 16

[48] Li, Y., Zhang, L., and Niu, Y., 2011, "Dynamic analysis of spherical 2-DOF parallel manipulator with actuation redundancy", in Proceedings of the 2011 IEEE International Conference on Mechatronics and Automation, Beijing, China, August 7-10, pp. 1350-1355. 16

[49] Zhao, Y., and Gao, F., 2009, "Dynamic performance comparison of the 8PSS redundant parallel manipulator and its non-redundant counterpart —the 6PSS parallel manipulator", Mechanism and Machine Theory, Vol. 44, pp. 991-1008. 15

[50] Raţ, N. R., Neagoe, M., Diaconescu, D., Stan, S. D., and Bălan, R., 2010, "Dynamic modeling and VR simulation of 3DOF medical parallel robots", Springer Science+Business Media B.V., DOI: 10.1007/978-90-481-3656-8_55, pp. 297-302. 15

[51] Byun, Y.-K., Cho, H.-S., Kim, W.-K., Baek, S.-E., Chang, H.-S., and Ro, K.-C., 1998, "Kinematic/Dynamic analysis of a 6 DOF parallel manipulator with 3-PPSP serial sub-chains and its implementation", in Proceedings of the 1998 IEEE/RSJ Intl. Conference on Intelligent Robots and Systems, Victoriam, B.C., Canada, pp. 1981-1986.

[52] Piras, G., Cleghorn, W. L., and Mills, J. K., 2005, "Dynamic finite-element analysis of a planar high-speed, high-precision parallel manipulator with flexible links", Mechanism and Machine Theory, Vol. 40, pp. 849-862. 16

[53] Cleghorn, W. L., Fenton, R. G., and Tabarrok, B., 1981, "Finite element analysis of high-speed flexible mechanisms", Mechanism and Machine Theory, Vol. 16, No. 4, pp. 407-424. 16

[54] Lee, M. K., and park, K. W., 1999, "Kinematic and dynamic analysis of a double parallel manipulator for enlarging workspace and avoiding singularities", IEEE Transactions on Robotics and Automation, Vol. 15, No. 6, pp. 1024-1034. 16

[55] Wu, J., Wang, L., and Guan, L., 2013, "A study on the effect of structure parameters on the dynamic characteristics of a PRRRP parallel manipulator", Nonlinear Dyn, DOI 10.1007/s11071-013-0960-2. 16

[56] Li, Y., Wang, J., Liu, X.-J., Wang, L.-P., 2010, "Dynamic performance comparison and counterweight optimization of two 3-DOF parallel manipulators for a new hybrid machine tool", Mechanism and Machine Theory, Vol. 45, pp. 1668-1680. 16

[57] Liu, X.-J., Wang, J., Gao, F., and Wang, L.-P., 2001, "On the analysis of a new spatial three degrees of freedom parallel manipulator", IEEE Transactions on Robotics and Automation, Vol. 17, No. 6, pp. 959-968. 16

[58] Liu, X.-J., Wang, J., Wu, C., and Kim, J., 2009, "A new family of spatial 3-DOF parallel manipulators with two translational and one rotational DOFs", Robotica, Vol. 27, No. 2, pp. 241-247. 16

[59] Cheng, H., Yiu, Y.-K., and Li, Z., 2003, "Dynamics and control of redundantly actuated parallel manipulators", IEEE/ASME Transactions on Mechatronics, Vol. 8, No. 4, pp. 483-491. 16

[60] Li, Y., and Xu, Q., 2009, "Dynamic modeling and robust control of a 3-PRC tranditional parallel kinematic machine", Robotics and computer-integrated manufacturing, Vol. 25, pp. 630-640. 16

[61] Lessard, S., Bigras, P. and Bonev, I.A., 2007, "A new medical parallel robot and its static balancing optimization", Journal of Medical Devices, Vol. 1, pp. 272-278. 20

[62] Nakadate, R., Tokunaga, Y., Solis, J., Takanishi, A., Minagawa, E., Sugawara, M. and Niki, K., 2011, "Development of a robot assisted carotid blood flow measurement system", Mechanism and Machine Theory, Vol. 46, pp. 1066-1083. 20

[63] Beer, J.M., Smarr, C.A., Chen, T.L., Prakash, A., Mitzner, T.L., Kemp, C.C. and Rogers, W.A., 2012, "The domesticated robot: design guidelines for assisting older adults to age in place", in Proceedings of ACM/IEEE International Conference on Human-Robot Interaction, New York, NY, USA, pp. 335-342. 20

[64] Lu, Y., Zeng, L. and Bone, G.M., 2009, "Multisensor system for safer human-robot interaction", in proceedings of IEEE International Conference on Robotics and Automation, Barcelons, Spain, pp. 1767-1772. 20

[65] Duchaine, V., Lauzier, N., Baril, M., Lacasse, M.A., and Gosselin, C. 2009, "A flexible robot skin for safe human robot interaction", in proceedings of IEEE International Conference on Robotics and Automation, Kobe, Japan, May 12-17, pp. 3676-3681. 20

[66] Yoon, S.-S., Kang, S., Yun, S.-K., Kim, S.-J., Kim, Y.-H. and Kim, M., 2005, "Safe arm design with MR-based passive compliant joints and visco-elastic covering for service robot applications", Journal of Mechanical Science and Technology, Vol. 19, No. 10, pp. 1835-1845. 20

[67] Choi, D.-E., Yang, G.-H., Choi, J., Lee, W., Cho, C. and Kang, S., 2011, "A safe joint with a joint torque sensor", in proceedings of International Conference on Ubiquitous Robots and Ambient Intelligence (URAI), Incheon, Korea, November 23-26, pp. 331-336. 20

[68] Kishi, Y., Yamada, Y. and Yokoyama, K., 2012, "The role of joint stiffness enchancing collision reaction performance of collaborative robot manipulators", in proceedings of IEEE/RSJ International Conference on Intelligent Robots and Systems, Vilamoura, Algarve, Portugal, October 7-12, pp. 376-381. 20

[69] Conti, F. and Khatib, O., 2009, "A new actuation approach for haptic interface design", The International Journal of Robotics Research, Vol. 28, No. 6, pp. 834-848. 20

[70] Park, J.-J., Song, J.-B., and Kim, H.-S., 2008, "Safe joint mechanism based on passive compliance for collision safety", Recent Progress in Robotics: Viable Robotic Service to Human, pp. 49-61. 20

[71] Park, J.-J., Kim, H.-S. and Song, J.-B., 2009, "Safe robot arm with safe joint mechanism using nonlinear spring system for collision safety", in proceedings of IEEE International Conference on Robotics and Automation, Kobe, Japan, May 12-17, pp. 3371-3376. 20

[72] Gan, D., Tsagarakis, N. G., Dai, J. S. and Caldwell, D. G., 2011, "Stiffness design for compliant manipulators based on dynamic analysis of the impact configuration", in proceedings of ASME IDETC/CIE, Washington, DC, USA, August 28-31, DETC2011-47636. 20

[73] Kim, B.-S., Park, J.-J. and Song, J.-B., 2007, "Double actuator unit with planetary gear train for a safe manipulator", in proceedings of IEEE International Conference on Robotics and Automation, Roma, Italy, April 10-14, pp. 1146-1151. 20

[74] Walker, D.S., Thoma, D.J. and Niemeyer, G., 2009, "Variable impedance magnetorheological clutch actuator and telerobotic implementation", in proceedings of IEEE/RSJ International Conference on Intelligent Robots and Systems, St. Louis, USA, October 11-15, pp. 2885-2891. 20

[75] Lauzier, N. and Gosselin, C., 2011, "Series clutch actuators for safe physical human-robot interaction",   IEEE International Conference on Robotics and Automation, Shanghai, China, May 9-13, pp. 5401-5406. 20, 27

[76] Len, T., Kunz, J. and von Stryk, O., 2010, "BioRob-Arm: a quicky deployable and intrinsically safe, light-weight robot arm for service robotics applications", Robotics(ISR), International Symposium on and German Conference on Robotics (ROBOTIK), June 7-9, pp. 1-6. 20

[77] Vermeulen, M. and Wisse, M., 2010, "Intrinsically safe robot arm: adjustable static balancing and low power actuation", International Journal of Social Robotics, Vol. 2, No. 3, pp. 275-288. 20

[78] Lauzier, N., Grenier, M. and Gosselin, C., 2009, "2 DOF Cartesian force limiting device for safe physical human-robot interaction", in proceedings of IEEE International Conference on Robotics and Automation, Kobe, Japan, May 12-17, pp. 253-258. 20

[79] Lauzier, N. and Gosselin, C., 2010, "3-DOF Cartesian force limiting device based on the delta architecture for safe physical human-robot interaction", in proceedings of IEEE International Conference on Robotics and Automation, Anchorage, Alaska, USA, May 3-8, pp. 3420-3425. 20

[80] Gosselin, C., Kong, X., Foucault, S., and Bonev, I., 2004, "A fully decoupled 3-dof translational parallel mechanism", in Proceedings of the Fourth Chemnitz Parallel Kinematics Seminar / 2004 Parallel Kinematic Machines International Conference, pp. 596-610. 56, 57

[81] Richard, P.-L., Gosselin, C., and Kong, X., 2007, "Kinematic analysis and prototyping of a partially decoupled 4-DOF 3T1R parallel manipulator", ASME Journal of Mechanical Design, Vol. 129(6), pp. 611-616. 56, 58

[82] Gosselin, C. M., Masouleh, M. T., Duchaine, V., Richard, P.-L., Foucault, S., and Kong, X., 2007, "Parallel mechanisms of the multipteron family: kinematic architectures and benchmarking", in Proceedings of IEEE International Conference on Robotics and Automation, Roma, Italy, pp. 555-560. 56

[83] Altuzarra, O., Pinto, C., Sandru, B., and Amezua, E., 2009, "Pareto-optimal solutions using kinematic and dynamic functions for a Schönflies parallel manipulator", in Proceedings of the ASME IDETC/CIE, San Diego, California, USA, DETC2009-86723. 56

[84] Briot, S., and Bonev, I. A., 2010, "Pantopteron-4: a new 3T1R decoupled parallel manipulator for pick-and-place applications", Mechanism and Machine Theory, No. 45, pp. 707-721. 56

[85] Glazunov, V. A., Levin, S. V., Shalyukhin, K. A., Hakkyoglu, M., and Tung, V. D., 2010, "Development of mechanisms of parallel structure with four degrees of freedom and partial decoupling", Journal of Machinery Manufacture and Reliability, Vol. 39, No. 5, pp. 407-411. 56

[86] Briot, S., and Arakelian, V., 2011, "On the dynamic properties of flexible parallel manipulators in the presence of type 2 singularities", Journal of Mechanisms and Robotics, Vol. 3, 031009. 56

[87] Zubizarreta, A., Cabanes, I., Marcos, M. and Pinto, C., 2009, "Dynamic modeling of planar parallel robots considering passive joint sensor data", Robotica, Vol. 28, pp. 649-661. 56

[88] Almeida, R. Z. H., and Hess-Coelho, T. A., 2010, "Dynamic model of a 3-dof asymmetric parallel mechanism", The Open Mechanical Engineering Journal, Vol. 4, pp. 48-55. 56

[89] Khalil, W. and Guegan, S., 2004, "Inverse and direct dynamic modeling of Gough-Stewart robots", IEEE Transactions on Robotics, Vol. 20, No. 4, pp. 754-762. 56

[90] Abdellatif, H., and Heimann, B., 2009, "Computational efficient inverse dynamics of 6-DOF fully parallel manipulators by using the Lagrangian formalism", Mechanism and Machine Theory, No. 44, pp. 192-207. 56

[91] Liu, M.-J., Li, C.-X., and Li, C.-N., 2000, "Dynamics analysis of the Gough-Stewart platform manipulator", IEEE Transactions on Robotics and Automation, Vol. 16, No. 1, pp. 94-98. 56

[92] Zhao, Y., and Gao, F., 2009, "Inverse dynamics of the 6-dof out-parallel manipulator by means of the principle of virtual work", Robotica, Vol. 27, pp. 259-268. 56

[93] Gosselin, C., 2009, "Compact dynamic models for the tripteron and quadrupteron parallel manipulators", in Proceedings of the Institution of Mechanical Engineers, Part I: Journal of Systems and Control Engineering, pp. 1-11. 17, 56, 57, 59, 64